UNIVERSITY OF OKLAHOMA

GRADUATE COLLEGE

DETAILED LITHOSTRATIGRAPHIC CHARACTERIZATION AND SEQUENCE STRATIGRAPHY OF A COMPLETE WOODFORD SHALE OUTCROP SECTION IN SOUTHERN OKLAHOMA

A THESIS

SUBMITTED TO THE GRADUATE FACULTY

in partial fulfillment of the requirements for the

Degree of

MASTER OF SCIENCE

By

HENRY ARMANDO GALVIS PORTILLA
Norman, Oklahoma
2017

Downloaded from SHAREOK. Persistent Handle URL: https://hdl.handle.net/11244/51866

DETAILED LITHOSTRATIGRAPHIC CHARACTERIZATION AND SEQUENCE STRATIGRAPHY OF A COMPLETE WOODFORD SHALE OUTCROP SECTION IN SOUTHERN OKLAHOMA

A THESIS APPROVED FOR THE
CONOCOPHILLIPS SCHOOL OF GEOLOGY AND GEOPHYSICS

BY

Dr. Roger Slatt, Chair

Dr. Matthew Pranter

Mr. Brian Cardott

© Copyright by HENRY ARMANDO GALVIS PORTILLA 2017
All Rights Reserved.

ACKNOWLEDGEMENTS

First, I would like to express great appreciation to Dr. Roger Slatt for believing in me and giving me the opportunity and honor to work under his guidance on this wonderful research project. His hard work, commitment and technical excellence inspired me many times to achieve my goals and materialize this project. I will always remember and admire him for the great assertiveness on his mentoring and leadership style.

This research would not have been possible without the generous funding from industry sponsors to the Institute of Reservoir Characterization and the Woodford Shale Consortium project at the University of Oklahoma. Sponsors included: Marathon Oil, Newfield Exploration, Pathfinder Exploration, Longfellow Energy, Tiptop Energy, BHP Billiton, Chevron, Ward Petroleum, ConocoPhillips, Nostra Terra Oil & Gas, Chaparral Energy, BP, Vitruvian Exploration, Potts-Stephenson Exploration, Payrock Energy, Casillas Petroleum, Apache Corporation, Chandler Engineering, Jones Energy, Gastar Exploration, Rebellion Energy, Halliburton, Jetta Operating company, Council Oak Resources, and Paisano Energy. Additionally, I wish to thank the School of Geology and Geophysics at the University of Oklahoma for providing resources and facilities for me to conduct the field work and the numerous laboratory analysis.

My appreciation is extended to the Speake family for generously allowing us access to their land. I am very grateful to them because all field trips to the Speake Ranch were a truly enjoyable experience not only for doing good geology at the quarry, but also for its peacefulness and the breath of fresh air it offered.

I wish to thank my thesis committee members, Dr. Matthew Pranter and Mr. Brian Cardott for their valuable comments and suggestions at my thesis defense and after, which led to improvements of this manuscript.

I also thank friends and colleagues for the enlightening discussions and fruitful feedback during research seminars and field trips, including Carlos Molinares, Richard Brito, Emilio Torres, David Duarte, Ifunanya Ekwunife, Sayantan Ghosh, and Benmadi Milad.

Lastly, I would like to thank my partner of life and beloved Daniela Becerra. Beyond her tireless technical support and smart insights throughout this thesis, I felt very fortunate for having received her constant enthusiasm, motivation and emotional support. Daniela always managed to make me see the bright side of things and showed me the glass half-full when many others have seen it as half-empty. I could not have done this thesis without her assistance. If multi-authorship were permitted for master theses, this would be entirely shared with Daniela. Also, I am very grateful for my family, mom, dad and sisters, who have always had the highest expectations and best wishes for whatever my pursuits are.

TABLE OF CONTENTS

List of Tables viii

List of Figures ix

ABSTRACT xiii

1. INTRODUCTION 1

1.1. Area of study 3

1.2. Regional Geological Background 5

1.3. Woodford Shale Stratigraphy 8

2. METHODOLOGY 11

2.1. Field Methods 11

2.2. Lithofacies Classification 13

2.3. Laboratory Methods 17

2.3.1. X-Ray Fluorescence (Elemental Chemostratigraphy) 19

2.3.2. X-Ray Diffraction (Bulk Rock Mineralogy) 20

2.3.3. Rock-Eval Pyrolysis and Leco-TOC 23

3.2.4. Petrographic Analysis 24

3.2.5. Rock Hardness (Micro-rebound Hammer) 24

2.4. Sequence Stratigraphy 27

3. OUTCROP CHARACTERISTICS 33

3.1. Woodford Shale Formational Contacts 33

3.1.1. Basal Contact: Hunton Group – Woodford Shale 35

3.1.2. Upper Contact: Woodford Shale – Sycamore Formation 40

3.2. Lithofacies Characterization 44

3.2.1. Argillaceous Shales 44
3.2.2. Siliceous Shales 47
3.2.3. Brown Siliceous Shales 49
3.2.4. Siliceous Mudstones 51
3.2.5. Cherts 53
3.2.6. Siliceous-Dolomitic Shales 55
3.2.7. Dolomitic Mudstone 57
3.3. Woodford Shale Internal Characteristics 59
3.3.1. Lower Woodford (LW) 59
3.3.2. Middle Woodford (MW) 60
3.3.3. Upper Woodford (UW) 61
4. ORGANIC GEOCHEMISTRY 70
4.1. Organic Richness 70
4.2. Kerogen Type 78
4.3. Thermal Maturity 80
5. ELEMENTAL CHEMOSTRATIGRAPHY 82
5.1. Detrital-sensitive elements 82
5.2. Carbonate-Sensitive Elements 86
5.3. Redox-Sensitive Elements 90
5.4. Vertical Chemostratigraphic Zonation 96
5.5. Elemental Proxies and Mineralogical Composition 101
5.6. Elemental Proxies and Lithofacies 104
6. ROCK HARDNESS 109

7. SUMMARY OF ROCK CHARACTERISTICS 111

8. SEQUENCE STRATIGRAPHY 114

8.1. Description of Stratigraphic Sequences 116

8.2. Synopsis of Sequence Stratigraphy Framework 124

8.3. Outcrop-to-Subsurface Stratigraphic Correlation 127

9. RESERVOIR IMPLICATIONS 130

10. CONCLUSIONS 140

RECOMMENDATIONS AND FUTURE WORK 143

REFERENCES 146

LIST OF TABLES

Table 1. Summary of main elements and their significance in chemostratigraphic interpretations 20

Table 2. Main parameters and definitions of the obtained variables from Rock-Eval pyrolysis and Leco-TOC 23

Table 3. Matrix of elemental enrichment ratios (ER) by cluster 97

Table 4. Summary of rock characteristics distributed by the informal Woodford subdivision..... 112

Table 5. Summary of rock characteristics distributed by lithofacies..... 113

LIST OF FIGURES

Figure 1. Location of the study area 4

Figure 2. Regional structural setting of southern Oklahoma.. 6

Figure 3. Tectonic evolution of the Southern Oklahoma Aulacogen 7

Figure 4. Regional paleogeography of North America's mid-continent region during the Late Devonian and Early Mississippian 8

Figure 5. Generalized stratigraphic chart of the Arbuckle Mountains and Ardmore Basin. Typical well log responses of the Woodford Shale in the Ardmore Basin 10

Figure 6. Field methods conducted in this study. 11

Figure 7. Typical cyclical heterogeneity between soft and hard beds 13

Figure 8. Field-based lithofacies classification of Woodford Shale mudrocks 15

Figure 9. Seven dominant lithofacies across the entire Woodford Shale interval 16

Figure 10. Location and distribution of samples across the entire Woodford Shale section 18

Figure 11. XRD patterns of seven selected samples from bulk-rock analysis 22

Figure 12. Micro-rebound hardness tester Equotip Piccolo 2 26

Figure 13. Schematic criteria for interpreting high-frequency cycles and their bounding surfaces based on Gamma ray parasequences (GRP). 28

Figure 14. Generalized 2nd order sequence stratigraphic model applied in this work ... 30

Figure 15. Wells used in this study for stratigraphic correlations and to tie the Speake Ranch outcrop with the subsurface of the Ardmore Basin 31

Figure 16. Typical weathering response of the Woodford Shale of south-central Oklahoma 34

Figure 17. Outcrop characteristics and lithostratigraphy of the basal formational contact between the Hunton and lower Woodford shale. 38

Figure 18. Lithological characteristics of the basal formational contact between Hunton and Woodford Shale 39

Figure 19. Outcrop characteristics and lithostratigraphy of the upper formational contact between the Woodford Shale and its overlying Sycamore Limestone 42

Figure 20. Lithological characteristics of the upper formational contact between the Woodford Shale and its overlying Pre-Sycamore deposits 43

Figure 21. Typical characteristics of the Argillaceous Shales lithofacies. 46

Figure 22. Typical characteristics of the Siliceous Shales lithofacies. 48

Figure 23. Typical characteristics of the Brown Siliceous Shales 50

Figure 24. Typical characteristics of the Siliceous Mudstones 52

Figure 25. Typical characteristics of Cherts 54

Figure 26. Typical characteristics of Siliceous-Dolomitic Shales 56

Figure 27. Typical characteristics of the Dolomitic Mudstones 58

Figure 28. Correlation between gamma ray responses and the Soft-to-Hard ratios per foot by Woodford members. 62

Figure 29. Integration of vertical distribution of lithofacies, soft-to-hard ratios and distribution of bed thicknesses by informal Woodford members 63

Figure 30. Bulk rock mineralogical composition plotted by Woodford members 66

Figure 31. Bulk rock mineralogical composition plotted by rock types based on weathering responses in outcrops, as hard and soft beds 67

Figure 32. Ternary diagram for identification of Woodford Shale lithofacies based on mineralogical proportions of quartz, clays and carbonates 68

Figure 33. Mineralogy vs organic richness (TOC)..... 69

Figure 34. Organic richness as determined by TOC contents 72

Figure 35. Distribution of TOC contents across Woodford members..... 74

Figure 36. Geochemical logs across the entire Woodford section 75

Figure 37. TOC contents plotted by lithofacies and mineralogy..... 77

Figure 38. Kerogen type as determined by pyrolysis Rock-Eval parameters 79

Figure 39. Kerogen type and maturity assessment via integration of HI and Tmax 81

Figure 40. Vitrinite reflectance distribution in south-central Oklahoma..... 81

Figure 41. Cross plots of detrital-sensitive elements differentiated by hard (green dots) and soft (red dots) beds..... 85

Figure 42. Cross plots of carbonate-sensitive elements differentiated by hard (green dots) and soft (red dots) beds..... 89

Figure 43. Cross plots of Sr vs carbonate-sensitive elements differentiated by hard (green dots) and soft (red dots) beds..... 90

Figure 44. Cross plots of Molybdenum vs TOC and sulfur 91

Figure 45. Cross plot of Mo vs TOC for interpreting degrees of basin restriction 92

Figure 46. Cross plots of Vanadium vs TOC and More anoxic conditions during the depositions of soft beds. 93

Figure 47. Cross plots of Uranium vs TOC and Mo 95

Figure 48. Vertical log of most common chemostratigraphic proxies across the entire Woodford section 100

Figure 49. Cross plots of elemental proxies (XRF) vs quartz contents (XRD)..... 102

Figure 50. Cross plots of elemental proxies (XRF) vs clay contents (XRD)..... 103

Figure 51. Cross plots of elemental proxies (XRF) vs carbonate contents (XRD)..... 104

Figure 52. Box plots of elemental proxies plotted by lithofacies..... 108

Figure 53. Distribution of rock hardness values by lithofacies. 110

Figure 54. Outcrop-based sequence stratigraphic framework of the complete measured section at Speake Ranch 123

Figure 55. Idealized vertical variations of main features and controls across a second-order depositional sequence within the Woodford shale of this study..... 126

Figure 56. Outcrop-to-subsurface Gamma ray correlation of sequence stratigraphic framework..... 129

Figure 57. Typical interbedding observed in the Woodford shale at Speake Ranch outcrop..... 131

Figure 58. Differences between soft and hard beds..... 133

Figure 59. Differences between soft and hard beds as determined by TOC, clay and quartz contents, Si/Al ratios, brittleness index and hardness values 134

Figure 60. Idealized one-foot models to which Woodford shale strata can be vertically stacked as function of bed thickness and soft-to-hard ratios..... 136

Figure 61. Idealized Reservoir quality and completion quality as interpreted via stacking patterns between soft and hard beds..... 137

Figure 62. Vertical plot at one-foot resolution that shows the stratigraphic variability of soft-to-hard ratios, bed thickness and rock Hardness..... 139

ABSTRACT

This work presents a detailed rock-based and stratigraphic documentation of an unpublished and recently discovered Woodford Shale outcrop in the south flank of the Arbuckle Mountains (southern Oklahoma). The exposed section comprises the entire Woodford Shale (320 ft), as well as its basal and overlying formational contacts with the Hunton Group and Sycamore Limestone respectively.

The basal contact is unconformable, and records the shallower carbonate deposits of the heavily karstified and bioturbated Hunton Group, sharply capped by the lowermost Woodford, which records the onset of a transgressive phase, represented by non-organic greenish/brown claystones and coarse grained glauconitic sandstones, that fines upward into organic-rich shales of the lower Woodford.

The upper contact between the Woodford Shale and the Sycamore Limestone is transitional, and suggests a general upward increase in paleo-oxygenation and terrigenous input, represented by non-organic, bioturbated greenish/grey siltstones that grades into marlstones of the early Mississippian.

Within the Woodford Shale strata, seven main lithofacies were recognized honoring textural, rock fabric, organic richness and mineral composition (siliceous, argillaceous or dolomitic). Vertical stacking of these lithofacies, tied with outcrop Gamma-ray profiles and elemental chemostratigraphic proxies, revealed a cyclical pattern interpreted as fourth-order parasequence cycles superimposed upon a major second-order depositional sequence. A Maximum Flooding Surface (MFS) is recognized near the transition between the middle and upper members of the Woodford Shale. Maximum organic richness accompanied by clay-rich facies were interpreted to occur

within early stages of the Transgressive System Tract (TST). The Highstand system tract (HST) appeared largely dominated by biogenic pelagic supply in the form of radiolarian-rich cherts.

Outcrop-to-subsurface Gamma ray correlations of parasequences surfaces and third-order stratigraphic cycles demonstrates the possibility of developing a high frequency sequence stratigraphic framework for the Woodford Shale in the subsurface of the Ardmore Basin; indeed the long-distance correlation of many of the sequences and surfaces attest to good lateral continuity for individual cycles.

Reservoir quality of this section was assessed using the vertical arrangement of lithofacies, from which we hypothesized that potential target zones are interpreted to be composed by high-frequency interbeddings of organic-rich 'soft' beds (acting as source) and 'hard' brittle beds (acting as more frackable or fractured rocks). According to this model, and relating our sequence stratigraphic framework, a potential target zone is interpreted to be within the late Transgressive System Tract (TST) and early Highstand System Tract (HST) where the soft to hard ratio and bed thicknesses of beds is about equal.

1. INTRODUCTION

In Oklahoma, USA, the Late Devonian-Early Mississippian Woodford Shale has proved great success in the production of oil and gas. Given its excellent source/reservoir rock properties, several authors have examined Woodford outcrops in southern Oklahoma. The most significant outcrop studies range from radioactivity surveys (Krystyniak, 2005; Paxton and Cardott, 2008), sedimentological and stratigraphic descriptions (Ham et al., 1973; Fay, 1989; Fishman et al., 2013; Puckette et al., 2013, Bontempi, 2015), biostratigraphic zonations (Urban, 1960; Over, 1992; Over, 2002), organic geochemistry (Comer and Hinch, 1987; Kirkland and others, 1992; Nowaczewski, 2011), up to the use of more advanced tools such as Handheld X-Ray Fluorescence (Treanton, 2014; Turner, 2016; Ekwunife, 2017) and geomechanical tests (Becerra-Rondon, 2017). However, in spite of that, valuable information from new outcrops in new areas still remains underinvestigated, and with the potential to attain more comprehensive understanding of the stratigraphy and lithofacies, which can be translated into useful parameters to assess reservoir/completion quality of the Woodford Shale in the subsurface.

Motivated by the economic importance of this unconventional resource and the current questions from operators that have shifted from “where are the hydrocarbons” to “what are the most optimum zones for drilling and completion”, this work aims to provide geological support to better target the Woodford Shale in the Ardmore Basin of south-central Oklahoma. To achieve this, a complete Woodford Shale outcrop section is characterized and tied to subsurface well logs through a sequence stratigraphic framework.

First, we documented in detail the stratigraphic relation and nature of the formational contacts. Secondly, we proposed a comprehensive classification scheme for Woodford lithofacies, which are characterized using qualitative and quantitative parameters obtained at different scales and under different analytical techniques, including: conventional petrography, scanning electron microscopy (SEM), X-Ray Diffraction (XRD), X-Ray Fluorescence (XRF), Rock-Eval Pyrolysis, Leco-TOC, and rock hardness.

Then, at a larger scale, stacking patterns of lithofacies and parasequences were interpreted into a sequence stratigraphic framework that later was used to correlate with subsurface well logs. Finally, we propose a geological assessment of reservoir and completion quality, where potential target zones are interpreted to be composed by high-frequency interbeddings of organic-rich 'soft' beds (acting as source) and brittle 'hard' beds (acting as more frackable or fractured rocks), which relate our high frequency sequence stratigraphic framework into the best horizontal drilling/completion target; the important zones are interpreted to be within early stages of Highstand System tracts.

1.1. Area of study

Regionally, the study area is located along the southern flank of the Arbuckle Mountains. It covers portions of Carter and Murray counties in south-central Oklahoma (Figure 1). Surface mapping of the area reveals a nearly east-west outcrop belt, where the Woodford Shale crops out through roadcuts, creeks, and quarries. Within this belt, some of the most visited Woodford Shale exposures occur along the southbound side of Interstate 35, including Henry House falls quarry and OHMEGCO quarry (Figure 1). While useful, all of these outcrops expose incomplete (covered) Woodford Shale sections. Fortunately, however, a complete Woodford section in this belt is exposed in a private quarry under the name 'Speake Creed Ranch', with geographic coordinates 34°22'40.36"N and 97°20'17.26"W (SE ¼ Section 18, Township 2S, Range 1W).

The Speake Ranch outcrop section is about 11 miles west of the Interstate 35 (Figure 1). The total vertical stratigraphic exposure is approximately 355 ft thick, comprising the entire lower, middle and upper informal members of the Woodford Shale (~320 ft), the uppermost portion of the underlying Hunton Group (20 ft) and the lowermost portions of the overlying Sycamore Limestone (15 ft). Thus, it offers a unique, fresh and complete Woodford Shale section that preserves the stratigraphic relations with its bounding units (Figure 1).

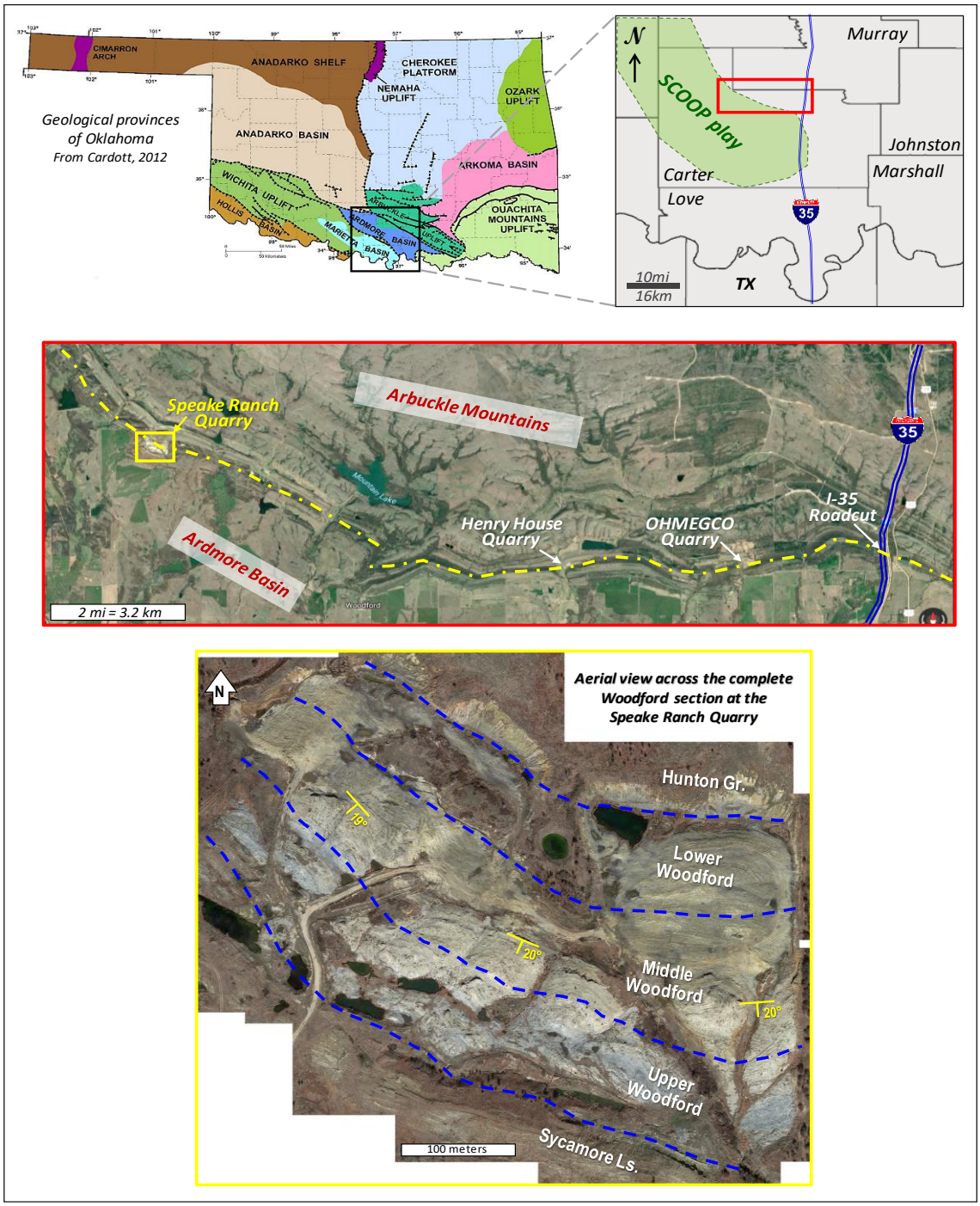

Figure 1. Location of the study area. Upper left: Geological provinces of Oklahoma highlighting portion of south-central Oklahoma and the Arbuckles Mountains (modified from Cardott, 2012). Middle: Location of Woodford Shale outcrops along the nearly E-W outcrop belt. The Speake Ranch quarry is the westernmost outcrop of this belt in the Arbuckle Mountains. Lower: Aerial view of Speake Ranch quarry across the complete Woodford section. Contacts with its over- and underlying bounding units are mappable over 100's of meters in the area. Hunton and Sycamore limestones are more competent than the Woodford Shale. Bedding strike is about N47-55°W dipping around 20°SW.

1.2. Regional Geological Background

The Ardmore Basin is a fault-bounded northwest depression of Pennsylvanian age in south-central Oklahoma. Its formation is related to the development of the Southern Oklahoma Aulacogen (SOA). During the Proterozoic to early Paleozoic, extensional failure of the continental lithosphere occurred in the form of a three-arm rift, from which two of the three arms connected to define the early Paleozoic paleocontinental margin (Figure 2), while the third arm was aborted forming the SOA developed as a NW-SE trough into a rigid craton (Hoffman et al., 1974; Allen, 2000) (Figure 2). During the early Cambrian, regional rifting along the aulacogen created a graben that experienced maximum subsidence (Suneson, 1996), allowing the SOA to be a major depocenter in the Ordovician (Figure 3). Between the Cambrian to Early Devonian accumulation of marine limestones, sandstones, and shales took place within the SOA, over a broad epeiric sea known as the Oklahoma Basin (Carlucci et al., 2014). At about the end of the Devonian the Acadian Orogeny occurred, leading to the first uplift event. Following the Acadian uplift, there was another period of deposition until the Early Pennsylvanian (Figure 3), represented by about 6,250 feet of rock recorded by the Woodford, Sycamore, Caney and Springer formations (Allen, 2000). Later, the Wichita Orogeny recorded a major pulse of deformation from the Late Mississippian to Early Pennsylvanian, during this period the Criner Hills uplifted about 16,000 ft above sea level; erosion of these mountains spilled sediments into the Ardmore and Marietta basins (Allen, 2000). At the end of the Pennsylvanian the Arbuckle Orogeny took place and the Caddo and Arbuckle anticlines were developed and deeply folded, then Permian strata filled both sides of these anticline structures (Figure 2) (Allen, 2000).

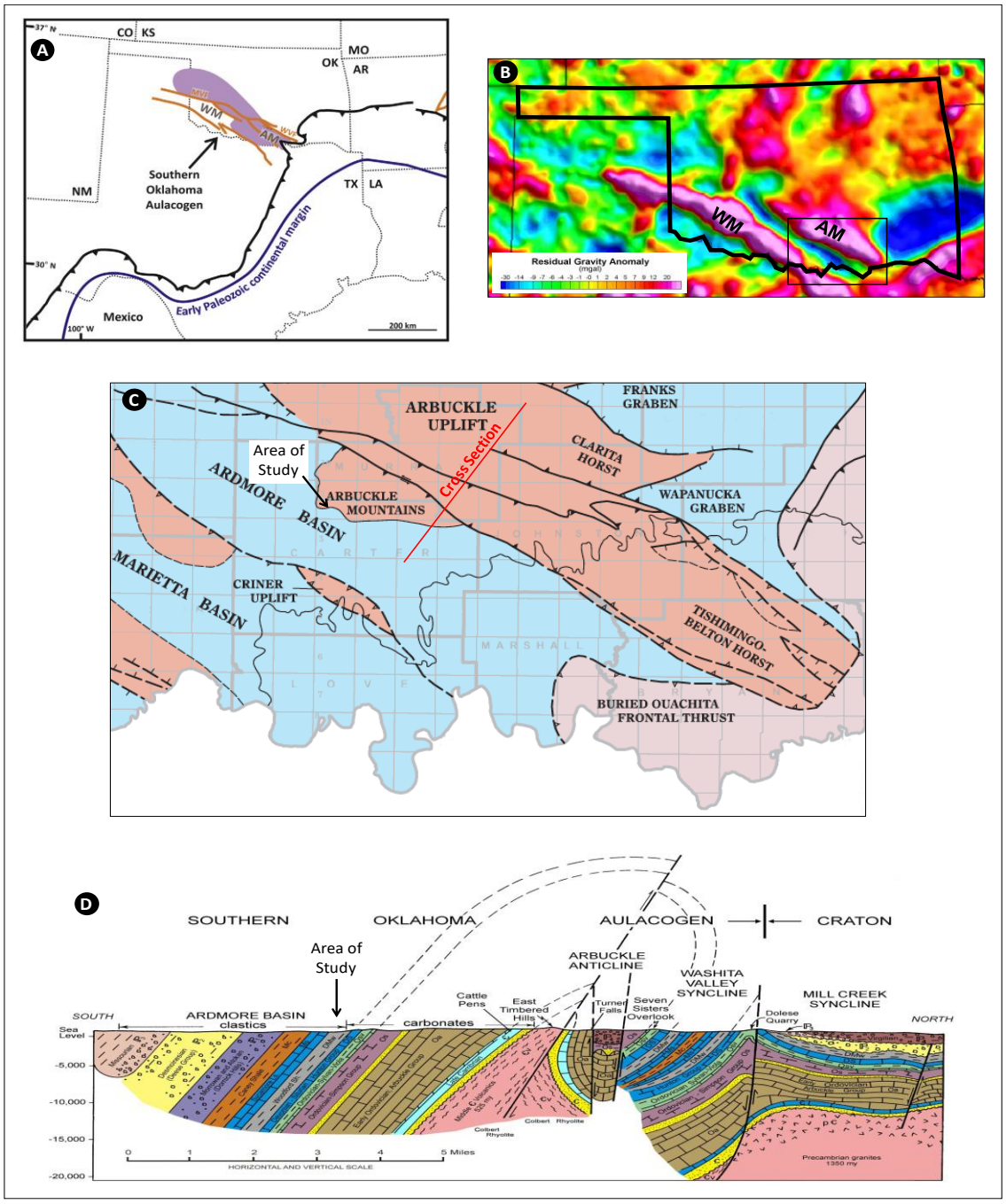

Figure 2. Regional structural setting of southern Oklahoma. A) Tectonic map of the Southern Oklahoma Aulacogen during the early Paleozoic (from Brueseke et al., 2016). B) Gravimetric map highlighting the uplifted basements of the Arbuckle Mountains (AM), Wichita Mountains (WM) and the depression of the Ardmore Basin in between (from Keller and Stephenson, 2007). C) Tectonic map showing the location of the study area in the southern flank of the Arbuckle Mountains (from Northcutt and Campbell, 1995). D) Schematic cross section across the southern flank of the Arbuckle Mountains. The Woodford Shale strata in the study area dip toward the south into the Ardmore Basin (From Keller 2012, originally in Ham et al., 1973).

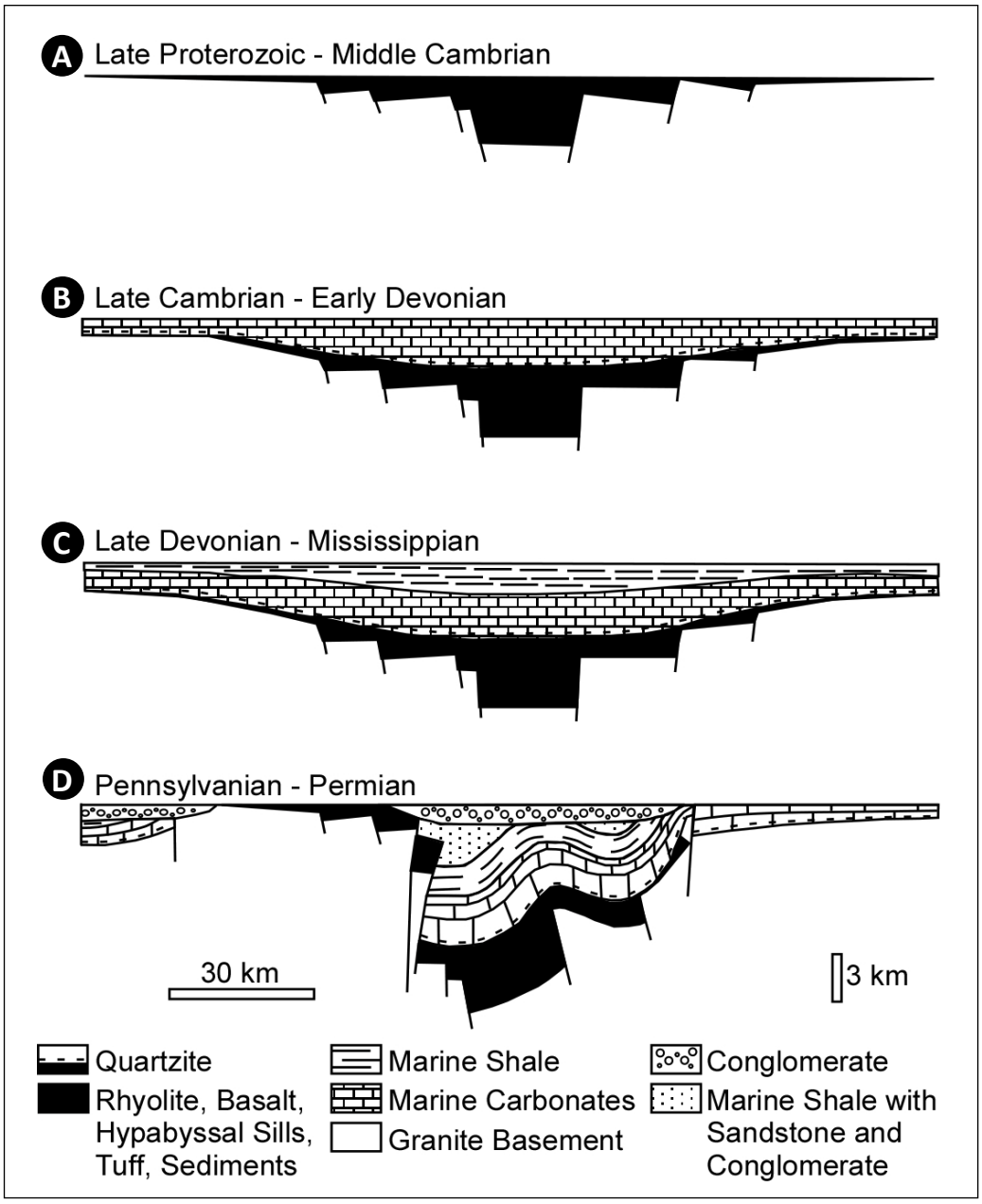

Figure 3. Tectonic evolution of the Southern Oklahoma Aulacogen. A) Middle Cambrian extension, characterized by normal faulting (rifting), and filling with volcanic deposits. B) Late Cambrian to Early Devonian subsidence and deposition of mostly limestones with minor sandstones and shales. C) Subsidence from the Late Devonian to Late Mississippian and deposition of organic-rich marine shales and minor sandstones and limestones. D) Folding and thrusting during Wichita and Arbuckle orogenies (from Hoffman et al., 1974).

1.3. Woodford Shale Stratigraphy

The Late Devonian-Early Mississippian Woodford Shale occurs in Oklahoma, Texas, Arkansas, Kansas and New Mexico (Conant and Swanson, 1961) under a variety of names. Its deposition is related to an extensive intra-cratonic sea, deeper to the southeast and shallower to the northwest (Figure 4) (Kirkland et al., 1992; Comer, 2005). This broad epicontinental sea covered much of North America's mid-continent region at that time (Figure 4), and along with near-equatorial latitudinal conditions favored the vigorous organic productivity and deposition of organic-rich fine-grained rocks (Kirkland et al., 1992; Algeo et al., 2007). Laterally equivalent units of the Woodford Shale are the Chattanooga, New Albany and Ohio Shale formations, which are also significant hydrocarbon source rocks and potential unconventional reservoirs.

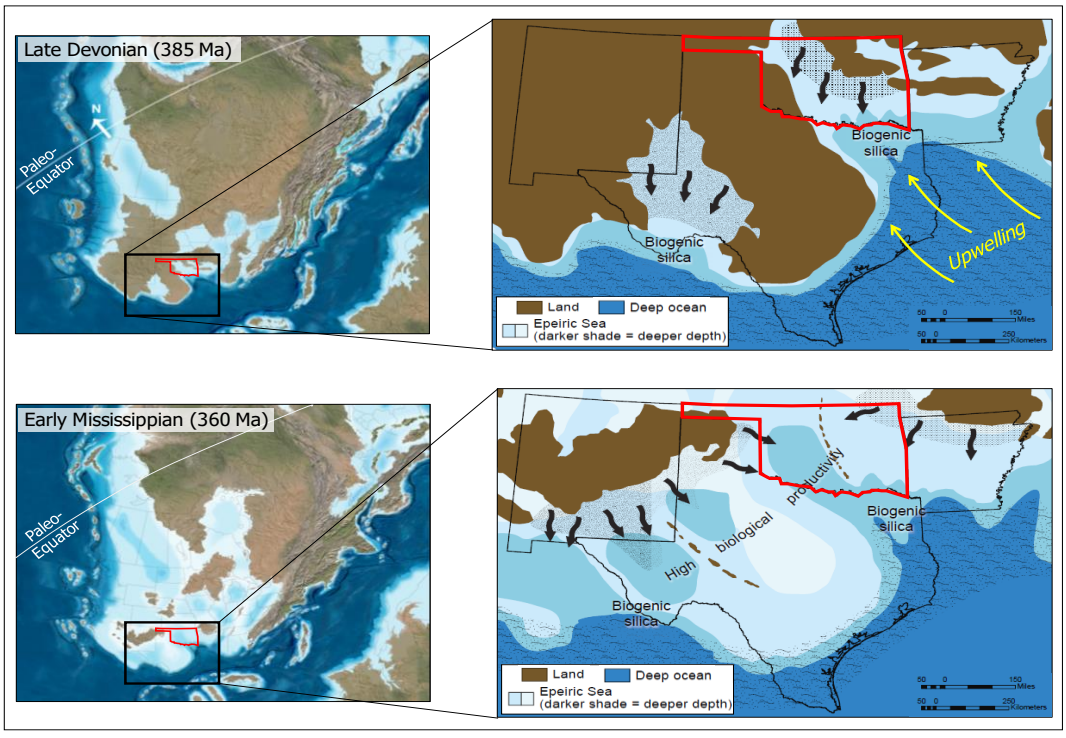

Figure 4. Regional paleogeography of North America's mid-continent region during the Late Devonian and Early Mississippian, showing the extensive epeiric sea covering most of the area of Oklahoma (modified from Comer, 2008).

In southern Oklahoma, where the Woodford Shale crops out, it ranges from about 230 to 400 ft. thick, and lies unconformably over the Silurian/Early Devonian Hunton Group and is conformably overlain by the Mississippian Sycamore Limestone (Figure 5) (Ham et al., 1973; Fay, 1989; Serna-Bernal, 2013; Fishman et al., 2013). Based on well-log signatures, palynomorphs, and geochemical proxies, the Woodford Shale comprises three informal members, upper, middle, and lower (Sullivan, 1985; Hester et al., 1990; Lambert, 1993; Miceli-Romero and Philp, 2012).

The upper Woodford is about 65-90 ft thick, and contains numerous cherty beds interbedded with fissile shale beds that contain variable amounts of clays (25-60%) and carbonate minerals (Fishman et al., 2013); phosphate nodules/concretions are common in this member. The organic richness (TOC>8wt.%) and the occurrence of phosphatic nodules and chert suggest that the upper Woodford member was deposited in relatively deep marine waters close to the oxygen minimum zone (Kirkland et al., 1992), and under dysoxic to suboxic conditions during a HST with high sedimentation rates (Miceli-Romero and Philp, 2012).

The middle Woodford is the most laterally extensive and thickest member, and is also the member that contains the most organic-rich strata (Lambert, 1993); it is approximately 70-120 ft thick, and is dominantly composed by black, fissile, clay-rich mudstones; this member has been interpreted as deposited under anoxic conditions, during a major transgressive event (Miceli-Romero and Philp, 2012).

The lower Woodford is about 52 ft thick. Its thickness is inversely proportional to the Hunton Group thickness suggesting paleo-topographic controls on the distribution of facies of this lower interval (Blackford, 2007; Slatt et al., 2012, McCullough, 2014); it

is predominantly clay-rich and fissile, with a few and scattered thin chert beds that increase in number towards the top of the member (Fishman et al., 2013).

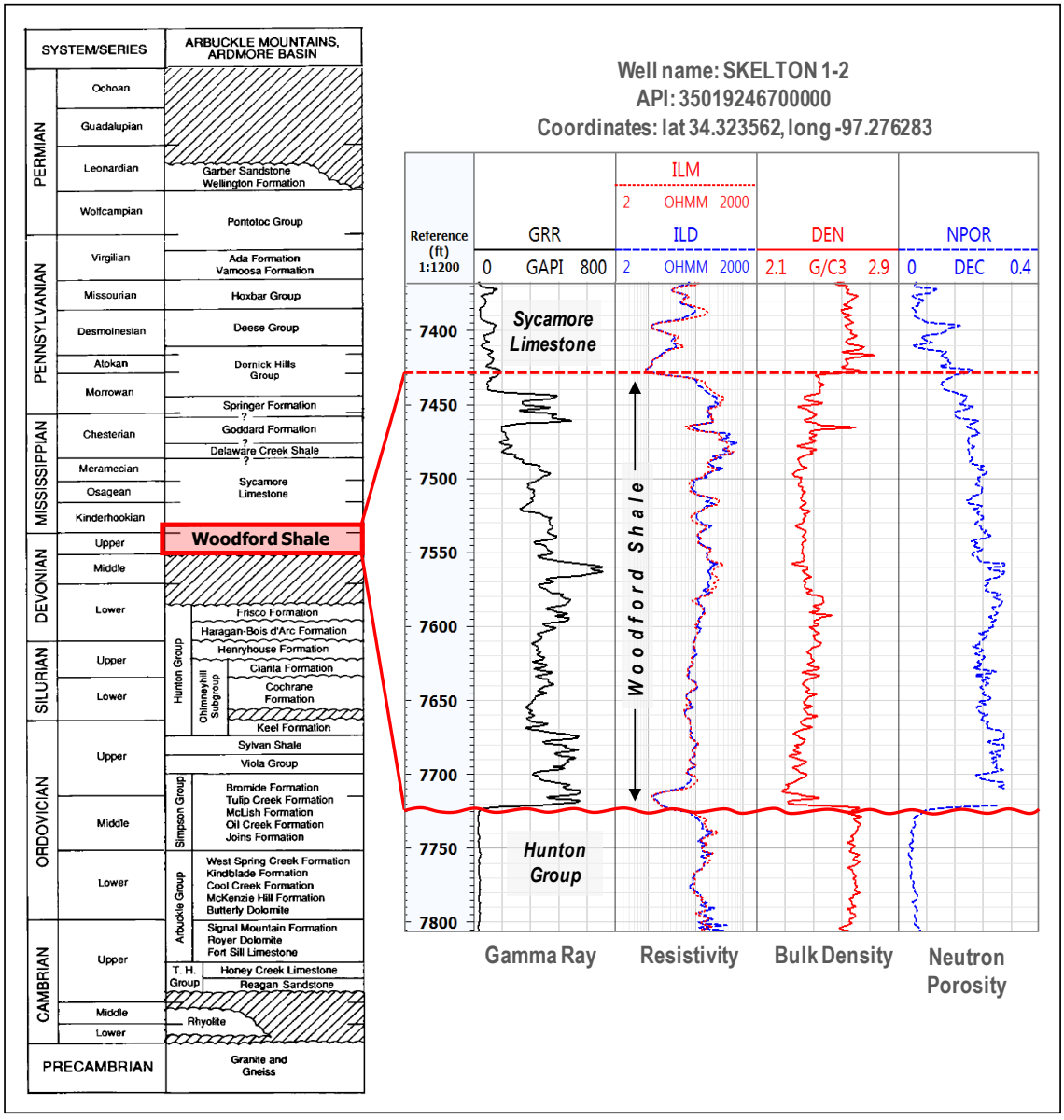

Figure 5. Left: Generalized stratigraphic chart of the Arbuckle Mountains and Ardmore Basin. The Woodford age interval is from the Late Devonian to Early Mississippian. (from Johnson and Cardott, 1992). Right: typical well log responses of the Woodford Shale in the Ardmore Basin. Well location is about 5 miles south of the Speake Ranch quarry (in Carter county).

2. METHODOLOGY

2.1. Field Methods

Field methods comprised section measurement, outcrop Gamma ray surveying, and rock sampling (Figure 6). First, the true stratigraphic thickness of the exposed succession was determined through the conventional method of using a Jacob's staff and compass. Structural control (strike/dip) was taken at 5-ft increments in order to avoid or account important structural deformation through the measured path. While measuring the section, trenches were dug and marker tabs were posted at one foot increments (Figure 6). Then, five radioactivity measurements were taken at every one foot using a hand-held scintillometer (Model RS-120 Super-SCINTTM), which yields values of natural radioactivity in 'counts per second' (cps). These measurements were then averaged into a mean value per foot so that it can be related with Gamma ray profiles of subsurface well logs.

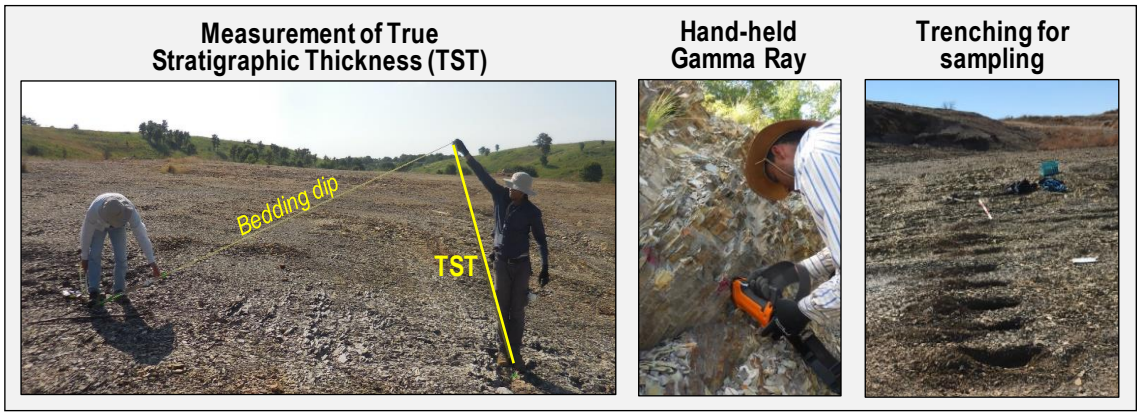

Figure 6. Field methods conducted in this study included measurement of true stratigraphic thickness, recording of gamma-ray readings each foot, and rock sampling in trenches on each foot.

At the bed scale the outcrop is rhythmically represented by two highly distinctive rock types (Figure 7). In order to keep a record of much of this field-scale heterogeneity, two hand-size samples were collected per foot, one 'hard' sample (indurated) and a 'soft' one (fissile). Additionally, in each foot, the average bed thickness per rock type was measured in order to estimate a soft-to-hard ratio, which basically relates the cumulative thickness of 'soft' beds over the cumulative thickness of 'hard' beds per foot (Figure 7). In this work, the systematic recording of bed thickness and the soft-to-hard ratio became very important because they reveal the degree of vertical anisotropy per unit foot. By combining such variables, multiple scenarios are illustrated to accommodate cycles of soft and hard beds (Figure 7). To illustrate, one foot (~30cm) may be made of 50% soft and 50% hard beds, however there might be several combinations in which the alternations of soft and hard beds are stacked to accommodate such 50/50; for example, that foot could have either two beds (each ~15 cm), four beds (each ~7.5 cm), six beds (each ~5cm) or eight beds (each ~3.75), and, all of them are accommodating the same 50/50 soft-to-hard ratio.

Similarly, Slatt and Abousleiman (2011) introduced the terminology of brittle-ductile couplets illustrating the applicability of this concept on the Woodford Shale fracability. Also, contributions of Laubach et al. (2009), Caldwell (2013), Ferril et al. (2014), and Breyer et al. (2016), emphasize the study of mechanical-stratigraphic relationships as important controls on fracture development and creation of connectivity within interlayered reservoirs, as is the case of other unconventional shale plays (Eagle Ford, Duvernay, Monterey, Niobrara, Wolfcamp, etc).

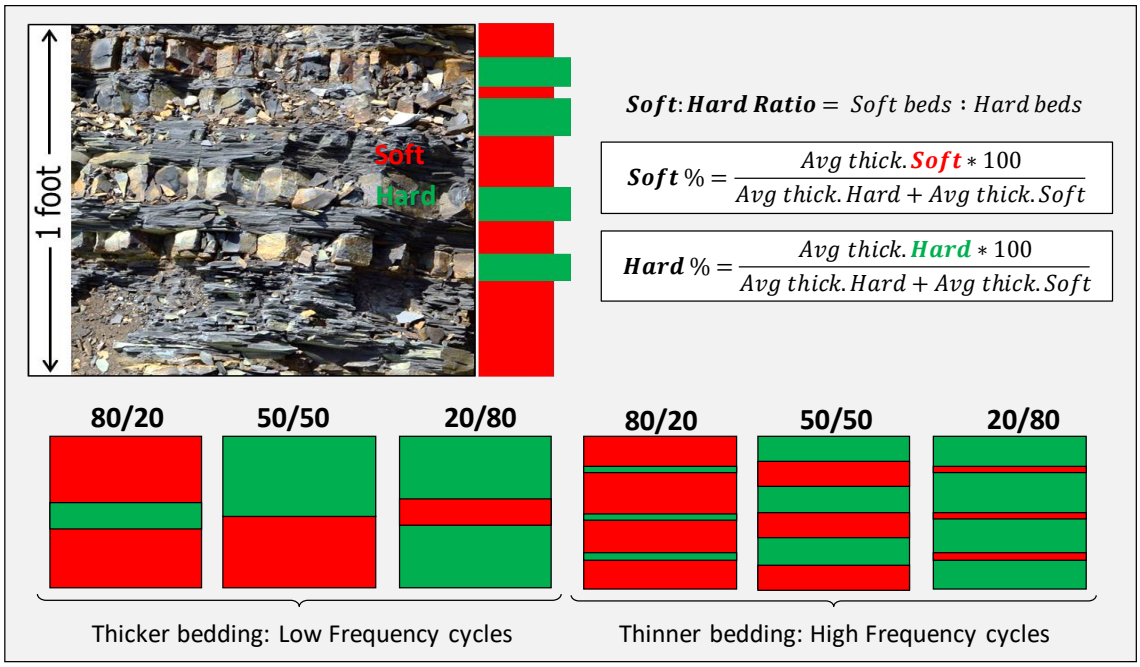

Figure 7. Typical cyclical heterogeneity between soft and hard beds. Soft beds are laminated and fissile, while hard beds are blocky with more vertical fractures. The soft-to-hard ratio is measured by extracting the average bed thickness per bed per unit foot. From this concept of the soft-to-hard ratio several scenarios can be recognized across the entire Woodford Shale. For example, high frequency cycles are made of thinner beds whereas low frequency cycles consist of thicker beds.

2.2. Lithofacies Classification

In mudrocks, at least 50% of its components are clay- and silt-sized (<62,5µm). Mudrocks make up the majority of the Woodford Shale lithofacies. Field observations clearly suggest that fissility of mudrocks is an effect of the degree of weathering. As one digs more into an outcrop, the mudrock parting responses usually grades from fissile, platy, slabby up to a blocky and sometimes non-fissile rock (Lewan, 1978). Thus, the extent to which we can use fissility as a descriptive attribute for outcrop samples is completely arguable as considered by Macquaker and Adams (2003), Milliken (2014), and Lazar et al. (2015). In spite of that, I believe that weathering responses of a mudrock

depend on its inherent texture and composition; it is quite intriguing to me how two adjacent beds that have been subjected to the same surficial conditions (i.e. rain, wind, snow, vegetation, etc.) appear today as highly contrasting 'soft' and 'hard' beds (Figure 7). Reasoning about that, and following terminology in Ingram (1953), Potter et al. (2005) and O'Brien and Slatt (1990), It is appropriate for the Woodford Shale strata to use a nomenclature that primarily distinguishes fissile (soft) from non-fissile mudrocks (hard) (Figure 8), and referring non-fissile rocks as mudstones and fissile rocks as shales. Following the field-based distinction between soft and hard beds, further in this thesis, results from organic contents, elemental and mineralogical composition, and mechanical properties corroborate their distinctive character across the complete Woodford Shale section

'Soft' mudrocks are fissile in outcrops, represented by sheet-like broken pieces and numerous bed-parallel planes of weakness (Figure 8). According to Ingram (1953) and Potter et al. (2005), thinner parting responses are related to higher amounts of phyllosilicate minerals in the rock. Similarly, it is suggested that thicker parting responses are related to either less argillaceous minerals or more siliceous/calcareous components within the rock. Varieties of these 'soft' mudrocks within the Woodford Shale include shales and claystones (Figure 8).

'Hard' mudrocks, on the other hand, are well indurated (non-fissile and blocky) in outcrops, with no or a few evident bed-parallel planes of weakness (Figure 8). Reaction to HCl acid defines two categories of 'Hard' mudrocks, the calcareous and non-calcareous. In the 'hard' non-calcareous mudrocks, their physical appearance helps to differentiate between mudstones and cherts, the latter defined for presenting the typical

conchoidal fracture and waxy luster on fresh surfaces. In the 'hard' calcareous category, the vigor of the HCl reaction and degree of crystallinity helped us to differentiate between crystalline dolomites and micritic limestones (Figure 8).

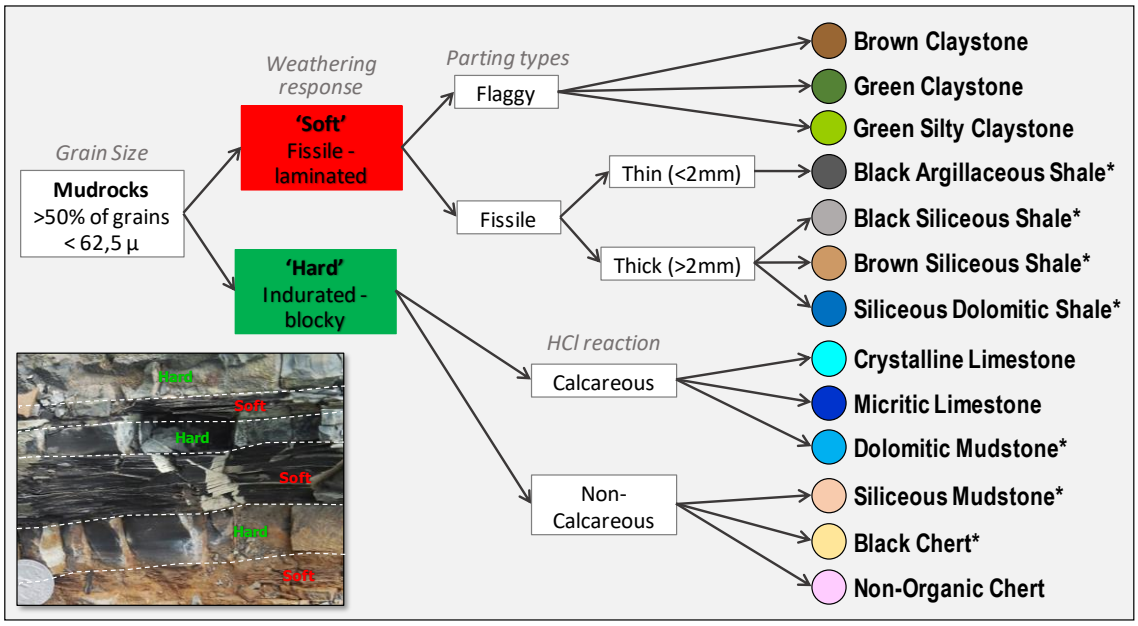

Figure 8. Field-based lithofacies classification of Woodford Shale mudrocks. The first criterion distinguishes between hard and soft beds based on weathering responses, then textural and compositional descriptors are added based on parting responses and HCl reaction. Thirteen lithofacies were recognized throughout the section. However, seven lithofacies were determined as the most dominant in the Woodford Shale interval (denoted with asterisks) after refining using XRD, XRF, Petrography and SEM.

To name lithofacies, we propose a terminology that consists of a primary root name (based on fissility), that then is preceded by field-based adjectives such as silty, sandy, crystalline, bioturbated, green, brown, black, etc. Later, using petrographic techniques and mineralogical results, names of lithofacies are refined using guidelines in Lazar et al. (2015), from which other preceding adjectives are added such as siliceous, argillaceous, dolomitic, micritic, glauconitic, etc. At the end, the name of a rock within

our classification scheme is honoring fundamental characteristics such as structure, texture and composition. In general, seven dominant lithofacies are identified within the Woodford Shale of this outcrop (Figure 9): i) Argillaceous Shale, ii) Siliceous Shale, iii) Brown Siliceous Shale, iv) Siliceous Mudstone, v) Chert, vi) Siliceous-Dolomitic Shale, and vii) Dolomitic Mudstone.

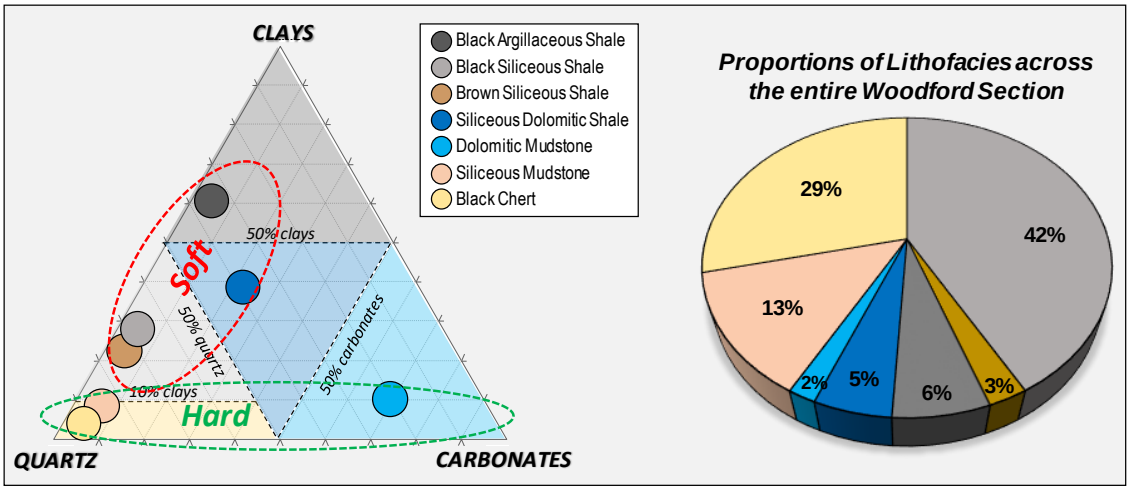

Figure 9. Seven most dominant lithofacies across the entire Woodford Shale interval. Left: ternary plot showing the relative proportions of clays, quartz and carbonates per lithofacies. Right: pie chart showing the relative abundance of each lithofacies across the Woodford Shale. Siliceous shales, cherts and siliceous mudstones are the most abundant lithofacies, making up more than 80% of the entire lithological record.

Further, the classification scheme was refined using bulk mineralogical results, from which we proposed a ternary diagram tailored for Woodford Shale samples (Figure 9). Minimum thresholds for defining a lithofacies are set at 50% for each principal component. Argillaceous Shales are made of at least 50% clay minerals, dolomitic mudstones are made of at least 50% dolomite, and siliceous mudstones and cherts are made of at least 50% quartz (Figure 9). An important observation in the case of the

quartz-rich lithofacies (quartz >50%) is that rocks with at least ~15% clays appear fissile in outcrops, as is the case of some siliceous shales made of admixtures of quartz (85%) and clays (15%) in which their physical appearance is of a fissile rock. This idea of fissility under low clay contents fall in agreement with Spears (1976) and Curtis et al. (1980), who not only tested the role of clay abundance in fissility, but also included other controls such as type of clay minerals, degree of crystallinity, mineral segregation, and organic content. Thus, it should not be a surprise that there are fissile rocks within the Woodford Shale with clay contents as low as 15%. Finally, the more mixed lithofacies corresponds with the Siliceous-Dolomitic Shale, which is made of about equal admixtures of quartz and clays, along with dolomite greater than 10% (Figure 9).

2.3. Laboratory Methods

Across the entire 350 ft of exposed section, over 550 samples were collected, from which X-Ray Fluorescence (XRF) and hardness tests were performed. Then, guided by the variability observed in the results obtained from the former techniques, representative subsamples were chosen to cover the complete spectrum of rock types. In total 136 subsamples were selected for TOC-Leco and Rock-Eval, 40 subsamples for petrography and X-Ray diffraction (XRD), and 9 subsamples for Scanning Electron Microscopy (SEM). In addition, 42 plugs were retrieved from the largest pieces of samples, of which six were used for uniaxial compressive strength (UCS) tests. Figure 10 summarizes the actual stratigraphic location of samples and the type of analyses conducted in this study.

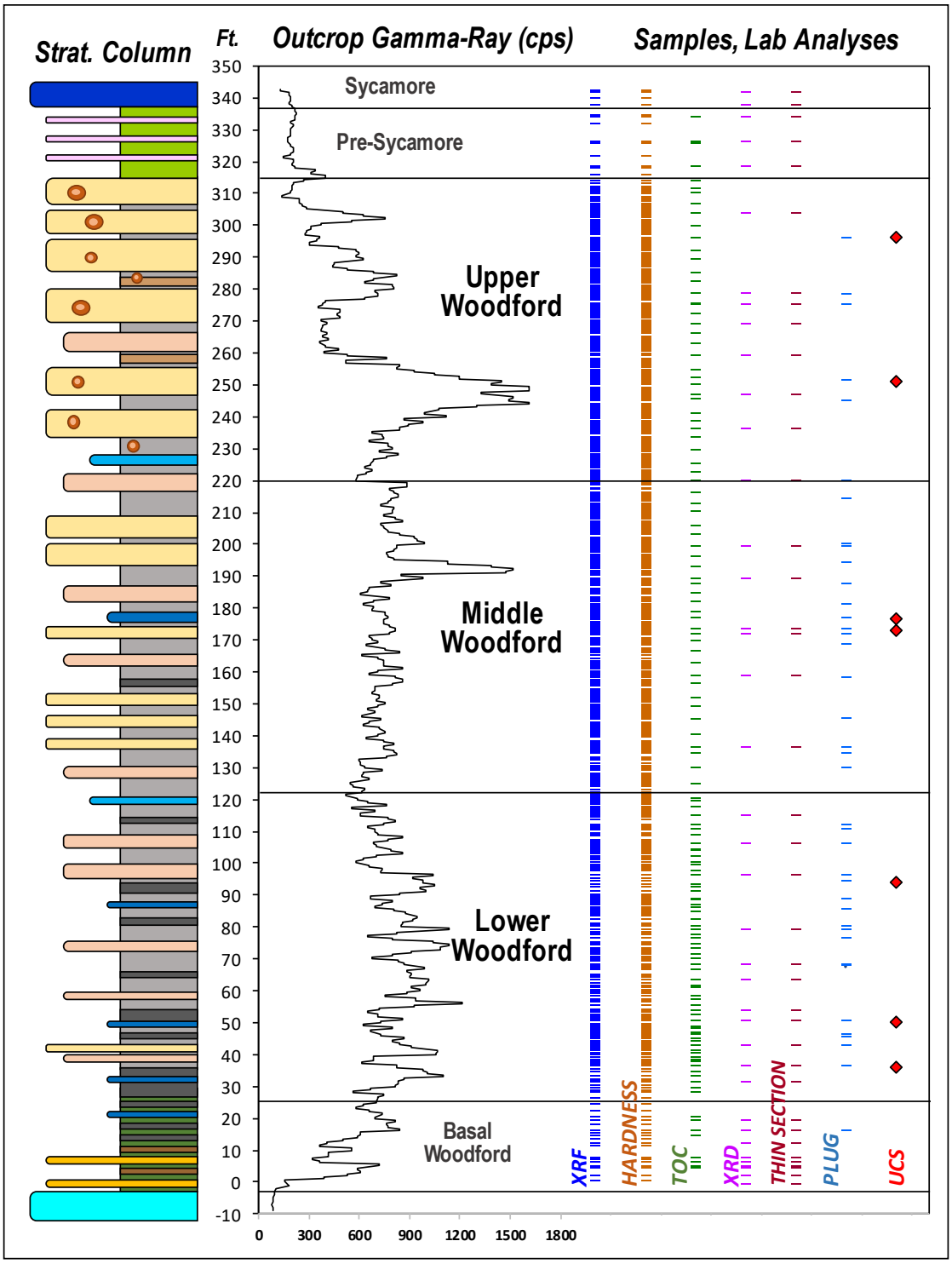

Figure 10. Location and distribution of samples across the entire Woodford Shale section. Notice the high resolution of sampling for most of the techniques conducted in this study. XRF and hardness guided the subsampling for TOC, XRD, and thin sections.

2.3.1. X-Ray Fluorescence (Elemental Chemostratigraphy)

The principle of this non-destructive technique uses the energy emitted by photons that resulted from the interaction of incident X-rays and atoms characteristic to specific elements in each sample. The spectrum of wavelengths from the energy release as well as their intensities are recorded by an XRF spectrometer that detects and counts proportions of some major and trace elements present in the sample.

To conduct XRF analyses, fresher and flattened surfaces were first obtained in all samples using a rock saw, then each sample was scanned for major elements under vacuum at 15 kV, 35 mA for 90 seconds. Then, at the same point, samples are scanned for trace elements with a Ti-Al filter at 40 kV, 17.1 mA for 60 seconds. The XRF spectrometer used in this study was a hand-held Tracer IV–SDTM manufactured by Bruker Co. Collected data was processed using as a reference the calibrations for mudrocks in Rowe et al. (2012), from which concentration of 30 elements are calculated in parts per million (ppm).

Recent contributions from Sageman and Lyons (2004), Algeo et al. (2007), Rowe et al. (2009), and Algeo and Rowe (2012), demonstrated the use of selected elements that are regarded as highly sensitive to changes in sediment sources, water chemistry and rock composition. Thus, out of the 30 calculated elements, about 15 were utilized for interpretations including: Silicon (Si), Titanium (Ti), Zirconium (Zr), Aluminum (Al), Potassium (K), Thorium (Th), Calcium (Ca), Strontium (Sr), Magnesium (Mg), Manganese (Mn), Vanadium (V), Molybdenum (Mo), Uranium (U), Sulfur (S), and Phosphorous (P). Table 1 summarizes the main elements along with their significance and/or main uses for chemostratigraphic interpretations.

Element	Proxy - Significance
Titanium (Ti)	Continental source and dust input
Zirconium (Zr)	Continental source
Silicon/Aluminum (Si/Al)	Quartz origin (biogenic or detrital)
Aluminum (Al)	Clay contents and feldspar
Potassium (K)	Clay contents and feldspar
Thorium (Th)	Clay contents and feldspar
Calcium (Ca)	Carbonate source and phosphates
Strontium (Sr)	Carbonate source and phosphates
Magnesium (Mg)	Carbonates, dolomitization
Manganese (Mn)	Carbonates, dolomitization
Uranium (U)	Organic matter richness, ?bitumen
Vanadium (V)	Bottom water anoxia, redox sensitive
Molybdenum (Mo)	Bottom water euxinia, redox sensitive
Sulfur (S)	Pyrite, reducing conditions, euxinia
Phosphorous (P)	Phosphate accumulation

Table 1. Summary of main elements and their significance in chemostratigraphic interpretations. The significance of each element/proxy comes from multiple references and is compiled in Turner (2016). (Bhatia and Crook, 1986; Pearce and Jarvis, 1992; Calvert and Pedersen, 1993; Pearce et al., 1999; Sageman and Lyons, 2004; Brumsack, 2006; Algeo and Lyons, 2006; Tribovillard et al., 2006; Algeo and Rowe, 2012)

2.3.2. X-Ray Diffraction (Bulk Rock Mineralogy)

The principle of this analytical technique uses the scattered energy that results from the interaction of electromagnetic waves (x-rays) with planes of atoms in crystals; basically, the resultant scattered light naturally causes many wave interferences that may be in phase (constructive interference) or out of phase (destructive interference) (Moore and Reynolds, 1997; Amonette, 2002). By relating the spacing of atomic planes and wavelengths of scattered x-rays, a diffractometer is capable of recording the intensities

of peaks of such constructive interference, known as diffraction peaks, and are regarded as diagnostic of specific mineral phases.

In this work, 42 randomly oriented powdered samples were prepared following standardized procedures described in Moore and Reynolds (1997) and summarized in the Laboratory Manual by Madden (2011). Per sample, 2 grams of crushed rock were pulverized to micron-sized powder, dried, and mounted on glass holders. Diffraction patterns were collected using a Rigaku Ultima IVTM diffractometer with Bragg-Brentano beam geometry and CuKα X-ray source. Scanning was performed from 2° to 70° 2θ with 0.02° steps and a count time of 2 seconds per step. Diffraction patterns were then interpreted using MDI Jade 2010 software where a statistical fitting between the calculated pattern and a mineral database was conducted. The identification of mineral phases was based on the position (2-theta) and d-spacing (Å) of individual diagnostic peaks according to Moore and Reynolds (1997), and their semi-quantification based on the intensities of peaks (counts).

Within the analyzed Woodford Shale samples (Figure 11), quartz clearly revealed its strongest intensities at 4.27Å and 3.35Å. For clay minerals, illite/mica was identified by strong reflections at 10.06Å, 4.49Å and 2.57Å (Figure 11); kaolinite with its peaks at 7.20Å, 3.58Å and 1.98Å. And finally, carbonate minerals such as dolomite and ankerite were identified by peaks at 2.89Å, 2.19Å and 1.78Å. Thus, based on the qualitative analysis of XRD patterns, quartz, illite/mica, kaolinite, and dolomite/ankerite are the main mineral phases identified within the Woodford Shale samples (Figure 11).

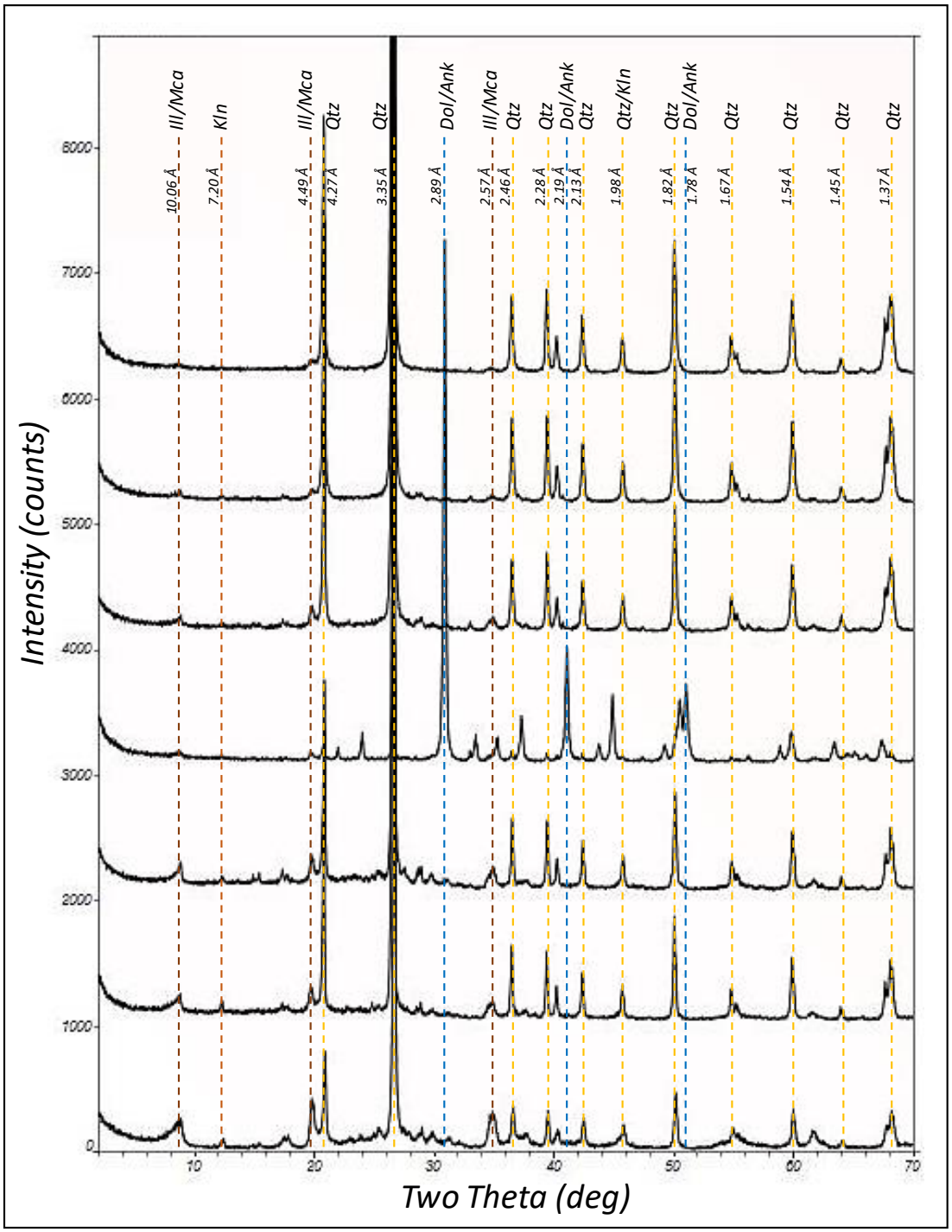

Figure 11. XRD patterns of seven selected samples from bulk-rock analysis. Vertical dashed lines indicate the peak position (2Θ) and standard d-spacing values for the main mineral phases identified within the Woodford Shale samples (Qtz: quartz; Ill/Mca: illite/Mica; Kln: kaolinite; Dol/Ank: dolomite/ankerite).

2.3.3. Rock-Eval Pyrolysis and Leco-TOC

For hydrocarbon source rock characterization, parameters obtained from Rock-Eval pyrolysis and Leco-TOC techniques persist as the main screening variables for the evaluation of source rock quality and organic richness. In this work, total organic carbon (TOC) from 136 samples was measured using a LECO carbon analyzer and, coupled with programmed pyrolysis analyses (Rock-Eval), values of S1, S2, S3, Tmax, HI, and OI were obtained per sample. Table 2 lists the main geochemical parameters obtained in this study through analyses of Rock-Eval pyrolysis and Leco-TOC.

Parameter	**Definition**	**Units**
TOC	Total Organic Carbon (from kerogen + bitumen)	Wt.%
S1	Free volatile hydrocarbons thermally released under 300°C (free oil/gas content)	mg HC/g rock
S2	Hydrocarbons generated during thermal cracking 300ºC to 550ºC (remaining potential)	mg HC/g rock
S3	Organic carbon dioxide generated during the S2 pyrolysis (indicator of kerogen oxidation)	mg CO2/g rock
Tmax	Temperature of maximum S2 generation, (indicator of thermal maturity)	°C
HI	Hydrogen Index = S2 x 100/TOC, used for kerogen type indicator (Van Krevelen plot)	mg HC/g TOC
OI	Oxygen Index = S3 x 100/TOC, used for kerogen type indicator (Van Krevelen plot)	mg HC/g TOC
S1/TOC	Normalized Oil Content = S1 x 100/TOC, indicator of oil saturation (producible oil)	

Table 2. Main parameters and definitions of the obtained variables from Rock-Eval pyrolysis and Leco-TOC. Compiled from Tissot and Welte (1984), Peters and Cassa (1994), and Jarvie et al., (2007).

3.2.4. Petrographic Analysis

Petrographic analysis of standard thin sections provided visual evidence about the various inorganic and organic constituents determined by XRF, XRD and TOC. Also, examination of the microfabrics allowed us to qualitatively assess reservoir quality through observations of cements and pore architecture. In this study, a total of 40 standard thin sections were analyzed using a Zeiss AxioImager Z1TM petrographic microscope. For supporting some petrographic observations of the microfabric, Scanning Electron Microscopy (SEM) analyses were conducted in 9 representative samples, covering the entire spectrum of lithofacies. Fresh broken surfaces were obtained following methodologies for SEM samples preparation in O'Brien and Slatt (1990). The equipment used for SEM analyses was a FEI Quantum 250 SEM with a coupled Bruker Electron Dispersive Spectrometer (EDS).

3.2.5. Rock Hardness (Micro-rebound Hammer)

In shales, obtaining experimentally-derived geomechanical parameters usually is a major problem. First, well cores are expensive to acquire, second, samples must meet specific dimensions (2:1 length-to-diameter) that are very difficult to achieve due to 'disking' while drilling with the coring bit (for plugs), and third, geomechanical tests such as uniaxial or triaxial are destructive and sometimes expensive lab techniques. Thus, cheaper and quicker-to-perform alternatives, like hand-held tools, have recently proved reliability to deriving mechanical properties of rocks; as is the case of the micro-rebound hammer that nowadays appears as the most widely used hardness tester for mudrock samples.

For this work, on the same sample surfaces scanned for XRF, hardness tests were collected by Becerra-Rondon (2017) using the Equotip Piccolo 2 hardness tester manufactured by Proceq S.A. This is a portable (pocket-size), battery-operated and non-destructive measuring tool (Figure 12). Essentially inside this tool, a hardness value (LH units) is obtained by comparing the rebound and impact velocities (Vr/Vi) of a spring-loaded body with a 3-mm tungsten ball tip (Figure 12); since ductile materials absorb more energy than brittle ones during an impact, with this technique it is expected faster rebound velocities translated into higher hardness values for 'Hard' samples, and conversely slower rebound velocities and lower hardness values for 'Soft' samples (Figure 12).

A total of 10 rebound experiments were performed on each sample, and their readings were computed into a mean HLD value per sample. Aoki and Matsukura (2008), Zahm and Enderlin (2010), and Lee et al. (2015) have demonstrated the reliability of converting LH values of mudrocks into Unconfined Compressive Strength (UCS) and other mechanical properties. Becerra-Rondon (2017) conducted Uniaxial Compressive Strength lab tests using Woodford samples from the Speake Ranch outcrop, incorporating previous publications, she also developed an empirical equation for transforming LH values into UCS (in Mpa), thus allowing for the Woodford shale samples to relate outcrop-based hardness with more meaningful mechanical properties as is the UCS.

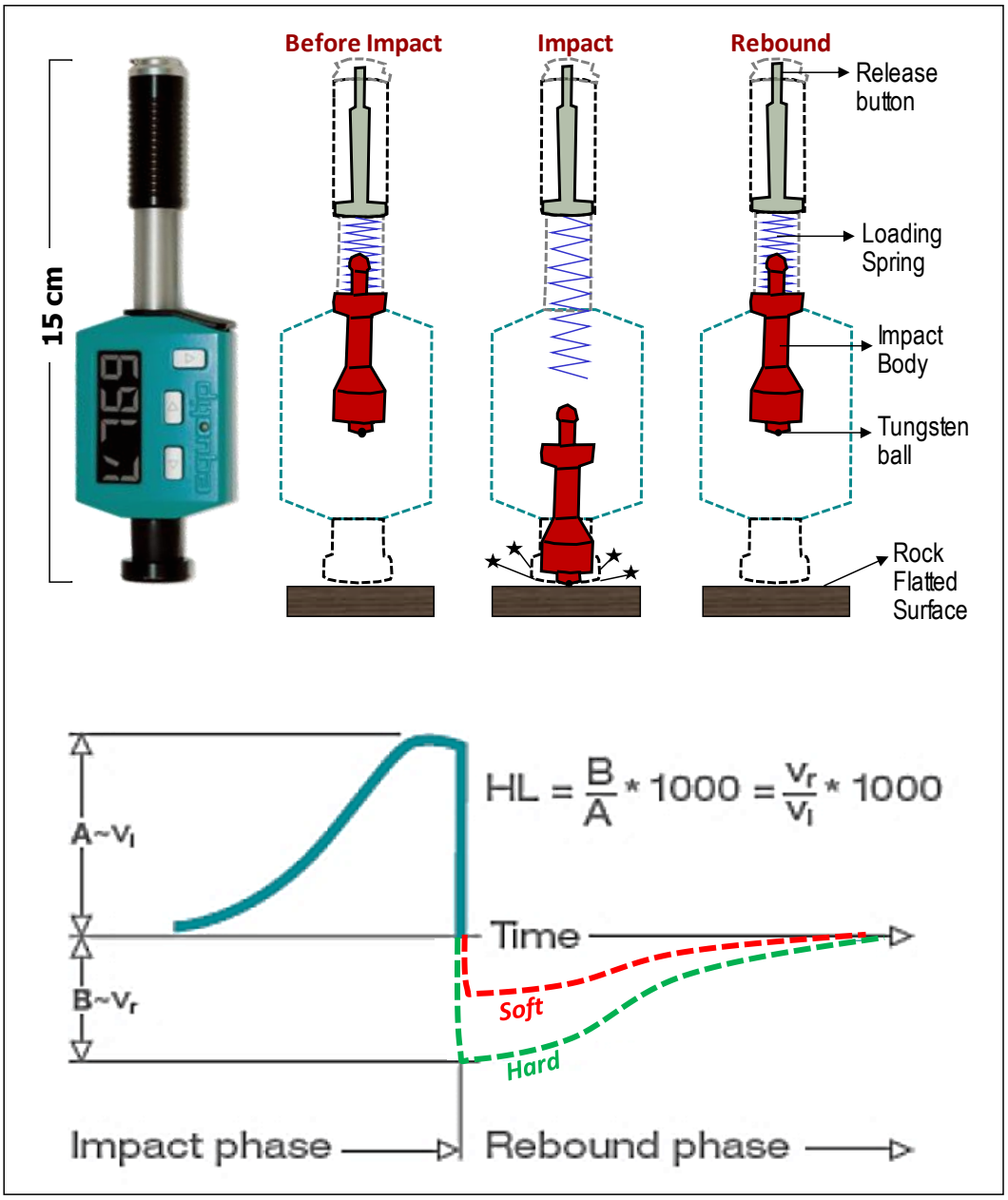

Figure 12. Micro-rebound hardness tester Equotip Piccolo 2. The tester is positioned perpendicular to the rock surface, then a spring-loaded impact body collide against the sample surface with an impact energy of 11 N-mm. The principle of rock hardness measurement uses the ratio between the rebound and impact velocities. During the rebound phase, a softer material is represented by slower rebound velocities, whereas a harder material will present faster rebound velocities translated into higher hardness values. Modified from Becerra-Rondon (2017).

2.4. Sequence Stratigraphy

Concepts and principles of modern sequence stratigraphy largely evolved from seismic stratigraphy at a time when unconventional shales were not the main resource play of interest (early in the 90's). Besides that, organic-rich shales have been largely regarded as black thin successions of few hundreds of meters lacking obvious vertical variations. Despite that, recent studies have demonstrated that the Woodford Shale, as many other unconventional shale successions, appears to show at a variety of scales, that relative sea level has risen and fallen in a cyclical manner, and because of this, general concepts of sequence stratigraphy are applicable to organic-rich shales that are deposited in a cyclical, predictable manner (Slatt and Rodriguez, 2012; Slatt, 2013a)

Thus, adopting concepts and models of sequence stratigraphy for unconventional resource shales in Slatt (2013a). First, based upon gamma ray responses we identified high-frequency stratigraphic cycles called Gamma Ray Parasequences (GRP). In this work, regardless of any temporal frame associated with each individual cycle/parasequence, the stratigraphic record of the Woodford Shale outcrop was subdivided into a series of 4th or possibly 5th order GRP's, which can be of three main types 1) Increasing-upward, 2) Decreasing-upward, and 3) Blocky (no-change upward). Then, a key feature for defining small scale stratigraphic cycles was the interpretation of turnaround points between stacked GRP's. In particular, regressive surfaces (rs) were identified where progradational trends change to retrogradational trends, and flooding surfaces (fs) identified where retrogradational trends change to progradational trends (Figure 13).

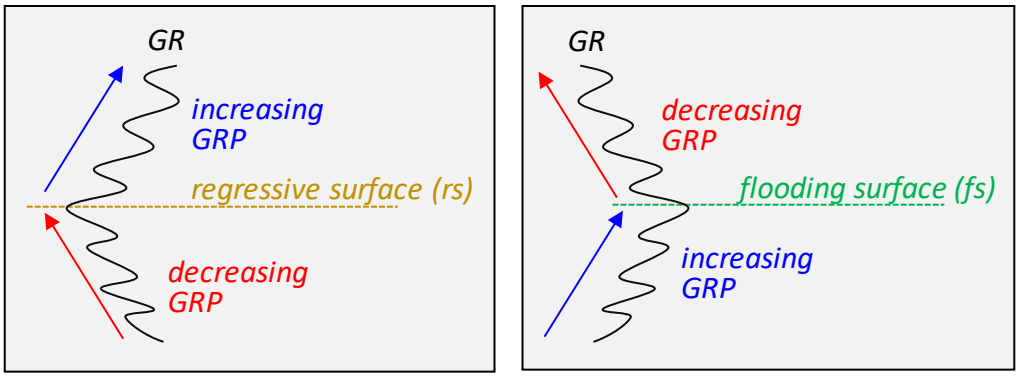

Figure 13. Schematic criteria for interpreting high-frequency cycles and their bounding surfaces based on Gamma ray parasequences (GRP). Regressive surfaces (rs) correspond with the turnaround point where stacked upward-decreasing GRP change to upward-increasing GRP. Flooding surfaces (fs) correspond with the turnaround point where stacked upward-increasing GRP change to upward-decreasing GRP.

Once the high-frequency GRP's and cycles were identified, these formed the building blocks for interpreting depositional sequences. Generally, in the Woodford Shale of this study smaller cycles (<50 ft. thick) build up bigger cycles and add detail to the large-scale features comprised within second-order systems tracts (>100 ft. thick) of depositional sequences. In this study, Gamma ray cycles/trends operate on a variety of scales, from a few feet to a few hundred feet, resulting in some intervals difficult to determine the right scale for individual GRP cycles. In some cases, surfaces (rs and/or mf) were too close together (of only few feet), or very high frequency cycles may be contained within a thicker, but systematic trend of increasing- or decreasing- gamma ray response. For that reason in this study there may be present more small scale regressive and flooding surfaces than were identified by Gamma ray responses.

A potential complication of interpreting surfaces and GRP's at very high resolutions, is that some geological features can be easily misinterpreted where facies and

their resultant gamma ray responses are the product of auto-cyclic controls, and anomalous paleoenvironmental conditions can be superimposed on larger changes of the relative sea level; for example in marine settings as was the Woodford Shale, especially where pelagic input is important small-scale GR trends can suggest progradation (with increase in biogenic silica) when they actually can record a deepening and decline of terrigenous supply. For such a reason individual GRP's were rather stacked and correlated with rock attributes such as lithofacies, bioturbation, mineralogy, elemental proxies and organic richness. Thus, allowing us to establish a long-term stratigraphic framework interpreted as second and third order sequences with superimposed fourth order GRP cycles.

Essentially, the interpretation of long-term sequences, consisted on identifying stratigraphic surfaces regarded for being laterally more continuous, as Maximum Flooding Surfaces (MFS) and Sequence Boundaries (SB). In between two SB's a relative sea level (RSL) cycle is recorded (Figure 14), that begins with a drop in the sea level to form the basal SB, then marine transgression occur up to a FS/MFS to form the Transgressive Systems Tract (TST), which usually within the Woodford Shale becomes more clay- and organic-rich upward; then a reduction in the rate of relative sea level rise forms the progradational Highstand System Tract (HST) (Figure 14), which within the Woodford Shale is often richer in biogenic quartz, less clay- organic-rich upward and grading up to the more bioturbated lithofacies towards the late stages of a HST.

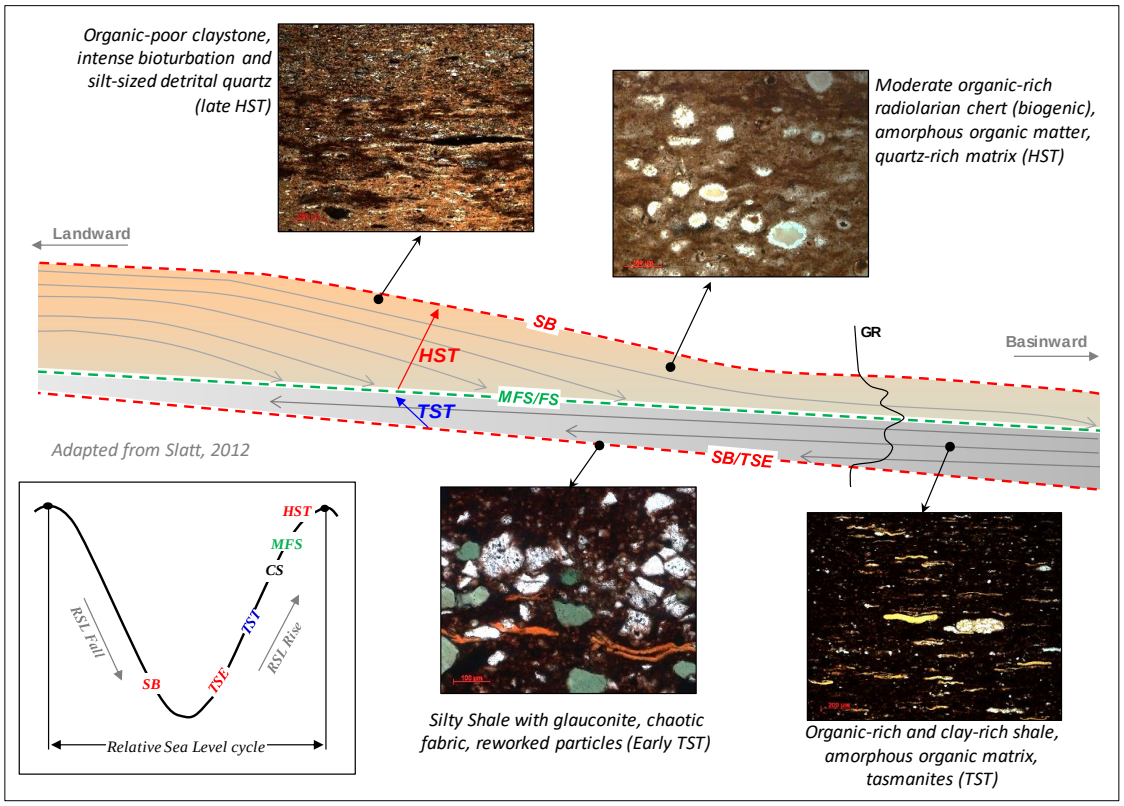

Figure 14. Generalized 2nd order sequence stratigraphic model applied in this work. Gamma ray log response typically increases upward within the TST, and cleans-upward during the HST. Representative thin sections from each part of the sequence stratigraphic model suggest an upward increase in clays and organic content up to the MFS, then in the progradational HST, detritus, burrowing and biogenic quartz dominates upward. Note: internal GRP's are not depicted in this generalized model, and small-scale features presented in this figure are not necessarily exclusive of a system tract of such 2nd order stratigraphic hierarchy (After Slatt and Rodriguez, 2012).

Finally, since outcrop observations and results of this work preserve all the direct evidence of rock attributes, the interpreted outcrop sequence stratigraphic framework constituted the model for correlating and interpreting sequences and GRP's in the subsurface of the Ardmore Basin (Figure 15). The correlation of outcrop sequences and GRP's to wireline log signatures allowed us the prediction of reservoir properties away from the outcrop.

Figure 15. Wells used in this study for stratigraphic correlations and to tie the Speake Ranch outcrop with the subsurface of the Ardmore Basin. Left vertical plot: Gamma ray motifs from 9 different wells displays the great similarity of GR responses between them. Average penetrated vertical thickness by wells varies from 290 to 400 ft. Right map: location of wells outlining the NW-SE section (yellow dashed line). All 9 wells were selected for being the closest vertical ones to the Speake Ranch outcrop

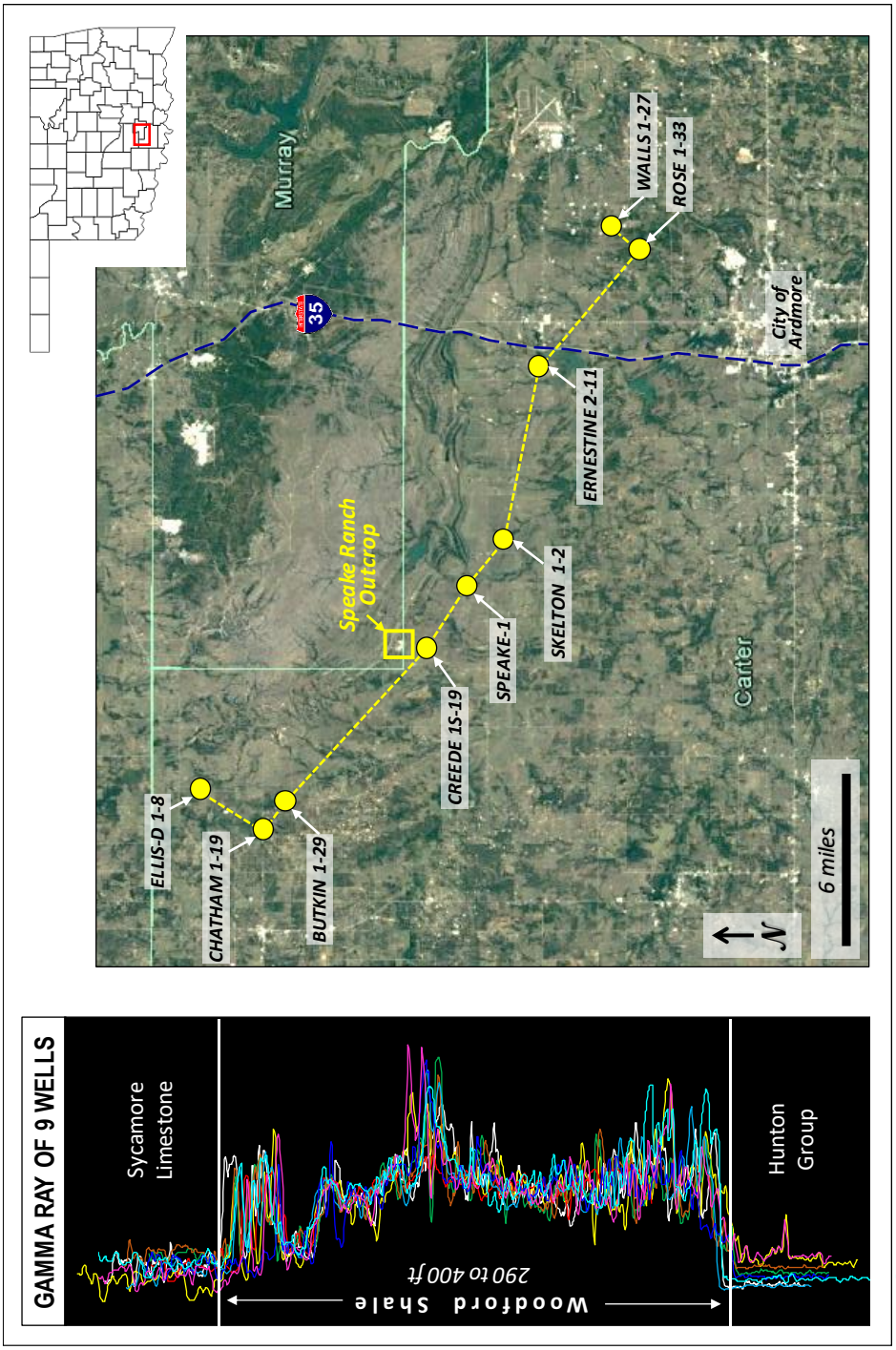
GAMMA RAY OF 9 WELLS
Sycamore Limestone
Woodford Shale
290 to 400 ft
Hunton Group
Murray
Carter
City of Ardmore
35
Speake Ranch Outcrop
ELLIS-D 1-8
CHATHAM 1-19
BUTKIN 1-29
CREEDE 1S-19
SPEAKE-1
SKELTON 1-2
ERNESTINE 2-11
WALLS 1-27
ROSE 1-33
N
6 miles

3. OUTCROP CHARACTERISTICS

From the very early outcrop descriptions in Taff (1902), Cooper (1932), Urban (1960), Ham et al. (1973), Comer and Hinch (1987), Fay (1989), Over (1992), and Kirkland et al. (1992), the stratigraphic knowledge of the Woodford Shale in south-central Oklahoma remains incomplete with regards to its bounding contacts, thickness, lithology, and depositional environments. In this work, taking advantage of the well-preserved and complete Woodford Shale exposure at the Speake Ranch Section (Figure 1), first, we describe field-based characteristics, such as formational contacts and lithofacies. Then, results for each analytical technique are presented in terms of the stratigraphic subdivision as well as their corresponding rock types and lithofacies.

3.1. Woodford Shale Formational Contacts

In south-central Oklahoma, the Woodford Shale sits stratigraphically in between two prominent resistant carbonate units, the underlying Hunton Group (Late Ordovician-Early Devonian) and the overlying Sycamore Formation (Early Mississippian). Regionally along outcrops in the Arbuckle Mountains, the typical Woodford Shale geomorphological response is of an easy-to-weather, fissile and shale-rich unit that erodes into valleys and ridges. According to published references, the Woodford Shale thickness is from 350 to 400 feet (Ham et al., 1973; Fay, 1989).

Similarly, at the Speake Ranch outcrop of this study, the Woodford Shale is bounded at its base by a highly resistant crystalline limestone of the Hunton Group, and at its top by another resistant limestone lithologically equivalent to Pre-Sycamore deposits (similar to a Welden Limestone?) (Figure 16). The true stratigraphic thickness

of the Woodford Shale at the Speake Ranch outcrop is about 335 feet, and was measured from the uppermost limestone of the Hunton Group to the lowermost limestone of the Sycamore Formation.

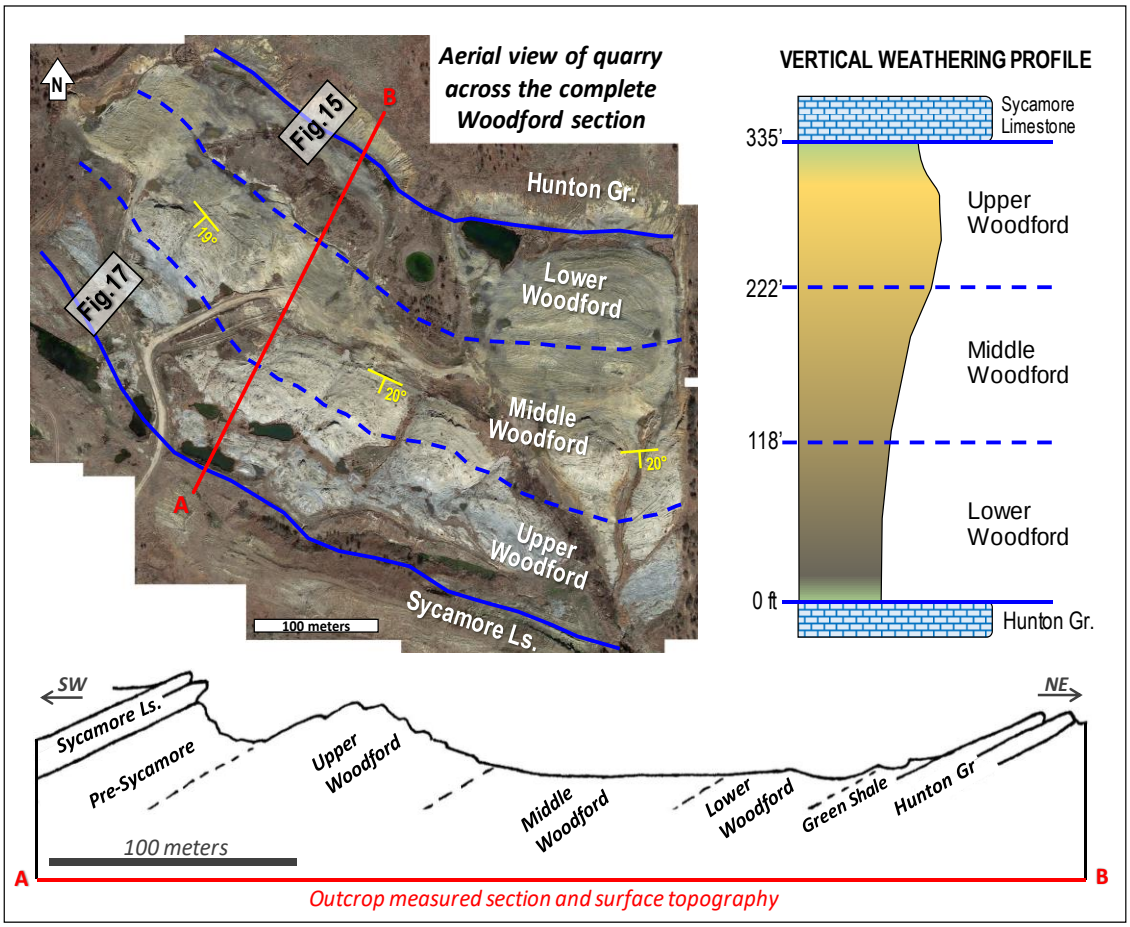

Figure 16. Typical weathering response of the Woodford Shale of south-central Oklahoma. Upper left: aerial view of Speake Ranch outcrop quarry outlining the Woodford formational contacts with its underlying Hunton Group and overlying Pre-Sycamore limestone. Upper right and lower: schematic weathering profiles highlighting large-scale variations in the resistance of the Woodford Shale strata; the lower Woodford and middle Woodford members are less resistant when compared with the upper Woodford member, which is more competent and usually develops ridges on outcrops. Both the basal-most and the upper-most portions of the Woodford are represented in outcrops by softer intervals that consists of greenish shales and usually develops ponded topographical reliefs.

3.1.1. Basal Contact: Hunton Group – Woodford Shale

Depositional models overall suggest a major regional unconformity between the Hunton Group and its overlaying Woodford Shale (Ham et al., 1973; Amsden and Klapper, 1972; Amsden, 1975). Distribution of thicknesses of these two units indicate an inverse relationship where the Woodford Shale attains its greater thickness at approximate thinner areas of its underlying Hunton Group (Hester et al., 1990; Blackford, 2007; McCullough, 2014). Moreover, there is seismic evidence of karsting features and incised valleys throughout this unconformity, which suggests a paleo-topographic control on the deposition and distribution of lithofacies of the lowermost Woodford strata (Gupta et al., 2011; Cardona-Valencia, 2014; Infante-Paez et al., 2016). Models to explain this unconformable relation are presented in Slatt et al. (2016) and Turner (2016), illustrating that during a rapid sea level fall, periods of subaerial exposure led to the development of incised valleys and sinkholes that were facilitated by the erosion and dissolution of the former Hunton carbonate platform, thus resulting in a configuration of semi-restricted mini-basins spread throughout the Hunton top; later, a rise in sea level and the onset of transgression led to sediment infilling and onlapping over the topographic lows, from where the deposition of organic-rich fine-grained rocks of the lower Woodford took place.

In this work, detailed field observations served to document and support such previous interpretations about the unconformable relationship between the Hunton and lower Woodford Shale (Figure 17). From base to top, the section begins with 10 ft of non-radioactive, thick bedded (~40 cm), yellowish to pale gray, massive and crystalline limestones (Figure 17) that exhibit numerous macroscopic burrows and well-preserved

cm-sized crinoid and brachiopod fragments (Figure 18A-B); dissolution features (karsting?) are common along bedding planes and joints. Average bulk composition of the crystalline carbonates reveal calcite (98%) as the major mineral constituent.

Stratigraphically above, in sharp contact is an interval of 15 ft thick, that throughout the outcrop develops low topography, within this interval, radioactivity responses abruptly increase from 150 to 750 cps (Figure 17). Lithologically, the interval consists of medium alternations (~12 cm) of non-organic, greenish and brown-reddish claystones (Figure 18C-D). Horizontal burrows and elongated calcareous nodules and/or hardgrounds (1 to 2 cm thick) are common within this interval. Bulk rock compositions of these greenish-brown claystones include I/S mixed layers (39%), quartz (30%), muscovite (16%), glauconite (7%), kaolinite (6%), and chlorite (2%). As a peculiarity of this pre-Woodford interval, two yellowish, thick bedded (~30 cm), massive, and resistant sandstone beds emerge from the 15-ft interval (Figure 17); these sandstones are very coarse-grained, conglomeratic and poorly sorted. Macroscopically, they exhibit crisscrossing networks of horizontal burrows along their bedding planes (Figure 18E), as well as lithified mud clasts. Microscopically they present a quartz-arenitic framework, with glauconite (15%), phosphate particles, pellets, broken brachiopods and crinoid fragments (Figure 18F); dolomite and calcite cements are common within sandstones. Bulk rock composition of sandstones reveals admixtures of quartz (56%), dolomite (24%), illite (8%), fluorapatite (9%) and glauconite (5%).

Upwards, at ~15 ft, yet with few and scattered cm- to mm-thick lenses of greenish claystones, the occurrence of organic-rich black shales gradually increases, accompanied by higher radioactivity readings (up to 1100 cps) (Figure 17). Black shales of this interval

are thinly fissile, papery-like, clay-rich and laminated. Pyrite/marcasite is abundant; their forms include disseminated crystals within the matrix, replacements of elongated burrows, and as nodules (up to 10 cm in diameter), that usually interrupt the shale parallel laminations. Black shales of this lowermost Woodford, on hand samples exhibit lighter and siltier lenses, that corresponds with laminar concentrations of detrital quartz grains and glauconite (Figure 18H). Average mineralogy of these black shales reveals a bulk rock composition made of illite/mica (60%), quartz (25%), glauconite (6%), kaolinite (6%) and pyrite (5%).

Above the Hunton Group in northern Oklahoma there is a Pre-Woodford deposit that is coarse grained, terrigenous, dolomite-cemented and with evidences of reworked particles (Misener-type sandstone) (Kuykendall and Fritz, 2001). Similarly, but in southern locations, we documented the occurrence of two thick sandstones bodies with such characteristics (Figure 17, Figure 18E-F). As mentioned earlier, they were found embedded within the transitional interval, above the carbonate Hunton Group and beneath the fissile black shales of the lower Woodford, these beds at the Speake Ranch outcrop most likely corresponds to lag deposits, related to the very early stages of marine transgression. Though laterally continuous in the area of study, these sandstone bodies have not been reported in other outcrops of the southern flank of the Arbuckle Mountains documented by Fay (1989), Kirkland (1992) and Paxton and Cardott (2008). However, there are two outcrops in the northern flank of the Arbuckle Mountains where very coarse clastic deposits occur above the Hunton Group and below the Woodford Shale. One outcrop is along the northeast side of State Route 77D where Andrews (2011), described a 2.5-ft. conglomeratic layer above the eroded Hunton limestone, and relates this basal

clastic Woodford with a transgressive lag. The second outcrop is in Murray County, 0.7 miles east of Interstate 35, where Bontempi (2015) described 5 inches of a glauconitic, phosphatic, dolo-chert-arenite at the basal-most Woodford Shale, and interpreted it as basal transgressive lag deposit as well.

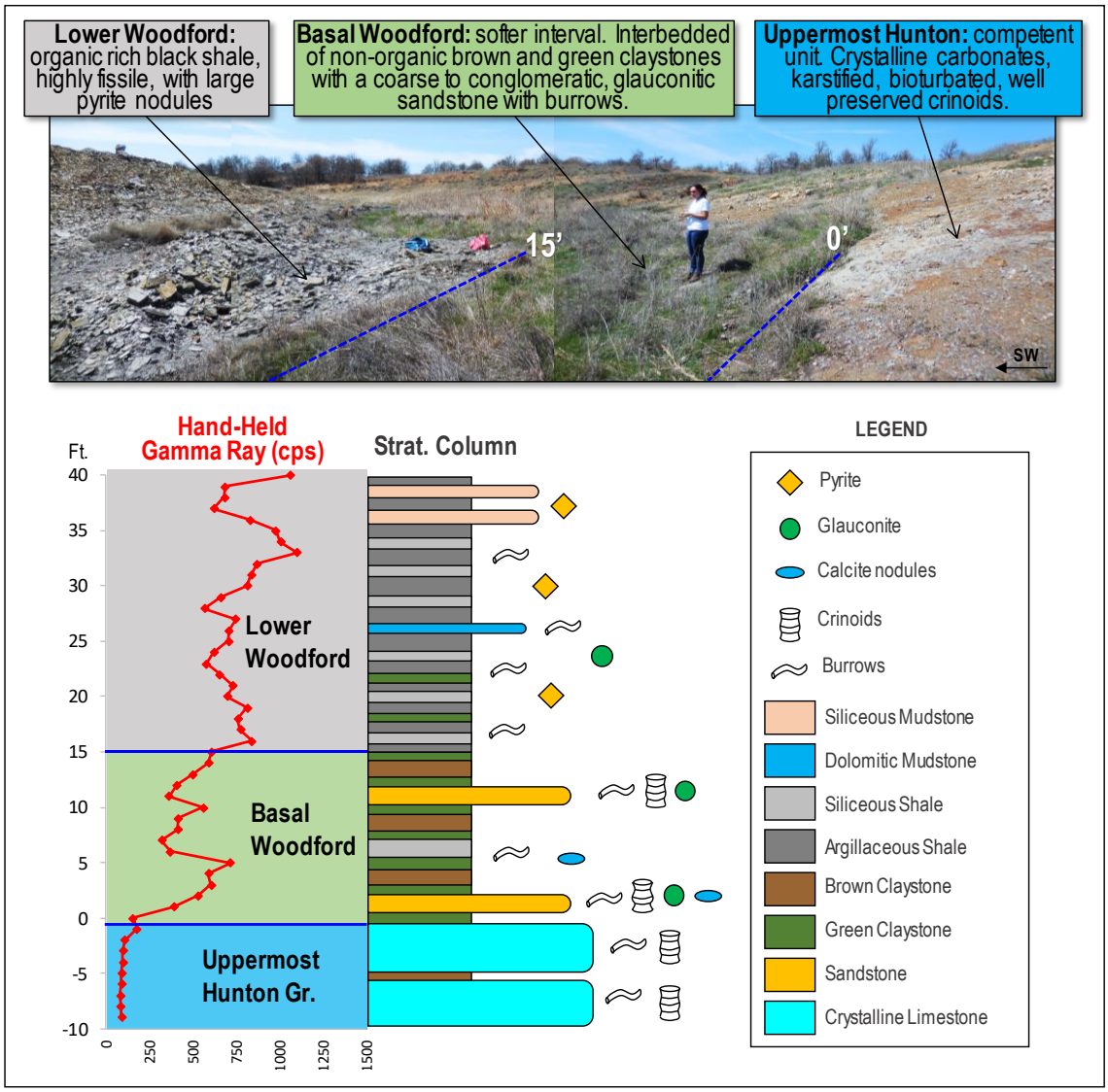

Figure 17. Outcrop characteristics and lithostratigraphy of the basal formational contact between the Hunton and lower Woodford shale. Geomorphological response shows a more competent Hunton overlaid by a softer interval made of non-organic claystones and sandstones. The lowermost occurrences of the typical black organic-rich shales of the lower Woodford Shale occur above 15 ft.

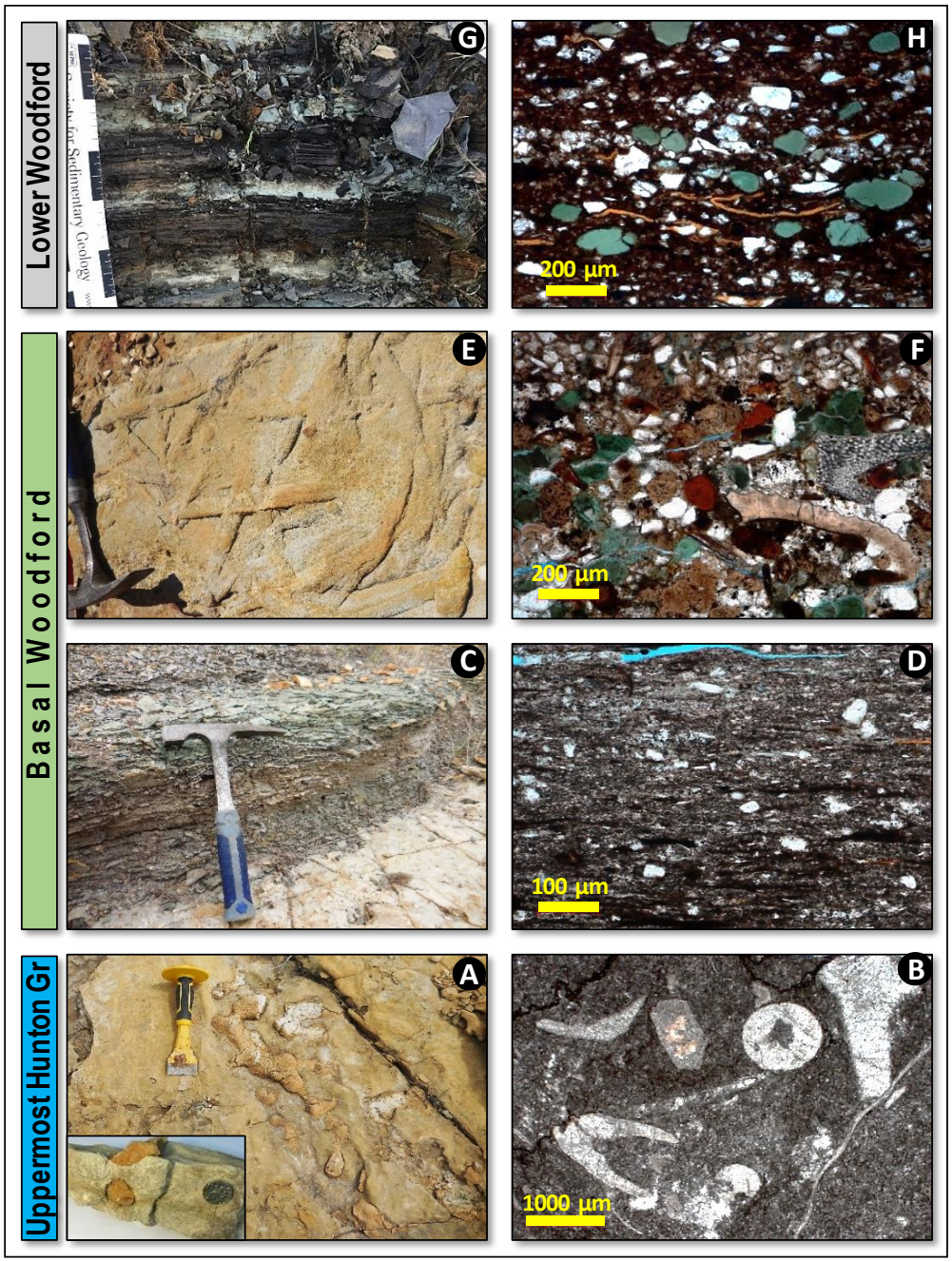

Figure 18. Lithological characteristics of the basal formational contact between Hunton and Woodford Shale. A) recrystallized calcite burrows in limestones, and dissolution along bedding planes and fractures. B) sparry calcite matrix with well-preserved recrystallized crinoids and brachiopods. C) interbedding of non-organic brown and green claystones (illite+kaolinite >70%). D) silt-sized angular quartz scattered within the clay-rich matrix. E) coarse grained to conglomeratic sandstone, thick-bedded, with burrowing networks along bed planes. F) sandstones are poorly sorted, with glauconite, phosphatic pelloids, fossil fragments and slightly cemented with calcite. G) fissile black shales interbedded with few thin beds of greenish claystones. H) organic rich shales with glauconite and silt-sized detrital quartz.

3.1.2. Upper Contact: Woodford Shale – Sycamore Formation

In south-central Oklahoma, the Sycamore Formation conformably overlies the Woodford Shale (Ham et al., 1969; Fay, 1989); the contact between these two units records the change in sedimentary facies, from the biogenic- and organic-rich sediments of the uppermost Woodford to more hybrid terrigenous and calcareous deposits of the Sycamore Formation (Early Mississippian) (Noble, 1995; Donovan, 2001). In the Arbuckle Mountains along Interstate-35 between the Upper Woodford and the ridge-forming Sycamore Formation, Donovan (2001) described a grey-greenish transitional interval (~60 ft.) of shales, cherts and limestones. Similarly, in this work at the Speake Ranch outcrop, we found and documented 21 feet of a distinctive softer and greenish interval that lies immediately above the black Woodford cherts and is capped by the competent, orange to yellowish limestone lithologically equivalent to a basal Sycamore limestone bed (Figure 19).

Starting from the uppermost Woodford (280 to ~315 ft.), this interval consists of alternations of organic-rich, dark grey, thick bedded cherts with medium bedded black siliceous shales (Figure 19). Radioactivity readings gradually decrease up to ~250 cps. Phosphate concretions and cm-sized tar balls are abundant, as well as fractures filled with bitumen. Upward at about 315 ft., a ponded topography marks the occurrence of a softer interval right above the 'typical' Woodford black cherts. This transitional interval is about 21 ft. thick, poorly-radioactive, and consists of interbeddings of light green silty claystones with thick bedded (~10cm) white, non-organic cherts (Figure 20). Several well-preserved brachiopod shells are found within the greenish facies, as well as bioturbation that is more evident in the white non-organic cherts (Figure 20). Average

mineralogy reveals a bulk rock composition for the greenish shales of quartz (65%), illite (18%), mica (9%), kaolinite (4%) and calcite (<3%). For the white cherts quartz makes up 88% and illite/mica makes up 11%.

Overlying the transitional zone at about 337 ft. is a resistant yellowish limestone interval (Figure 19), which can be considered as the lowermost occurrences of the Sycamore carbonates and may represent the earliest flourishing of carbonate deposits of the lower Mississippian. At this location, the lowermost Sycamore consists of yellowish to light grey, thick bedded (~50 cm), massive limestones (Figure 20). Petrographic and mineralogical analyses indicate that these beds are actually hybrid or impure limestones (marlstones?), consisting of silt-sized angular quartz (~60%) embedded within a micritic to pseudosparitic matrix (~30%). Minor constituents are pellets, glauconite and broken fragments of brachiopods, radiolarian, and spicules (Figure 20).

Whether the contact of the Woodford Shale with its overlying Sycamore deposits is conformable or not at the Speake Ranch outcrop and nearby outcrops, the abrupt shifting from organic-rich black cherts and shales to a non-organic greenish transitional shale zone that then grades into massive, competent limestones of the most basal Sycamore Formation (Figure 19) implies that the 'typical' Woodford deposition suddenly ceased and the settlement of carbonate conditions took place later within the upper portions of the transitional greenish zone. Moreover, through biostratigraphic studies, Noble (1995) and Schwartzapfel (1990) identified the early Mississippian (after the Woodford deposition) as a period of non-deposition (hiatus) or extremely slow accumulation, and stated that the deposition resumed over the late Mississippian (Meramecian) in the form of limestones and shales of the Sycamore Formation.

Therefore, it is suggested that the relationship between the Woodford and Sycamore is in essence para-conformable (hiatus), and the greenish transitional zone might not be genetically related to the Woodford Shale. Instead the terminology of 'Pre-Sycamore' can be adopted to refer to the greenish transitional zone capping the Woodford, as illustrated by Champlin (1958).

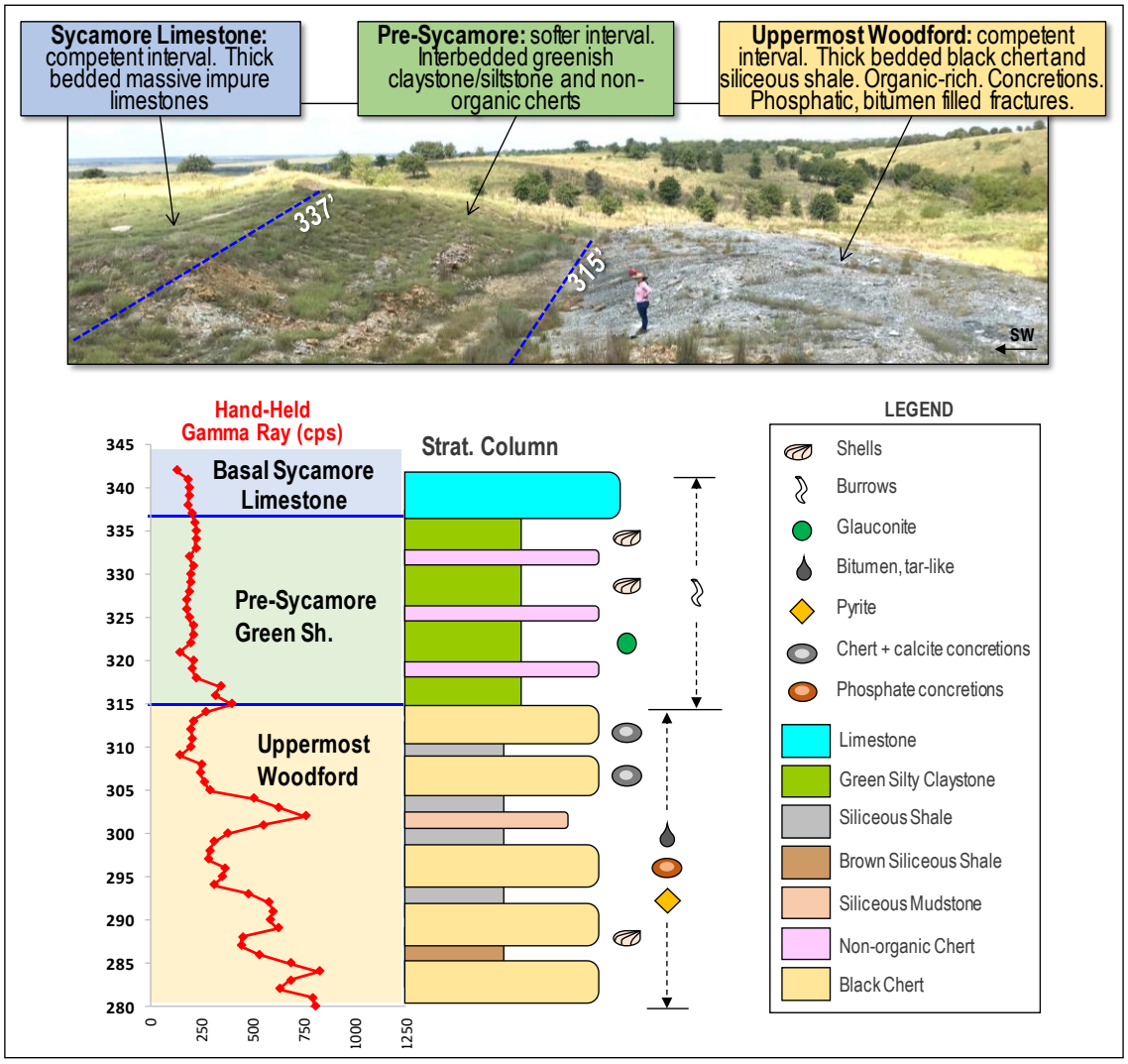

Figure 19. Outcrop characteristics and lithostratigraphy of the upper formational contact between the Woodford Shale and its overlying Sycamore Limestone. Geomorphological response shows a transitional softer interval between the uppermost Woodford (right side) and its overlying Sycamore Limestone (left side), this transitional interval consists of non-organic greenish silty claystones, highly bioturbated.

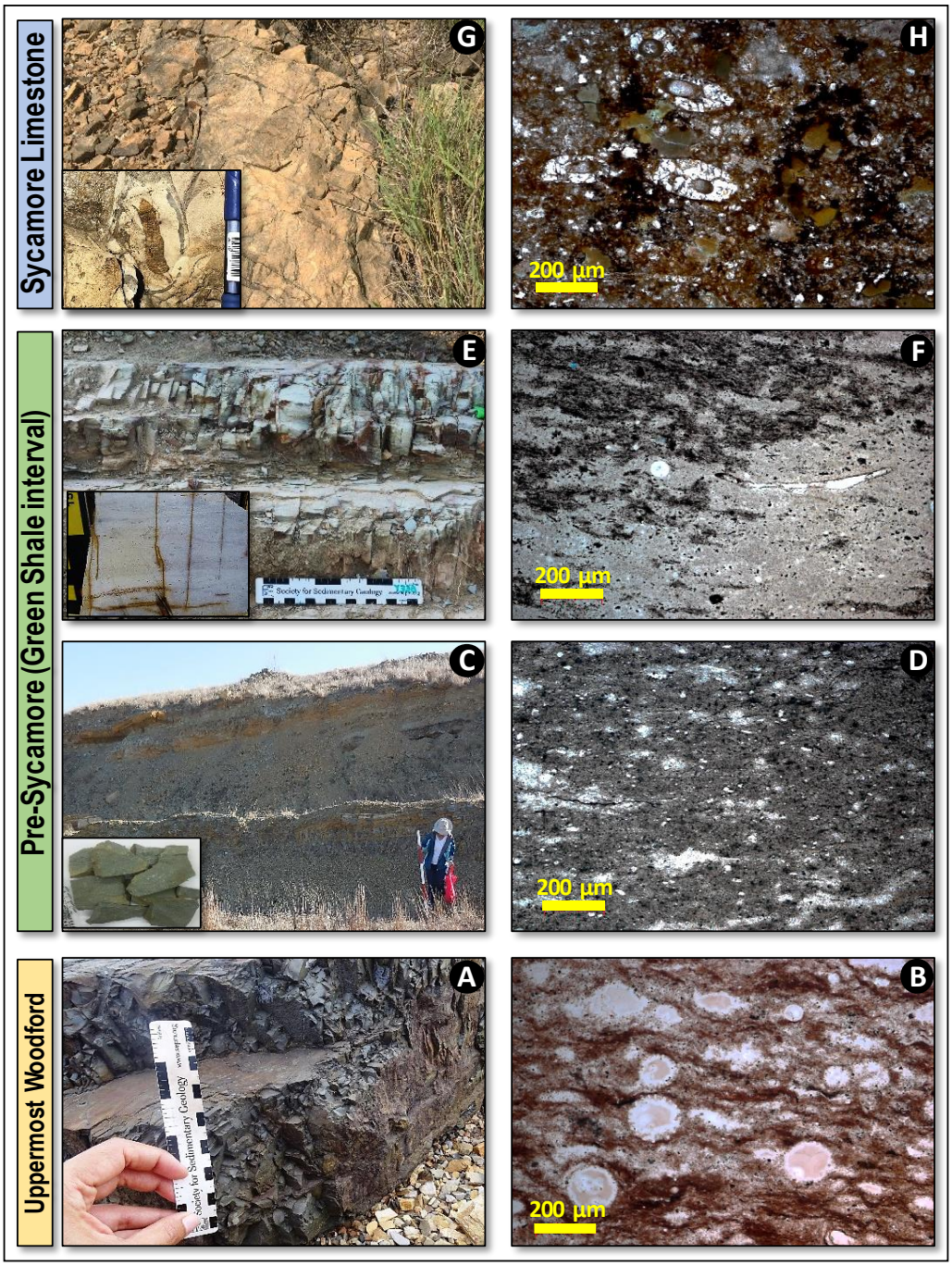

Figure 20. Lithological characteristics of the upper formational contact between the Woodford Shale and its overlying Pre-Sycamore deposits. A) thick-bedded black cherts are organic rich (TOC>4wt.%) and highly fractured (shrinkage-like?). B) well-preserved silicified radiolarians are abundant in cherts. C) softer interval (15ft) of greenish silty claystones. D) silt-sized quartz embedded in a non-organic clay-rich matrix. E) thick-bedded white cherts occur interbedded with the greenish claystones, these are non-organic and bioturbated. F) well-preserved brachiopod shells are in white cherts. G) thick-bedded limestones with macroscopic burrowing. H) impure limestones (marlstone?) contain micrite, dolomite, glauconite, and silt-sized quartz.

3.2. Lithofacies Characterization

As mentioned earlier in the lithofacies classification scheme in the methodology (pages 13 to 16), and illustrated in Figure 8 and Figure 9, only seven lithofacies are identified as representing most of the Woodford Shale strata at the Speake Ranch outcrop. From the most argillaceous to the most quartz-rich lithofacies, and finalizing with the calcareous ones, hereinafter these lithofacies are presented as follows: *i) Argillaceous Shales; ii) Siliceous Shales; iii) Brown Siliceous Shales; iv) Siliceous Mudstones; v) Cherts, vi) Siliceous-Dolomitic Shales;* and *vii) Dolomitic Mudstones.*

3.2.1. Argillaceous Shales

Within the Woodford Shale, this is the most clay-rich and fissile lithofacies (clays>50%); on outcrops, they are predominantly black to dark grey and exhibit very thin parting responses (papery-like). Sporadically its lamination is interrupted by coarsely-crystalline pyrite/marcasite concretions and pyritized macro-burrows.

On microscopic observations, the shale matrix is dark brown, mostly composed by clay-sized particles that overall exhibit parallel preferential alignments along with very fine laminations defined by concentrations of micas, organics and silt-sized quartz (Figure 21). The occurrence of silt-sized detrital quartz is almost exclusive to the lithofacies of Argillaceous and Siliceous Shales (Figure 21). However, within the Argillaceous Shales, they reach greater proportions up to 10% (visual estimates).

Along with the detrital quartz, other non-clay particles are palynomorphs, identified as either *Tasmanites*, acritarchs or pollen (Von Almen, 1970; Molinares, 2013), which in some cases could reach proportions of up to 20% of the whole rock (visual

estimates), their walls are light orange to yellow and ellipsoidal (Figure 21); within this lithofacies it is noted that most of the palynomorphs occur flattened or collapsed, with little or no evidence of cements filling their cavities (Figure 21). Radiolarians and spicules are very rare within this lithofacies, and when found they are poorly preserved.

Carbonate particles may occur but in very minor proportions in the form of dolomite/ankerite crystals scattered throughout the matrix. Silica-rich cements appear as micro-crystalline quartz replacing walls of palynomorphs, forming parallel-like micro-strings aligned within the shale matrix (Figure 21). Pyrite crystals appear dispersed throughout the matrix, as well as framboids (Figure 21). Other diagenetic minerals in trace amounts are gypsum and barite, which are likely related to veins.

Micro-deformation features of the Argillaceous Shales include a few examples of low angle pre-compaction fractures filled with sulfates.

The average bulk rock composition of the Argillaceous Shale is: illite/mica (57%), kaolinite (5%), quartz (42%), orthoclase (<5%), dolomite/ankerite (<7%), pyrite (3%), and gypsum (2%). TOC contents range from 11 to 21 wt.%, averaging 18 wt.%.

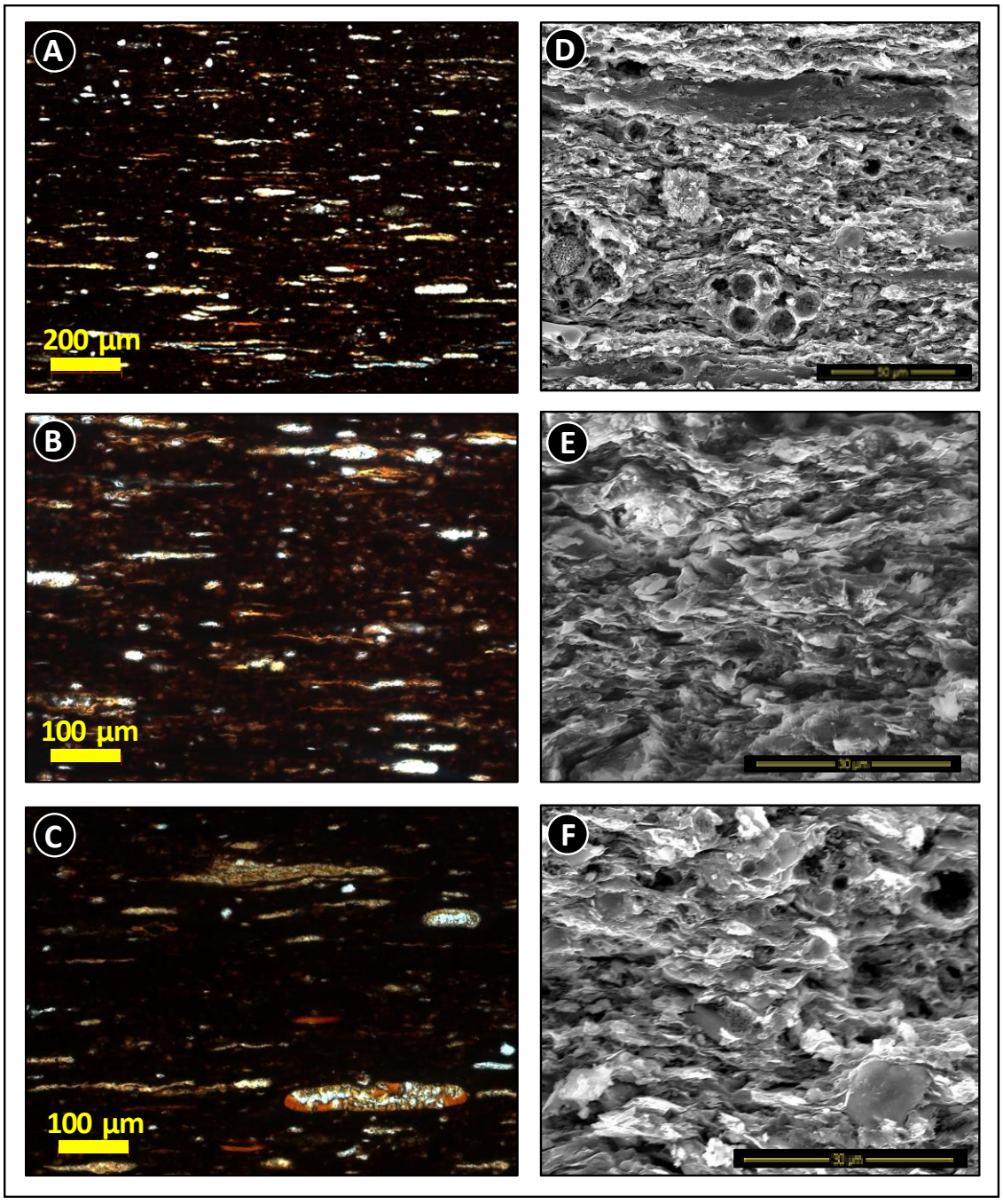

Figure 21. Typical characteristics of the Argillaceous Shales lithofacies. Features include parallel clay alignments, scattered silt-sized quartz, pyrite framboids, flattened/collapsed palynomorphs (*Tasmanites*), microcrystalline quartz replacing walls of *Tasmanites* like forming parallel micro-strings aligned with the matrix. A, B and C are thin section photomicrographs, and D, E and F are SEM images on fresh broken surfaces.

3.2.2. Siliceous Shales

Following in declining order of clay abundance, Siliceous Shales appear as the second most clay-rich lithofacies within the Woodford Shale, with clay contents varying from 15 to 50%; yet fissile in outcrop samples, its major constituent is quartz (45-85%).

This lithofacies is black to grey, slightly indurated, and with thicker parting responses. In particular, within the upper Woodford member, Siliceous Shales appear harder and differentially compacted due to the effect of adjacent nodular chert beds.

Microscopically, the shale matrix is dark brown and laminated, represented by admixtures of microcrystalline quartz, illite/mica, organics, and silt-sized detrital quartz (Figure 22). Other coarser particles embedded into the matrix include palynomorphs, characterized by yellow to orange organic walls, which are usually flattened and aligned following the lamination (Figure 22). Detrital silt-sized quartz grains appear scattered and as micro-lenses (Figure 22). Pyrite is commonly observed aggregated in bands, as framboids or replacing portions of organic materials. Radiolarian tests are rare to absent. Silica-rich cements in the form of chalcedony can be found as parallel micro-strings through the matrix, as well as replacing walls of palynomorphs (Figure 22).

Dolomite/ankerite is rare, but in some cases, occur as discrete subhedral microcrystals. Other secondary minerals in trace amounts are sulfates such as gypsum. Micro-deformation features of shales include few examples of low angle to parallel fractures filled with bitumen, quartz or gypsum. Average bulk rock composition of the Siliceous Shale lithofacies is: quartz (67%), illite/mica (20%), kaolinite (4%), dolomite/ankerite (<2%), pyrite (<5%), and gypsum (<2%). TOC contents vary from 8 to 17 wt.%, averaging 12 wt.%.

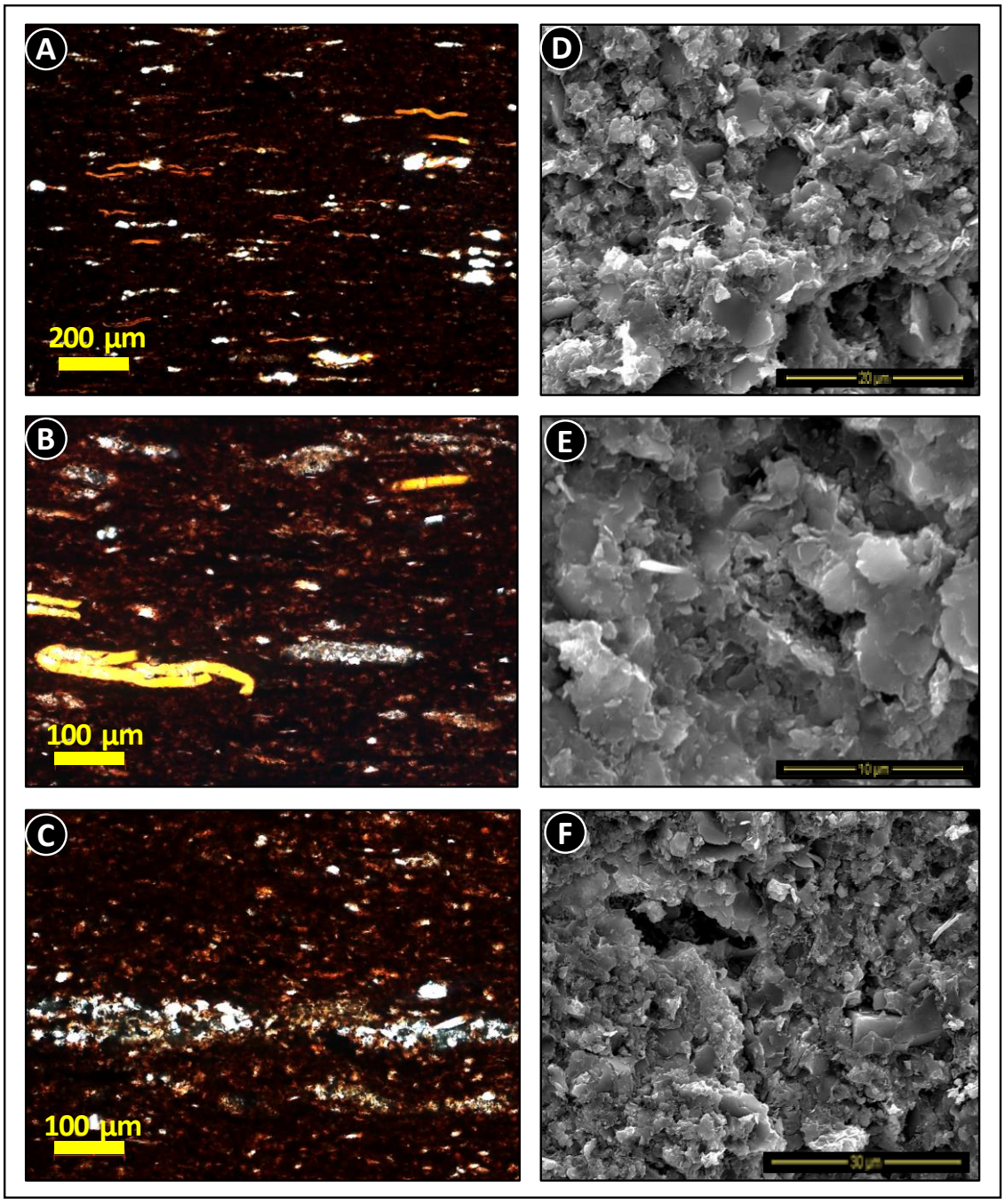

Figure 22. Typical characteristics of the Siliceous Shales lithofacies. The shale matrix is largely made of microcrystalline authigenic quartz and clays; embedded coarser particles include silt-sized detrital quartz in laminae and flattened *Tasmanites*. Siltier microlenses seem to provide better primary porosities within this lithofacies. A, B and C are thin section photomicrographs, and D, E and F are SEM images on fresh broken surfaces.

3.2.3. Brown Siliceous Shales

This lithofacies is a variety of the Siliceous Shales. In outcrops, they are light brown to brownish grey, fissile and with thicker parting responses (5-10 mm).

The most outstanding feature of this lithofacies is its anomalous light weight (low density?) when compared with the other lithofacies within the Woodford Shale; field tests reveal that these beds absorb moisture and dry rapidly (porous?). Also in outcrops, usually beds of this lithofacies host abundant phosphate concretions of the upper Woodford member.

Microscopic observations reveal a slightly laminated light brown matrix made of clay-sized microcrystalline quartz and clay minerals (Figure 23). In the form of a bitumen-impregnated matrix, this lithofacies seems to host vast amounts of organic materials possibly related to migrated bitumen, characterized by orange to dark brown fluidal-like material dispersed through the matrix (Figure 23); this previous observation of a bitumen saturated lithofacies is confirmed afterwards in the results of pyrolysis Rock-Eval.

The microfabric seems randomly oriented and open (in the sense of O'Brien and Slatt, 1990 to refer to phosphatic mudstones) (Figure 23). Silt-sized detritus are common within this lithofacies; palynomorphs and radiolarian tests are rare. Secondary features include bitumen in the form of saturated microfractures and laminar concentrations. Average whole rock composition of the light-weight Brown Siliceous Shales is: quartz (73%), illite/mica (19%), kaolinite (4.5%), fluorapatite (<3%), pyrite (<2%) and gypsum (<2%). TOC contents range from 3 to 12 wt.%, averaging 7 wt.%.

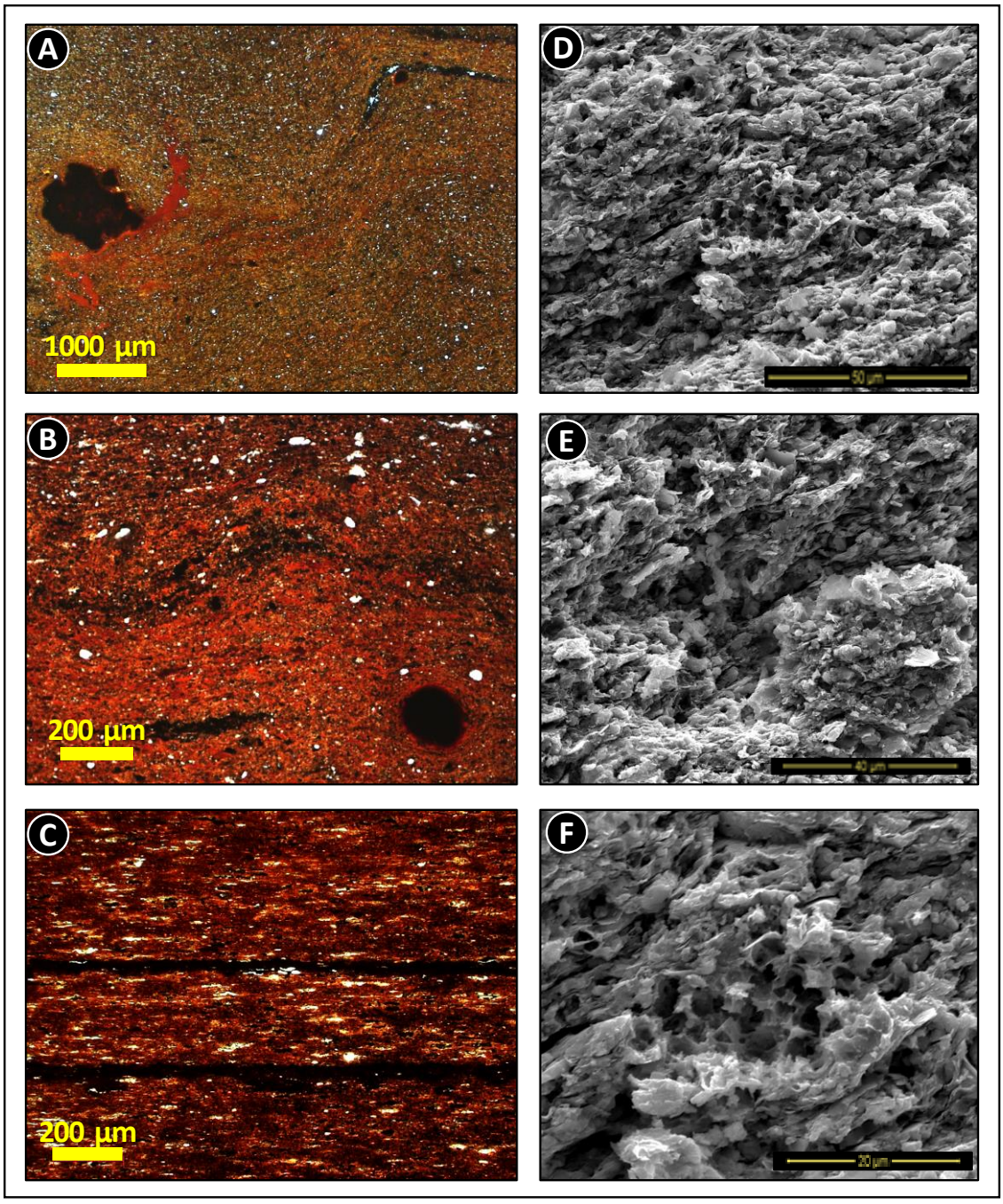

Figure 23. Typical characteristics of the Brown Siliceous Shales. The matrix is randomly oriented and porous, might be the case of a phosphatizied shale matrix; silt sized detrital quartz are embedded in the shale matrix. Bitumen occurs dispersed in the matrix as well as micro-fractures parallel to the lamination. A, B and C are thin section photomicrographs, and D, E and F are SEM images on fresh broken surfaces.

3.2.4. Siliceous Mudstones

This is the second most silica-rich lithofacies, where quartz amounts vary from 87 to 95%. In outcrops, they are dark grey, hard (non-fissile), blocky, and massive to slightly laminated.

Microscopic observations reveal a lighter colored matrix, that ranges from light orange to pale brown. Organic material is unevenly distributed as patches not aligned to preferential planes. The microfabric is slightly laminated to massive. Texturally, the matrix is made of equigranular aggregates of micro-crystalline quartz (Figure 24). There is little evidence of discrete grains of silt-sized detrital quartz within this lithofacies; however, there might be some traces of detritus that are incorporated into the tight quartz-rich matrix.

Fossil contents of the Siliceous Mudstones range from 10 to 40%, with abundant and scattered radiolarian and palynomorphs that are usually very well preserved. Most of them are rounded and silicified (Figure 24), retaining their original shapes, as well as filled with chalcedony and pyrite.

Micro-deformation features of this lithofacies include vertical to sub-vertical fractures, usually filled with chalcedonic quartz and bitumen. Average bulk rock composition of the Siliceous mudstone is: quartz (92%), illite/mica (<4%), kaolinite (<2%), dolomite/ankerite (<1%), and pyrite (<5%). TOC contents vary from 3 to 8 wt.%, averaging 4.5 wt.%.

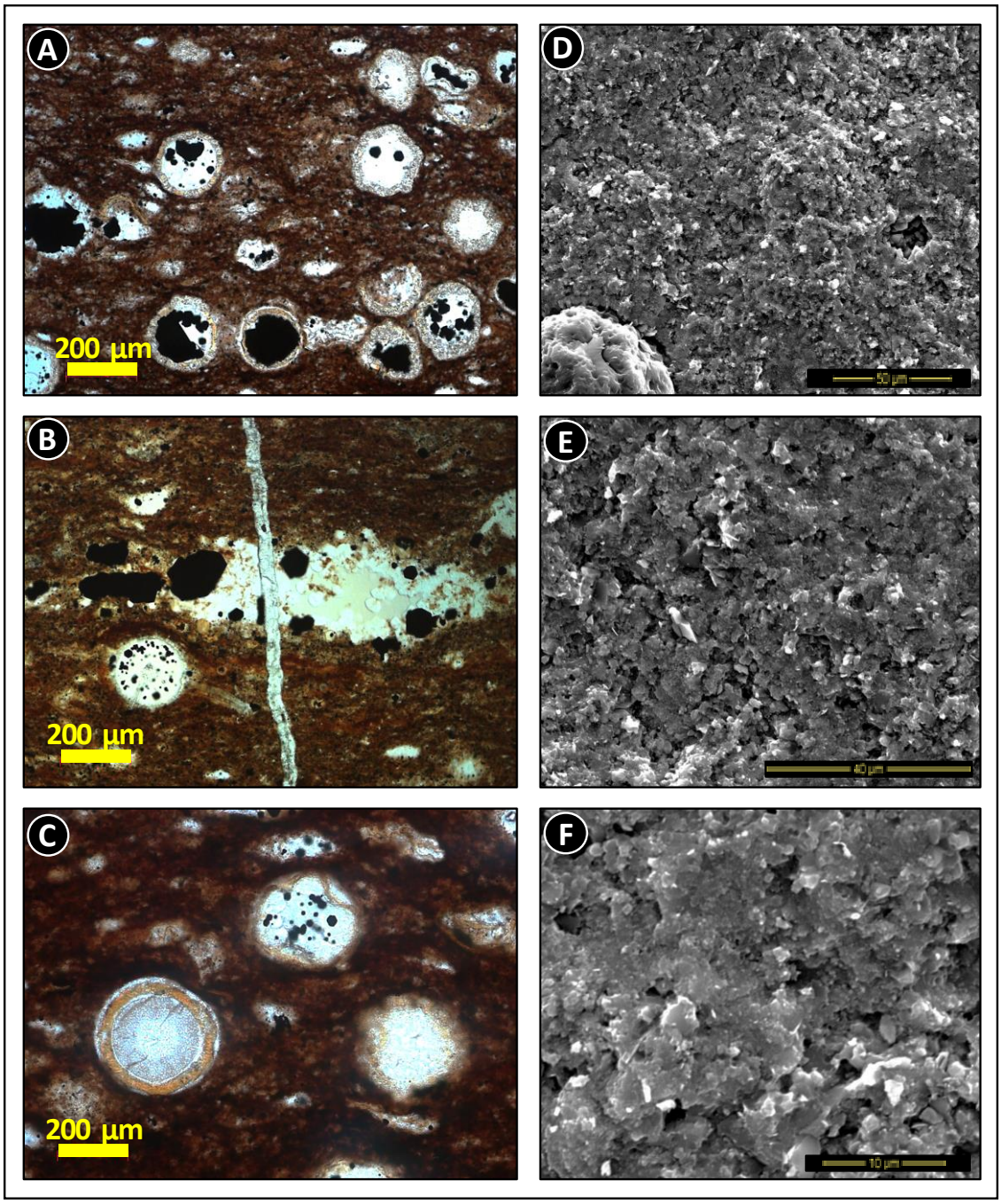

Figure 24. Typical characteristics of the Siliceous Mudstones. The microfabric is slightly laminated to massive. The shale matrix is made of aggregates of micro-crystalline quartz (no visible discrete grains contacts). Scattered through the matrix there are abundant well-preserved radiolarian and *Tasmanites* filled with chalcedony and pyrite. A, B and C are thin section photomicrographs, and D, E and F are SEM images on fresh broken surfaces.

3.2.5. Cherts

Within the Woodford Shale, this is the most silica-rich lithofacies, with quartz amounts ranging from 87 to 98%. In outcrop samples, chert beds are dark grey, hard, massive, blocky, and exhibit its typical conchoidal fracture. Also in outcrops, nodular bedded cherts that host phosphate concretions are common (mostly in the upper Woodford member).

Microscopically, cherts appear subtly laminated, defining laminar concentrations of silicified radiolarian tests (Figure 25). The chert matrix is predominantly composed by microcrystalline quartz aggregates, arranged in a very tight fabric, where there is no clear differentiation of grain contacts (Figure 25). Dark brown organic material is also present in cherts as scattered patches throughout the matrix.

Numerous and well-preserved radiolarian tests and palynomorphs are observed, which usually are internally replaced by chalcedony quartz (Figure 25). Pyrite occurs as finely disseminated crystals and sometimes associated with microfossils.

Deformation features include vertical to sub-vertical microfractures that are filled with bitumen, quartz or calcite. Also, vertical stylolites are common features throughout this lithofacies. Average bulk rock composition of cherts is: quartz (95%), illite/mica (<3%), kaolinite (<1%), dolomite/ankerite (<1%), and pyrite (<2%). TOC contents are the lowest among the Woodford lithofacies (2 to 4 wt.%).

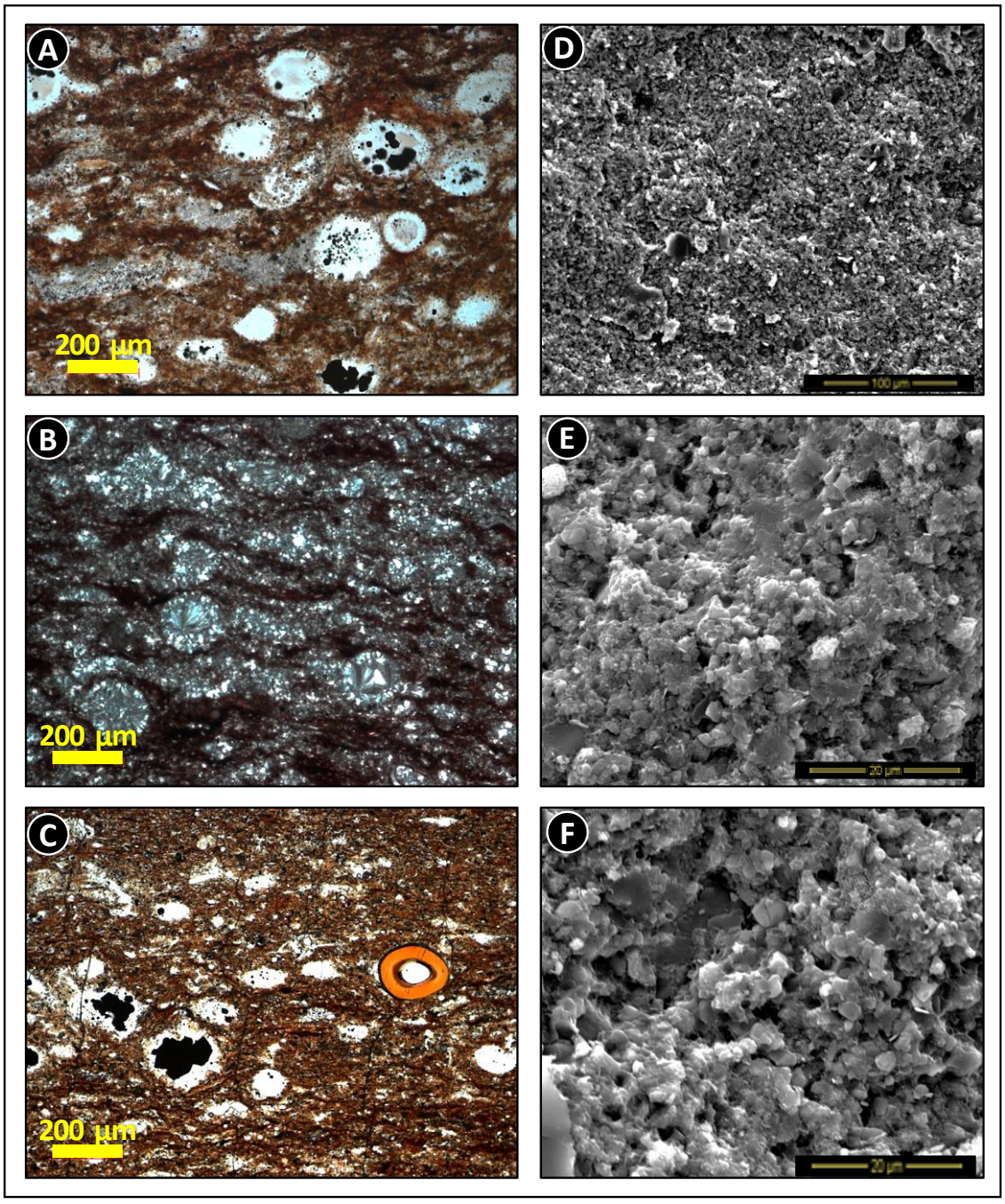

Figure 25. Typical characteristics of Cherts. The matrix is made of micro-crystalline quartz aggregates. Well-preserved radiolarian tests and *Tasmanites* are replaced by chalcedony quartz. Vertical microfractures are common, these are filled with bitumen and quartz. There is little to no evidence of detrital silt-sized quartz within cherts. A, B and C are thin section photomicrographs, and D, E and F are SEM images on fresh broken surfaces.

3.2.6. Siliceous-Dolomitic Shales

This is a variety of a shale lithofacies, where carbonate contents range from 15 to 50%, and coexist with quartz and clays in almost equal proportions. In outcrops, the Siliceous-Dolomitic Shales beds are black to dark grey, fissile, and slightly indurated, exhibiting thicker parting responses. Also, due to the occurrence of silt-sized dolomitic crystals, in outcrop samples this lithofacies appears slightly coarser than a regular Argillaceous or Siliceous Shale.

Microscopically, the matrix is dark brown, finely laminated, and displays preferential alignment of clay-particles and organics (Figure 26); flattened palynomorphs occur following the preferential orientation, as well as some dispersed silt-sized detrital quartz are common throughout the shale matrix (Figure 26).

Diagenetic dolomite/ankerite make up the majority of the calcareous component, occurring as discrete subhedral microcrystals scattered throughout the matrix, as well as replacing fossil particles (Figure 26). Silica-rich cements also occur, but in the form of parallel micro-strings following the lamination. Other diagenetic minerals, but in trace amounts, are sulfates such as anhydrite and barite, which occur mostly associated to microfracture fillings along with bitumen. Pyrite is present as framboids dispersed through the matrix and as replacements of fossil particles.

Average bulk rock composition of the Siliceous-Dolomitic Shales is: dolomite/ankerite (25%), quartz (37%) illite/mica (32%), kaolinite (<5%), pyrite (3%), and gypsum (<2%). TOC contents range from 8 to 14 wt.%, averaging 11 wt.%.

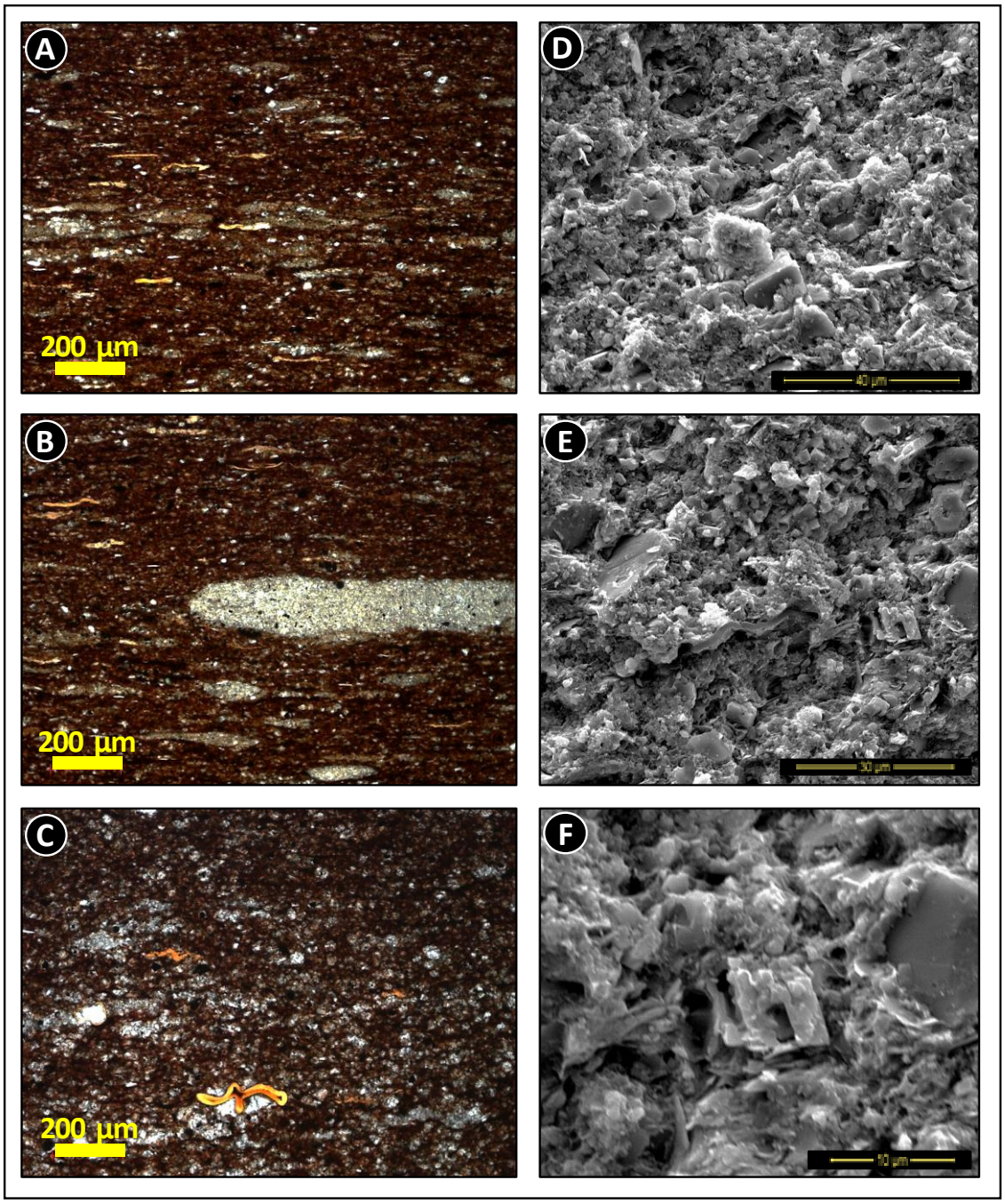

Figure 26. Typical characteristics of Siliceous-Dolomitic Shales. The microfabric is represented by lenticular dolomite aggregates (recrystallized burrows?), which are made of discrete subhedral dolomite crystals; coarser particles include flattened *Tasmanites* and detrital silt-sized quartz. Dolomite/ankerite crystals are partially leached or dissolved, revealing a type of intraparticle porosity within the dolomitic shales. A, B and C are thin section photomicrographs, and D, E and F are SEM images on fresh broken surfaces

3.2.7. Dolomitic Mudstone

Within the Woodford Shale strata, this is the most calcareous-rich lithofacies. Dolomite and/or ankerite make up the majority of the calcareous content (>20%). In outcrops, dolomitic mudstones are light grey, hard, blocky, and crystalline in appearance. In some cases, dolomitic beds occur associated with macroscopic burrows.

Microscopic observations reveal a recrystallized matrix, from which its primary depositional fabric or laminations have almost been completely removed (Figure 27). The rock framework is made of mosaics of very fine to coarse subhedral crystals of dolomite/ankerite (Figure 27). Remnants of organic material and clay minerals are visible that apparently have been trapped by the dolomite crystal overgrowths, thus resulting in concentrations of organics and clays along crystal-to-crystal borders. Depending on the degree of dolomitization, mudstones of this lithofacies exhibits significant changes in crystal size, and destruction of the depositional microfrabic.

Visible *Tasmanites* and radiolarians are rare, as they appear strongly replaced by dolomite. Deformation features include sub-vertical, branched calcite and gypsum veins. Average bulk rock composition of the Dolomitic Mudstones is: dolomite/ankerite (>20-50%), quartz (49%), illite/mica (9%), kaolinite (<2%), and pyrite (<3%). TOC contents are generally less than 2 wt.%.

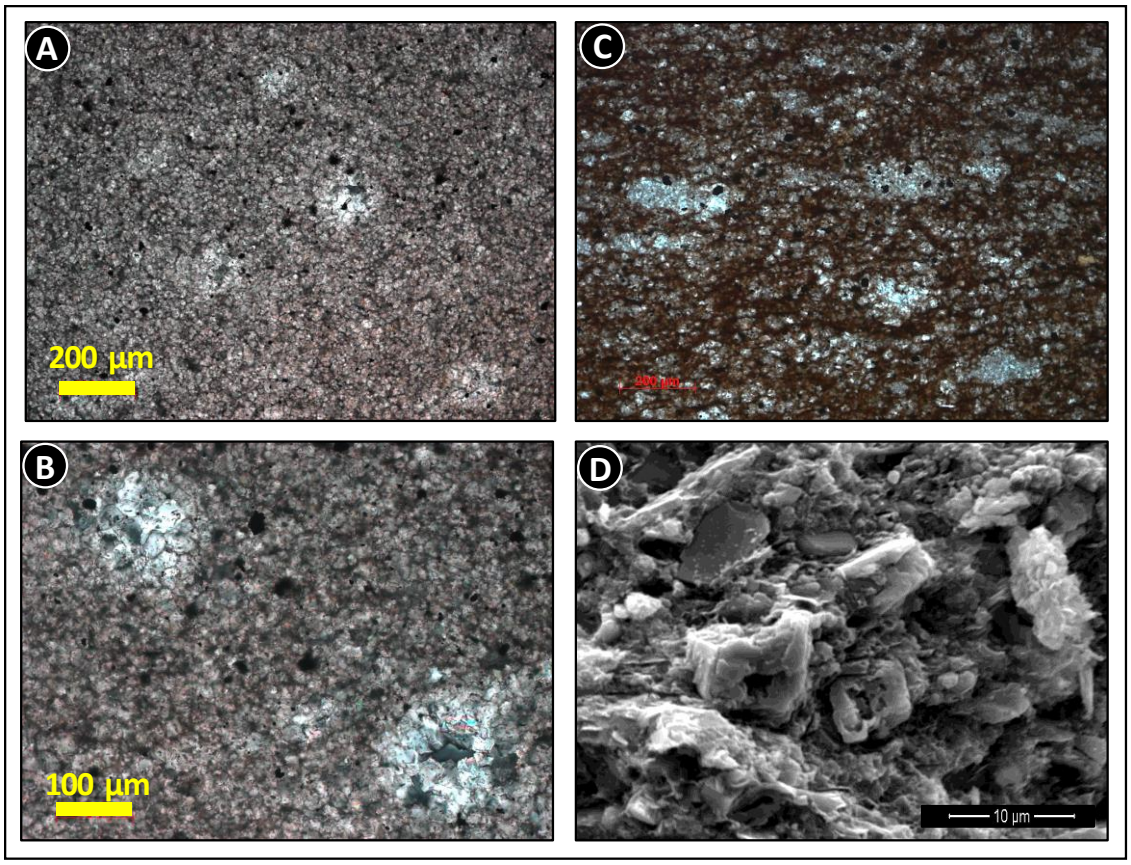

Figure 27. Typical characteristics of the Dolomitic Mudstones. The microfabric is recrystallized, with some remains of its primary depositional fabric. The matrix is made of mosaics of finely crystalline dolomite and ankerite, *Tasmanites* and radiolarian are strongly replaced by dolomite. A, B and C are thin section photomicrographs, and D is a SEM image on fresh broken surfaces.

3.3. Woodford Shale Internal Characteristics

For reporting results within the Woodford Shale I adopted the informal subdivision into lower, middle and upper members, as originally adopted by Sullivan (1985), Hester et al. (1990), and Lambert (1993). Though counterproductive in terms of time-rock stratigraphy as correctly discussed by Turner (2016), this informal subdivision has demonstrated consistency among industry and academia, finding it useful for communication.

Overall, the Woodford Shale at the Speake Ranch outcrop exhibits monotonous alternations of hard and soft beds, from which the soft-to-hard ratio was extracted per foot (Figure 7), and observed that gamma ray responses correlate with our obtained soft-to-hard ratios (Figure 28), resulting in that the softer an interval is, the higher the radioactivity is; in the Woodford, this observation can be easily explained since soft beds are the ones that present higher clay and organic contents.

3.3.1. Lower Woodford (LW)

The LW member at the Speake Ranch outcrop is about 105 ft thick (~32 meters) and generates topographic lows throughout the section (Figure 16), into this, soft beds dominate, making soft-to-hard ratios varying from 70/30 to 100/0, along with very high Gamma ray responses varying from 600 to 1300 cps, averaging 800 cps (Figure 28).

The ‘soft’ component is mostly represented by lithofacies of Argillaceous, Siliceous and Dolomitic shales that, when compared with other members, are the most abundant lithofacies within the lower Woodford (Figure 29). Hard lithofacies on the other hand, such as Siliceous Mudstones and Cherts, only account for less than 30% of

the lithology within this member (Figure 29). Distribution of bed thicknesses shows that soft beds are much thicker (>30cm) than hard beds (1-6cm) (Figure 29).

The contact between the lower and middle Woodford is represented by a major turnaround point in the gamma ray profile (Figure 29), which lithologically in the field coincides with a zone of bioturbated Dolomitic Mudstones.

3.3.2. Middle Woodford (MW)

The MW member at the Speake Ranch outcrop is about 104 ft thick (~31,6 meters), and is dominated by soft-to-hard ratios between 85/15 to 50/50, meaning that the proportion of hard beds increases gradually upward, while the soft ones decrease (Figure 29). Radioactivity readings in this member are more homogenous, mostly ranging from 650 to 900 cps (Figure 28).

Average bed thickness between soft and hard beds decreases and is less contrasting between them, varying from 1-12 cm and 1-6 cm respectively (Figure 29), implying the occurrence of high-frequency cycles of soft and hard beds.

Lithofacies within this member are largely represented by Siliceous Shales, Cherts and Siliceous mudstones (Figure 29). Clay-rich and dolomitic lithofacies (as the Argillaceous and Dolomitic Shales) decrease upward abruptly from its underlying lower Woodford member.

The contact between the middle and upper Woodford members sits at about 222 ft and is marked by the first occurrence of phosphate nodules/concretions of variable diameter (2-5cm), as well as by a trough in radioactivity (Figure 29).

3.3.3. Upper Woodford (UW)

The UW member at the Speake Ranch outcrop is about 92 ft thick (~28 meters), and generally more competent than its preceding members, and usually develops scarp slopes in outcrops (Figure 16).

Radioactivity responses are highly variable, ranging from 400 to 800 cps, with outlier values greater than 1300 cps nearby the most phosphatic-rich zone (Figure 28 and Figure 29). Average soft-to-hard ratios range from 40/60 to 5/95, making this the hardest interval among the Woodford members (Figure 29).

Distributions of bed thickness reveal a dominance of thicker hard beds (5-20cm) compared to the soft ones (<6cm). Cherts and Siliceous Shales are the most abundant lithofacies (Figure 29), making up about the 88% of lithofacies in this member.

Other field-scale features of this upper Woodford include the abundant occurrence of phosphate nodules/concretions of variable diameter (1-25cm), the nodular bedded geometry of the hard beds, and the bitumen (tar-like?) filled microfractures and cm-sized tar balls.

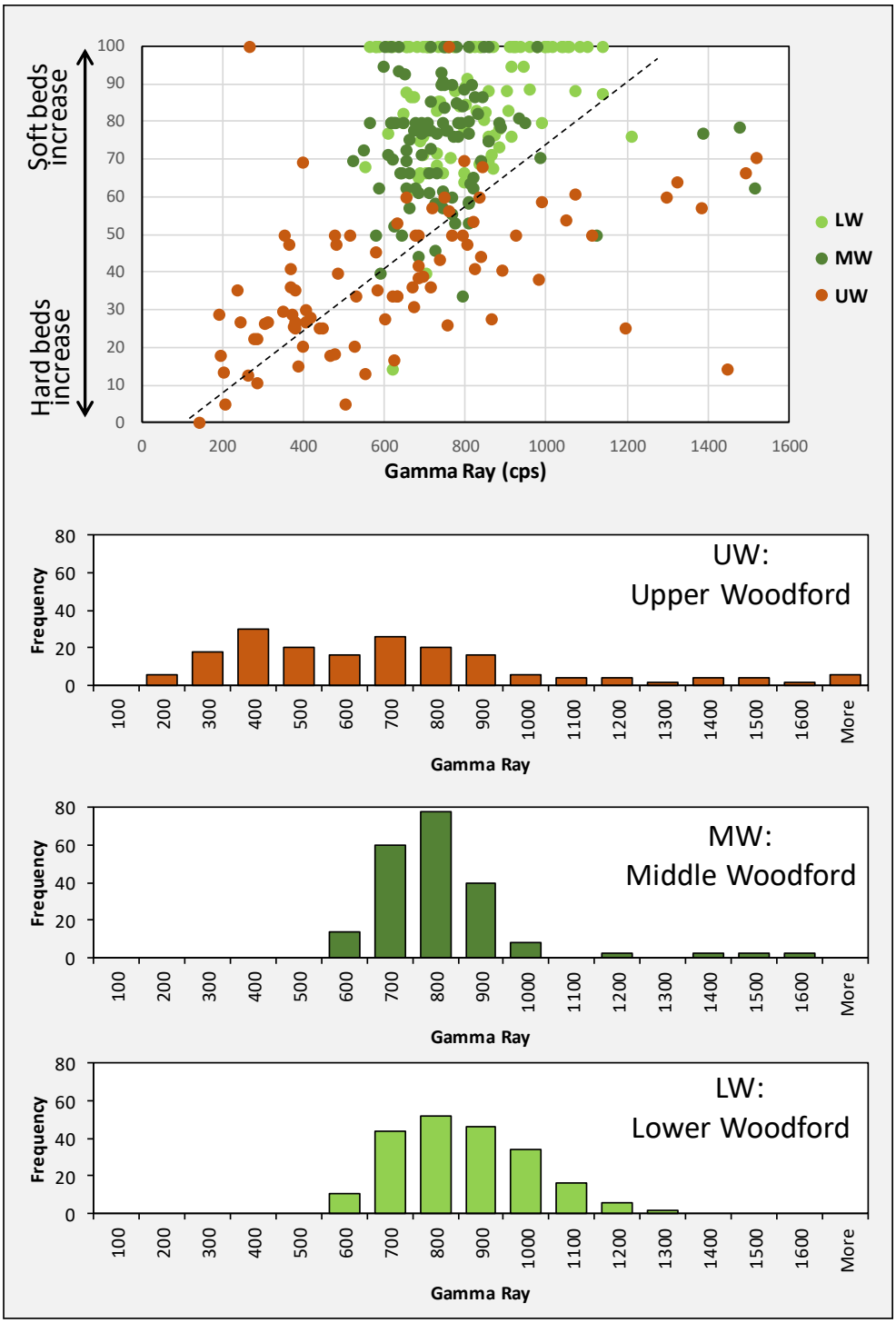

Figure 28. Correlation between gamma ray responses and the Soft-to-Hard ratios per foot by Woodford member. Notice the positive correlation between these two variables, implying a generalized increase in radioactivity with more soft beds per foot.

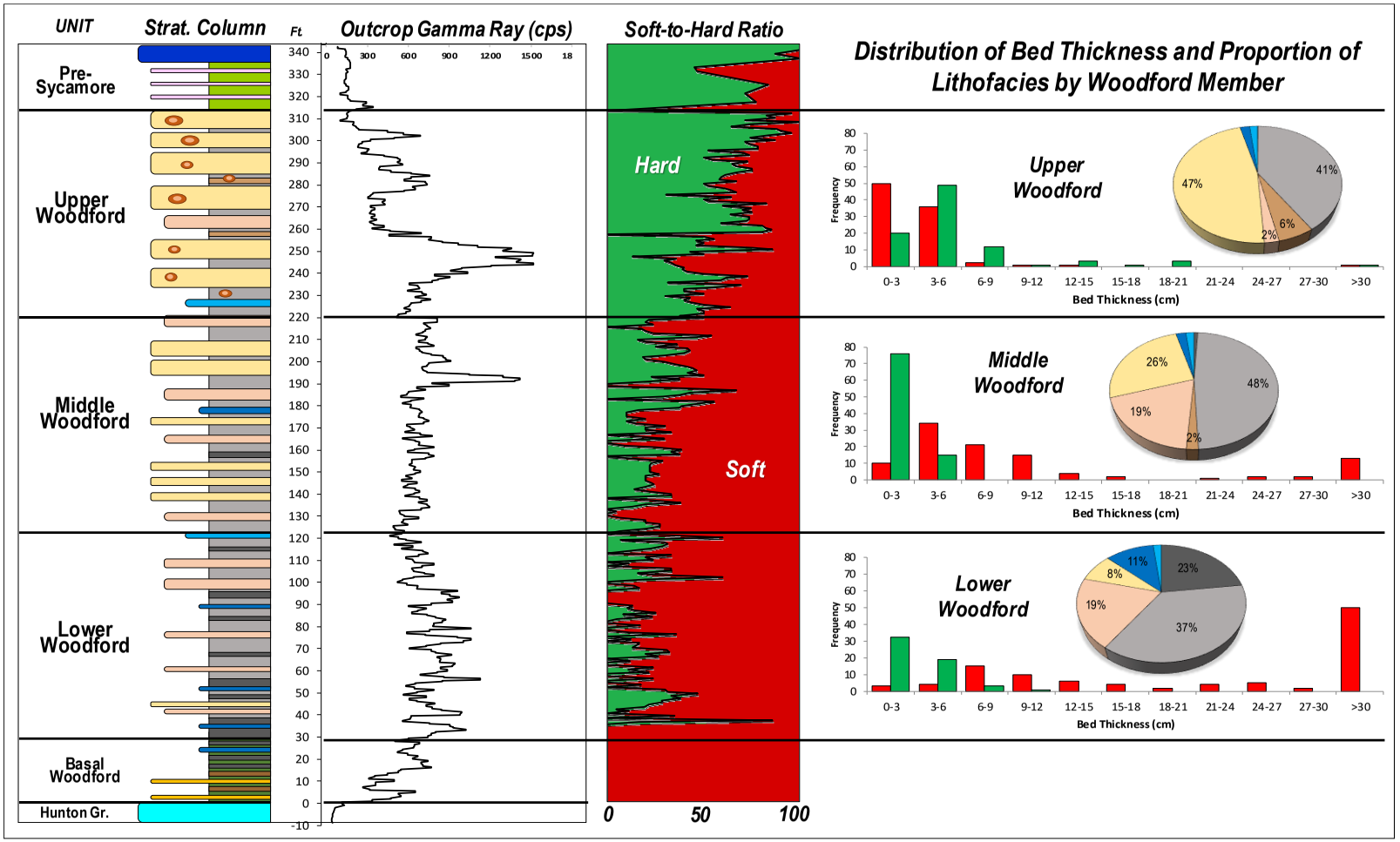

Figure 29. Integration of vertical distribution of lithofacies, soft-to-hard ratios and distribution of bed thicknesses by informal Woodford members. It is evident the upward increase of hard beds. The LW is dominated by thick soft beds of argillaceous and siliceous shales. The MW is characterized by a nearly 50/50 mix of soft and hard beds of siliceous shales and cherts. The UW is dominated by higher contents of hard beds of thick-bedded cherts, which are intercalated with thin beds of siliceous

4. MINERALOGY

Numerous authors have documented the mineral composition of the Woodford Shale in Oklahoma. Some of them have reported average bulk rock mineralogy regardless of the stratigraphic position and/or rock types, all agreeing that the Woodford Shale is composed by quartz (30-70%), illite/mica (5-40%), kaolinite (<10%), chlorite (<5%), calcite (5-25%), dolomite (0-50%), and pyrite (<10%).

Recent contributions by Caldwell (2013), Fishman et al. (2013), and Becerra-Rondon (2017) have made specific emphasis on reporting mineralogy by rock types, resulting in the Woodford mineralogy being highly contrasting among rock types even in adjacent beds. Also, this proves our measurement approaches to be more meaningful as composition can be related with geochemical, petrophysical, and geomechanical heterogeneities within the Woodford strata.

Overall the Woodford samples from this work show quartz is the dominant component and it is well dispersed throughout the section. From the most basal Woodford (beneath foot 30 ft), quartz amounts can be as minimum as 20%, up to almost entirely pure quartz samples (95-99%) at higher stratigraphic positions (around 270 ft) (Figure 30). Clay minerals are also well dispersed over the entire section but at much smaller proportions, ranging from 5 to 67% (Figure 30); main clay types within the Woodford samples include illite/mica, kaolinite and chlorite. One important finding from the clay mineralogy of the Woodford Shale at the Speake Ranch outcrop is that clay contents never surpass 70% of the bulk rock; even at the lowermost portions, the highest clay contents are accompanied by moderate amounts of quartz or carbonates (~30%) (Figure 30). Regarding carbonate contents, while abundant in some samples, their distribution

throughout the section is restricted to a few beds, and only dolomite and ankerite were identified as carbonate minerals in the Woodford strata.

Among the informal Woodford members, there is evident a decreasing upward of clay contents, where the lower Woodford appears as the most clay-rich interval (up to 67% clays), followed by the middle (3-30%), and then upward the least clay-rich strata of the upper Woodford member, where clay contents do not exceed 25% (Figure 30). Inversely, it can be noted that quartz amounts tend to increase upward, from about 60% in the lower Woodford to 71% and 90% in the middle and upper Woodford respectively. Carbonate contents are very low across the entire Woodford Shale of this sections; however, where carbonate-rich beds occur, these are mostly concentrated within the lower Woodford member (Figure 30).

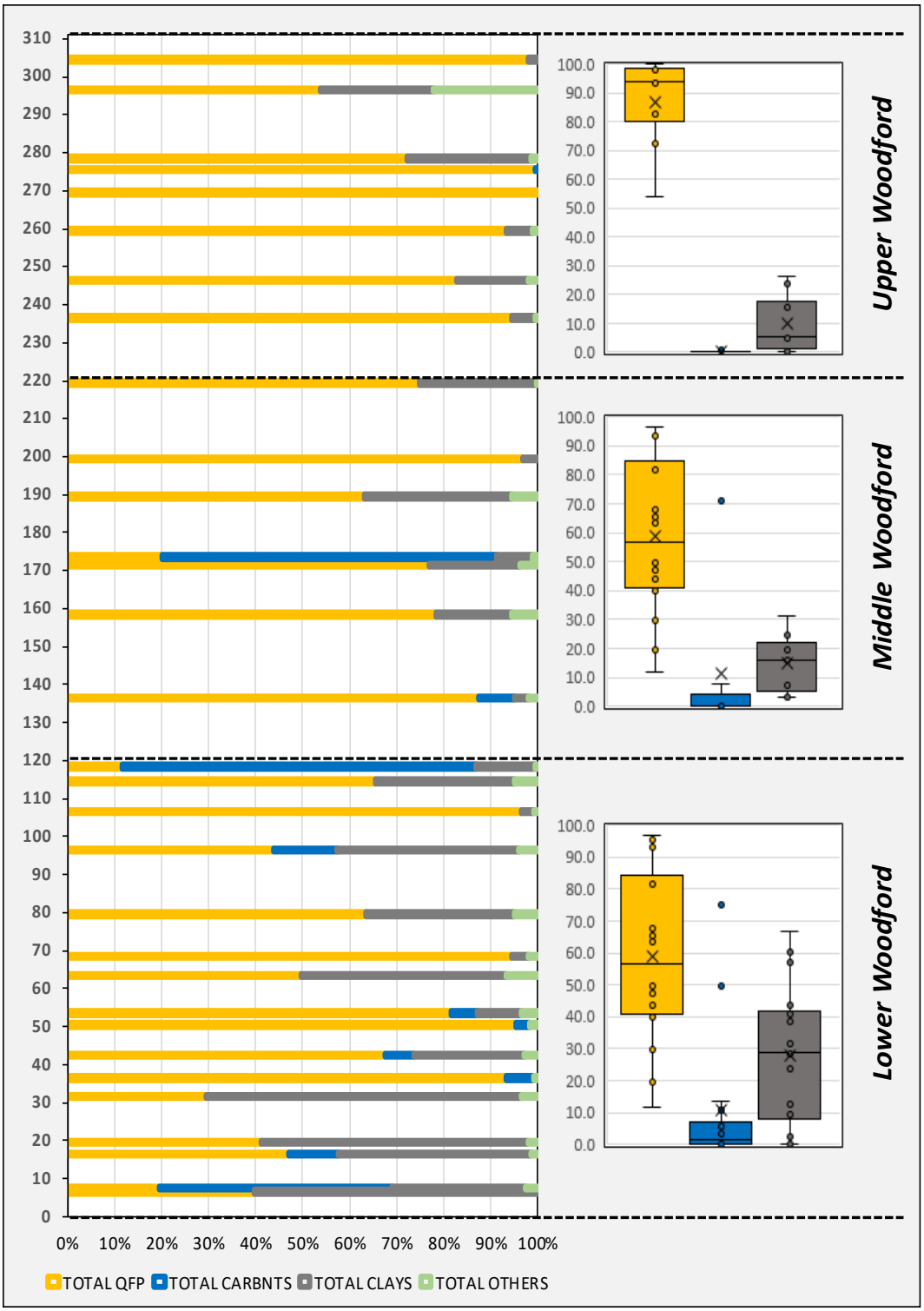

Figure 30. Bulk rock mineralogical composition plotted by Woodford members. In general, clay contents decrease upward, while quartz contents increase upwards.

In regard to the hard and soft rock types, it has been stressed their weathering responses in Woodford Shale outcrops, which are very distinctive and highly contrasting at the bed scale (Figure 7); supporting such observation, when mineralogical composition is plotted by rock type together, the two distinctive populations stand out by themselves (Figure 31).

Mineralogically, hard beds are much richer in quartz (~94%) than the soft ones (~57%); clay contents in soft beds appear to be about four times higher than in the hard beds (Figure 31). Therefore, given the quite discrete and sharp compositional boundaries between hard and soft beds, it might be beneficial sampling into two rock types in the field, so that the rhythmic nature of the Woodford Shale can be also preserved in lab results. Similarly, Comer and Hinch (1987) and Fishman et al. (2013) found that much of the geochemical and petrophysical heterogeneities in the Woodford Shale may be captured by using this couplet of rock types.

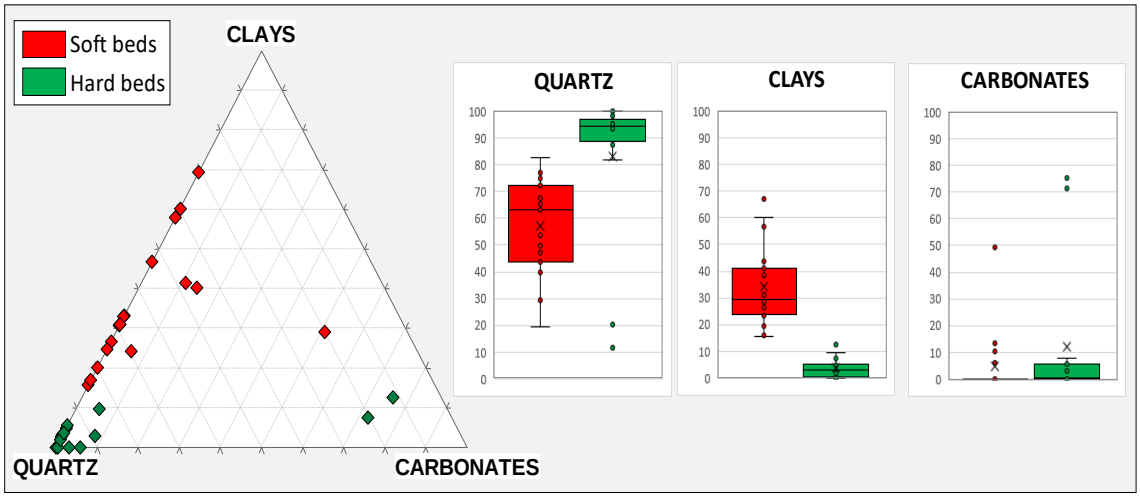

Figure 31. Bulk rock mineralogical composition plotted by rock types based on weathering responses in outcrops, as hard and soft beds. The differentiation between soft and hard beds confirm the highly contrasting mineralogical composition of these two rock types.

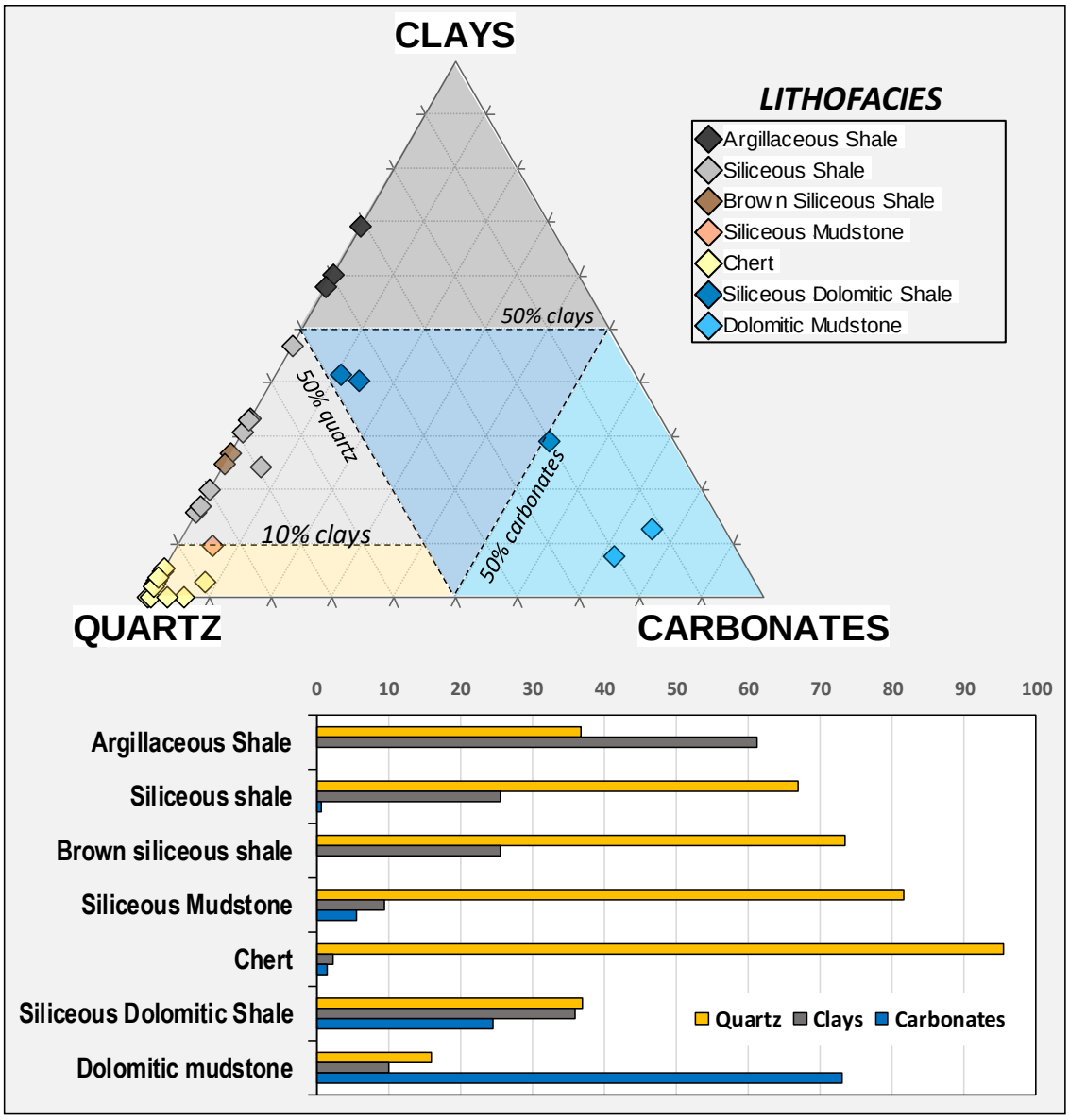

Figure 32. Ternary diagram for identification of Woodford Shale lithofacies based on mineralogical proportions of quartz, clays and carbonates. Bar chart below shows mineralogical admixture and their proportions per each lithofacies.

When plotted by lithofacies, distributions of quartz, clays and carbonates revealed that there are almost unique combinations between these three minerals per each lithofacies (Figure 32). It is noted that Argillaceous Shales present the highest clays contents (~60%), Cherts the highest quartz amounts (~95%), and Dolomitic Mudstones

the highest carbonate contents (~72%) (Figure 32). The more mixed lithofacies, such as the Siliceous Shales, are made of quartz (~70%) and clays (~25%) but with no carbonates; Siliceous Mudstones are made of quartz (~82%), clays (~10%) and carbonates (~5%), and finally the Siliceous-Dolomitic Shales that are made of about one third quartz, one third clays and one third carbonates (Figure 32).

Finally, mineralogical results are compared with organic richness (TOC), and we found a positive relationship between clay contents and TOC (Figure 33), meaning that within the Woodford Shale, most of the highest TOC contents (>6 wt.%) are hosted within clay-rich beds. And inversely, it is found that quartz-rich beds tend to present lower TOC contents (<6 wt.%). This observation was supported by visual observations of thin sections, as is the case of the Argillaceous and Siliceous Shales (Figure 21 and Figure 22), where the very dark colored matrix might be indicative of the high organic contents. Similarly, Comer and Hinch (1987), Fishman et al. (2013) and Becerra-Rondon (2017), using similar cross plots between minerals and TOC, concluded that, clay-rich beds are most prone to contain the higher TOC contents.

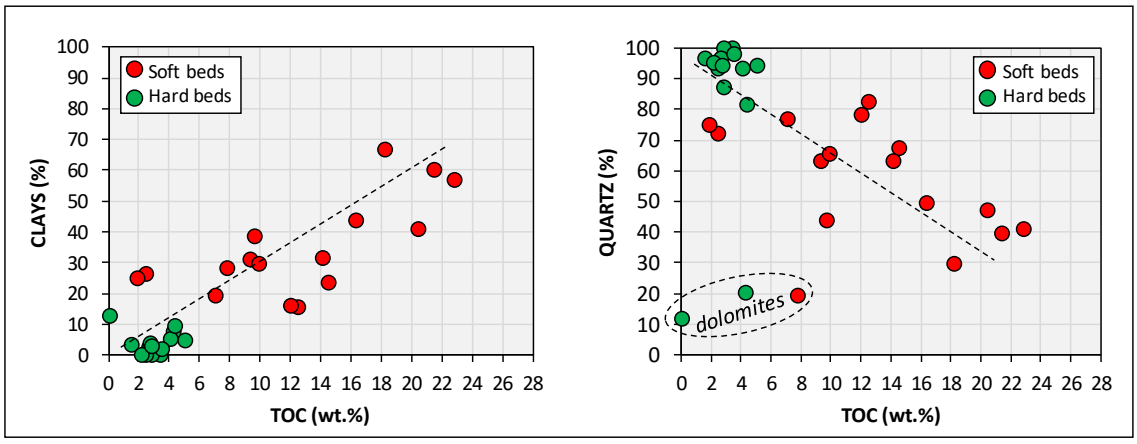

Figure 33. Mineralogy versus organic richness (TOC). Clay contents positively correlate with TOC, while quartz inversely correlates with TOC. Outlier points in the left plot corresponds with dolomitic beds, which have low TOC and low quartz.

4. ORGANIC GEOCHEMISTRY

Results of source rock characterization were addressed according to guidelines in Tissot and Welte (1984), Peters and Cassa (1994), and Jarvie et al. (2007). Organic richness and source rock quality was assessed via TOC-Leco and Rock-Eval pyrolysis respectively.

4.1. Organic Richness

Within high-frequency interbedded strata as is the Woodford Shale and other shale resources, TOC values should be interpreted with caution. Particularly, in this work it was found significant variations in TOC's and other geochemical parameters that are anomalously related to high-frequency stratigraphic and lithological controls (mostly at the bed scale). Preliminarily, I hypothesized that almost regardless of the stratigraphic position, similar rock types either found within the lower, middle or upper members, these would present very similar TOC contents no matter its location within the informal Woodford subdivisions, as evidenced by TOC values greater than 8 wt.% for the upper Woodford, which is a member known for much lower organic richness.

Comer and Hinch (1987), Kirkland et al. (1992) and Roberts and Mitterer (1992) noted that as well; they studied outcrop samples of the Woodford Shale and found that kerogen type and levels of thermal maturity were analytically the same; however, TOC concentrations in cherts and shales were markedly dissimilar. They explained the lower TOC contents in cherts due to dilution of organics caused by syn-deposition of biogenic silica, also suggested that shales over cherts might have 2.5 times more TOC concentrations (Roberts and Mitterer, 1992).

Across the entire Woodford Shale of this study, present-day TOC contents indicate this is a very good to excellent hydrocarbon source rock, values oscillate from 0.095 to 30.20 wt.% TOC (SD ±5.63), with averages of 12.02 wt.% and 3.33 wt.% for soft and hard beds respectively (Figure 34).

Traditionally, good correlations are anticipated between gamma ray and TOC. However, from in this work, vertical profiles and cross-plots revealed weak correlations between gamma ray and TOC (Figure 35). While quite anomalous the non-correlation between these two variables, this should be expected in outcrop studies; particularly in the Woodford Shale, given its high-frequency interlayering of soft (TOC ~12.02 wt.%) and hard (TOC ~3.33 wt.%) beds (Figure 34). What an actual radioactivity measurement represents is the cumulative response of U, Th, and K from all soft and all hard beds contained within the diameter of investigation of the detector. Thus, gamma ray would not correlate one-to-one with TOC unless a TOC value per foot accounts for the fraction of soft over hard within one foot. Indeed, the only case in which a direct one-to-one relationship can be seen between TOC and gamma ray is where the entire foot has the same gross lithology (i.e. 100% shale). Then one could assume that all the radioactivity response is due to a single lithology with homogeneous TOC in that foot. Connock (2015) recognized in cores samples the same complexity of vertical variability in TOC contents within the Woodford Shale, noticing TOC values oscillating between 10 to 5 wt.% in less than 1.5 ft.

The process of converting values from the bed-scale to 1-foot scale (comparable to well logs) is known as upscaling, and will be presented in Becerra-Rondon (2017).

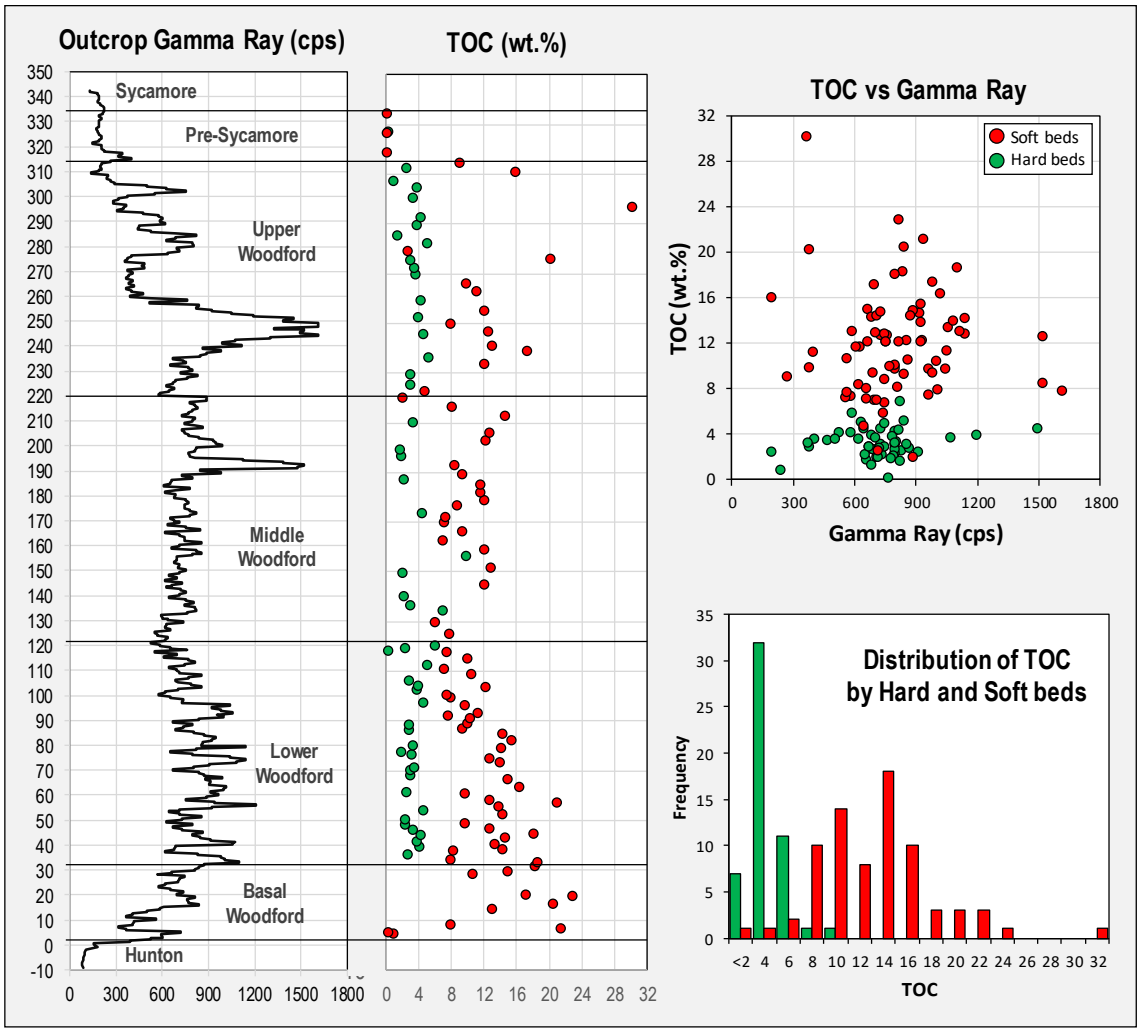

Figure 34. Organic richness as determined by TOC contents. Vertical profiles and histograms of TOC revealed two very distinctive populations of soft and hard beds. A TOC cutoff of about 6 wt.% represent the separation between these two rock types. Correlation of TOC with gamma ray is weak and may be influenced by the typical high-frequency intercalation of organic-rich and organic-poor beds. TOC values greater than 8 wt.% can be found even at high stratigraphic positions in the upper Woodford.

In terms of the informal Woodford subdivision, the lower Woodford member presents the highest average TOC contents (9.39 wt%) (Figure 35), where the maxima (16-24 wt.%) occur within the lowermost 40 ft of the interval, and then evidences a decreasing upward trend in organic richness, reaching its minimum mean values (~5

wt.%) at around the contact with its overlying middle member (Figure 34). Standard deviation within the lower member is ±5.72, indicating TOC values broadly spread from the mean.

The middle Woodford member has an average TOC of 7.43 wt.%. and presents the lowest standard deviation (±3.99). Internally, it reveals an overall constant range from about 2 to 14 wt.% (Figure 34). Interestingly, hard beds within this middle member reach their maximum values (8-10 wt.%) among the entire Woodford members (Figure 34 and Figure 35).

The upper Woodford member presents the broader range of TOC values within the entire Woodford, with a standard deviation of ±6.58 and a range from 0.86 to 30.2 wt.% (Figure 35). This member is the most variable in terms of TOC. At the base of the interval values range from about 4 to 14 wt.%, and then around the upper half, TOC values increase excessively reaching up to 30 wt.% (Figure 34**).**

In particular, within this upper interval, it is noted that at around 240-250 ft exist a super high radioactivity zone. However, the TOC contents across this zone do not depict the same high radioactivity trend (Figure 34**),** thus implying that radioactivity is not only affected by uranium associated to organic contents, but also should be affected by the presence of phosphates, which also concentrate significant uranium contents and affects radioactivity readings (Swanson, 1961).

Furthermore, when looking together the higher production index (PI>0.1) and the early mature Tmax values (436°C) (Figure 36), it can be suggested that the anomalous high TOC values of the upper Member might be associated with bitumen contamination perhaps migrated from nearby strata. Supporting this observation, normalized oil

contents normalized oil content (S1/TOC>50), shows anomalous high values across this entire upper Woodford (Figure 36), therefore the conclusion is that measured TOC contents of the upper Woodford member are accounting not only for kerogen, but also a significant contribution comes also from bitumen.

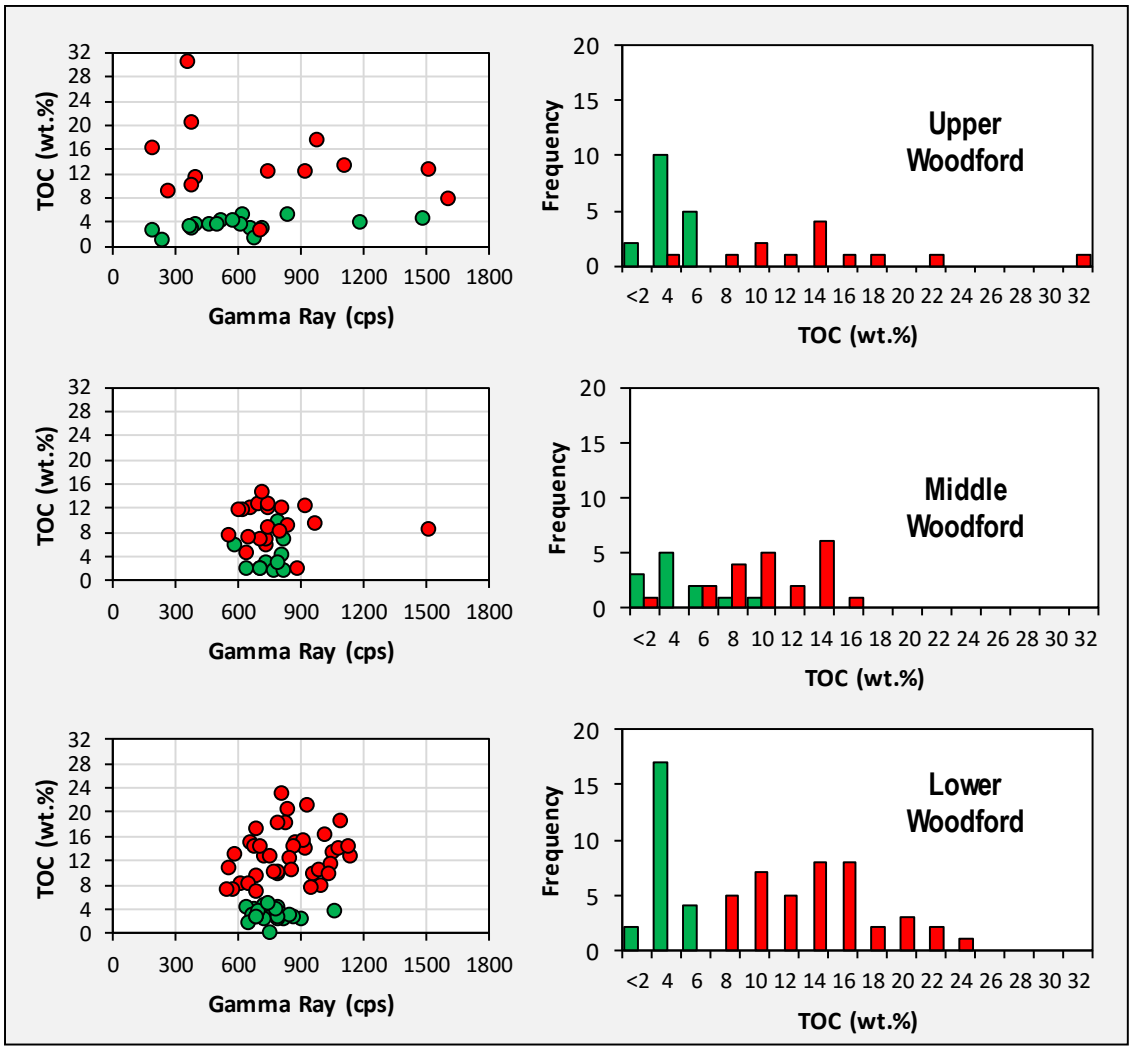

Figure 35. Distribution of TOC contents across Woodford members. Lower and middle members show narrower distributions, whereas the upper member shows a wider distribution most likely affected by bitumen which yields high TOC values. The comparison between TOC and gamma ray is made in order to demonstrate that high TOC values are not always indicative of high gamma ray. Rather, it should be considered other radioactive components in the upper Woodford such as phosphatic particles, which also increase the total gamma ray responses.

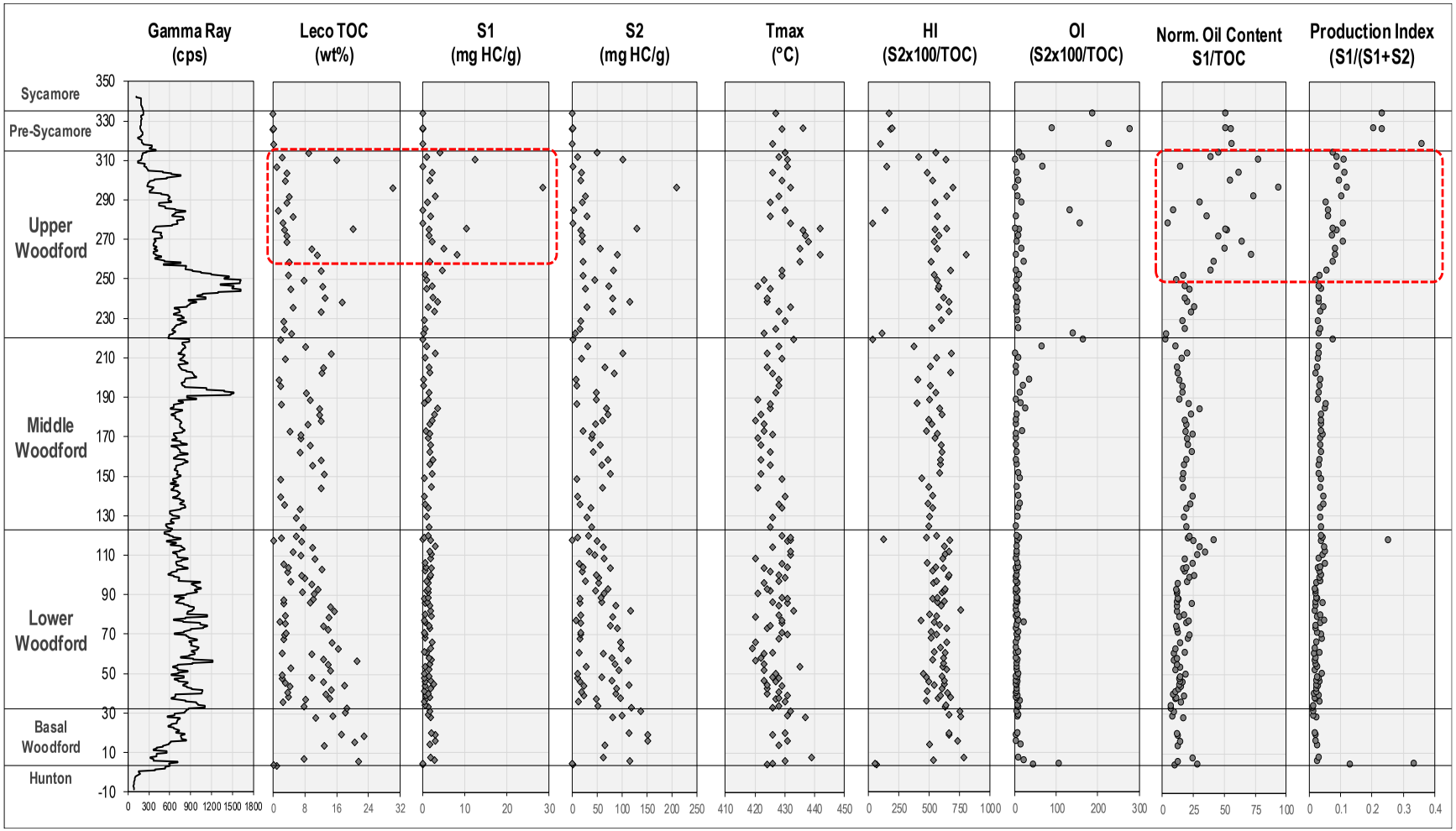

Figure 36. Ge
contamination f
about 436°C (ea

When compared with mineralogical composition and lithofacies, the higher TOC contents in the Woodford Shale occurred associated with clay-rich lithofacies (Figure 37). About 96% of samples with TOC values greater than 8 wt.%, were identified as Argillaceous, Siliceous or Dolomitic shales, which are lithofacies that contain more than about 15% clay minerals.

In general, throughout the Woodford Shale there is a positive relationship between clay contents and TOC (Figure 37). While still high in TOC, quartz-rich lithofacies of Cherts and Siliceous Mudstones tend to correlate negatively with TOC contents (Figure 37). Most of the samples with quartz contents greater than 80%, have TOC concentrations on average of 4.0 wt.% (Figure 37). Carbonate contents do not show a clear trend with TOC (Figure 37). However, when TOC is compared with the most dolomitic lithofacies (Dolomitic Mudstone), their TOC contents are less than 5.0 wt.%. This suggests that higher carbonate contents might be inversely related with TOC contents; this was visually confirmed via petrographic analyses, where samples with a more intense dolomitized matrix (coarser mosaics of crystals), the general mudstone appearance is much cleaner showing less visible dark organic material (Figure 27).

Summarizing, within the Woodford Shale at the Speake Ranch section the higher TOC contents tend to correlate with clay-rich beds, and independently from its stratigraphic position, clay-rich beds (clays>20%) are most likely to present TOC contents greater than 6 or 8 wt.%. Roughly speaking, a clay-rich bed within the Woodford contain 3 times more TOC than a quartz-rich bed. Even between adjacent beds, an argillaceous shale can be 3 times more organic rich than an adjacent chert bed.

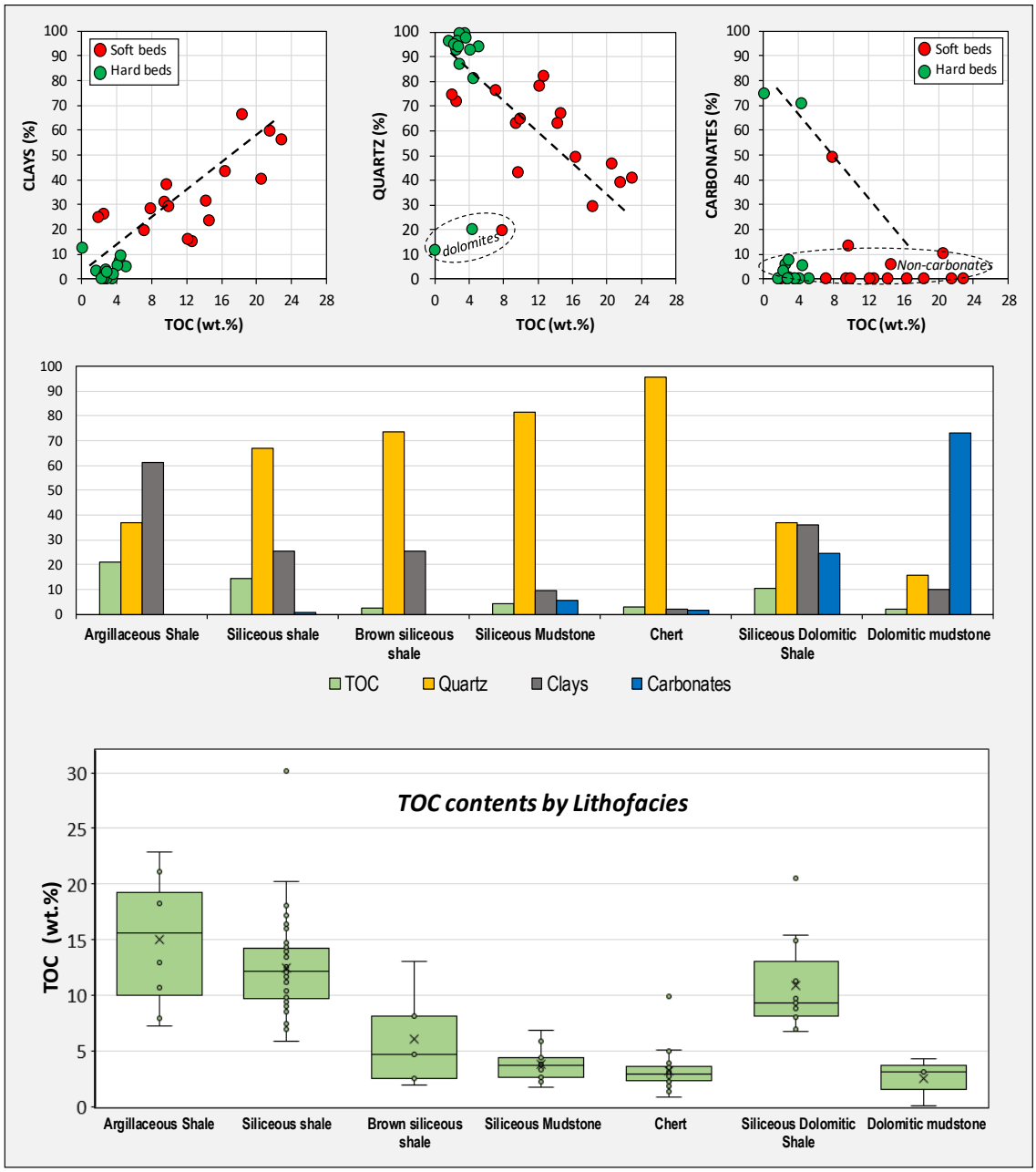

Figure 37. TOC contents plotted by lithofacies and mineralogy. Generally higher TOC contents coexist with clay-rich lithofacies (clays>15%). The higher the quartz, the lower the TOC, as evidenced by the lithofacies of Cherts, where quartz contents are maximum and TOC may be below 4%. Box plots of TOC by lithofacies show that lithofacies of shales (either Argillaceous, Siliceous or Dolomitic) present TOC contents greater than 6 wt.%.

4.2. Kerogen Type

Organic matter quality was assessed from parameters obtained from Rock-Eval Pyrolysis. Hydrogen Index (HI) and Oxygen Index (OI) are parameters derived from S2 and S3 peaks respectively. When plotted in a pseudo van-Krevelen diagram they can be used to determine kerogen type (Tissot and Welte, 1984). Figure 38 is a plot of HI versus OI for the informal Woodford members, and reveals that most samples contain very high HI (420 to 760 mgHC/gCOT) and low OI (<20 mgCO2/gCOT), and fall within the range of Type I to II kerogen (oil prone) (Figure 38). Points that plot between the range of Type II and III, with low HI (<200 mgHC/gCOT) and high OI (>60 mgCO2/gCOT), are interpreted as outliers either due to their carbonate-rich content or recent weathering, which apparently yields erroneous OI values. To overcome the biased effect of OI values, Langford and Blanc-Valleron (1990) and Cornford et al. (1998) proposed a more reliable plot relating S2 versus TOC in order to determine kerogen type. In such a plot the slopes represent the HI translated into kerogen types (Figure 38). Using Cornford's template, data points from this study outlined a well-defined trend corresponding to Type II kerogen (marine origin, oil prone) (Figure 38). Looking closer at kerogen types from each Woodford member, there is no evidence of segregation of kerogen types by members; instead the three of them appear scattered as a single cloud (Figure 38). This observation might be indicative of a common organic precursor or similar organofacies throughout the section. In recent contributions by Wang (2016) about kerogen types and organofacies of the Woodford Shale in Oklahoma, he concluded that overall the Woodford shale corresponds to a typical 'organofacies B' in the classification scheme of Pepper and Corvi (1995), which can be supported by the coexistence of siliceous-, clay-

rich, non-calcareous marine shales with low-to-moderate sulfur concentrations. Summarizing, kerogen quality of this work indicates a Type II kerogen for the entire Woodford section, agreeing with recent contributions of Nowaczewski (2011), Miceli-Romero and Philp (2012), Serna-Bernal (2013), Connock (2015), Wang (2016), and Villalba (2016).

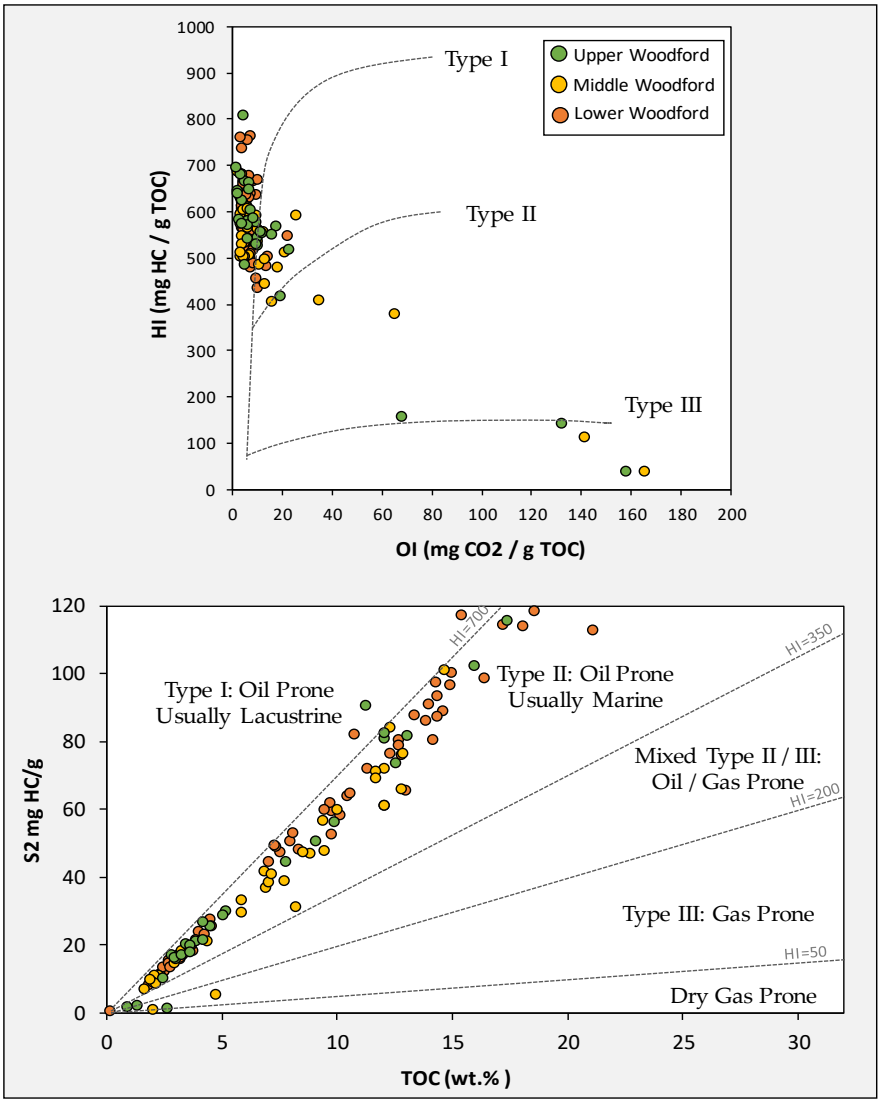

Figure 38. Kerogen type as determined by pyrolysis Rock-Eval parameters. Upper plot: Pseudo van Krevelen diagram for Woodford Shale samples suggest a mixture of Type I and II kerogen. Lower plot: Rock-Eval remaining hydrocarbon potential (S2) vs. TOC plot (Cornford et al., 1998), suggest a Type II kerogen for the entire Woodford.

4.3. Thermal Maturity

Thermal maturity of the Woodford Shale has been examined for many years, however the most complete and updated overview across different geological provinces of Oklahoma is by Cardott (2012, 2014). In particular, several vitrinite reflectance (%Ro) data points of outcrops samples are reported near the southern limb of the Arbuckle Mountains (Figure 40), ranging from 0.49 to 0.53% Ro (Cardott, 2012, 2014), which correspond with thermal maturity levels obtained in this study.

In this study, thermal maturity was first examined using parameters derived from Rock-Eval Pyrolysis. A cross plot of Tmax versus HI indicates that the Woodford Shale at the Speake Ranch Section is immature to early mature, with Tmax values from 419 to 442°C (mean 427°C) (Figure 39). A Tmax-based %Ro was calculated using the formula [%Ro=(0.0180xTmax)–7.16] (Jarvie et al., 2001). The calculated Ro values range from 0.38 to 0.79% Ro (mean 0.79% Ro). Finally, direct petrographic measurements of VRo% (provided by Cardott, 2017, written communication), revealed a mean random vitrinite reflectance of 0.60% Ro based on 40 measurements varying from 0.49-0.72%. Thus, both the Tmax-based %Ro and the measured %Ro suggest that thermal maturity of this Woodford section fits into the range of immature to early oil window. The low levels of thermal maturity can be attributed to tectonic uplift of the Arbuckle Mountains during the Pennsylvanian (Ham et al., 1973). Just southward to the area of study, thermal maturity seems to increase following the structural trends of the Ardmore Basin (Figure 40), oscillating from immature (0.49% Ro) in the northern part, up to dry-gas (2.45% Ro) in the deepest areas (~15,000 ft) (Cardott, 2012).

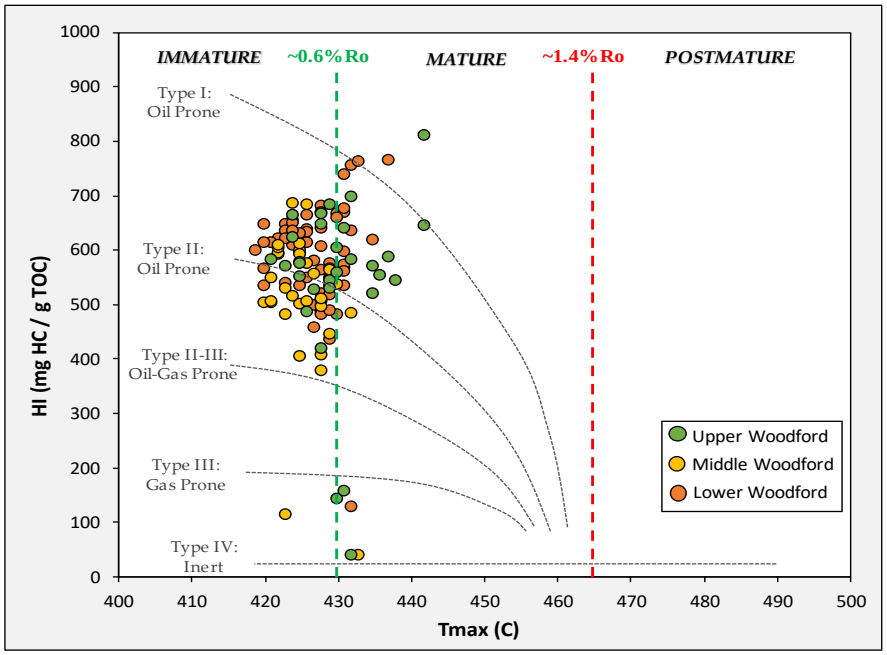

Figure 39. Kerogen type and maturity assessment via integration of HI and Tmax data.

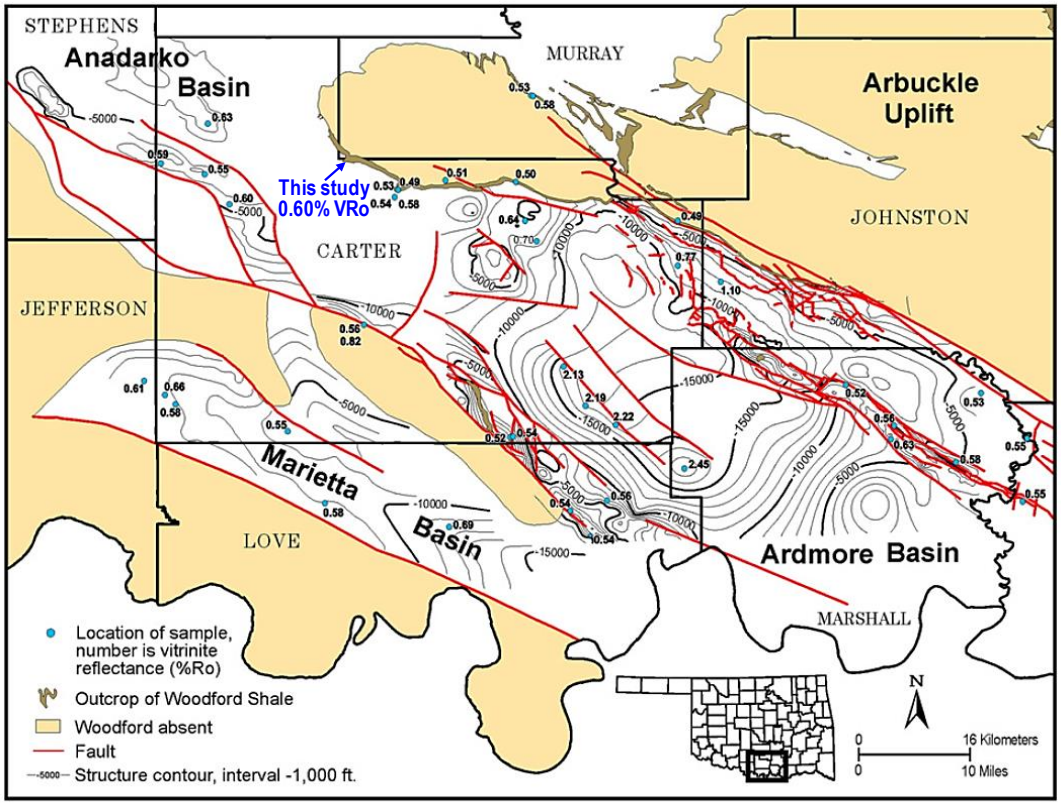

Figure 40. Vitrinite reflectance distribution in south-central Oklahoma. %Ro from this study is in the range of immature to early oil window (Basemap from Cardott, 2012, %VRo of this study was measured by Brian Cardott, 2017, written communication).

5. ELEMENTAL CHEMOSTRATIGRAPHY

Since vertical heterogeneities of the Woodford Shale at Speake Ranch outcrop are mostly represented by intercalations of hard and soft beds (Figure 7), two samples per foot were collected and analyzed in order to record such stratigraphic variability.

Commonly, aluminum (Al) is used as a proxy for fine-grained detrital sediments due to its low solubility and high stability under diagenetic and other environmental conditions (Dean and Arthurw, 1998). Because of this Al was used as the common abscissa for cross-plots between elements, allowing the distinction between quartz-rich (depleted in Al) and clay-rich (enriched in Al) beds. Also, to synthetize the presentation of results, elements were grouped into three categories based on their uses for interpretations: 1) detrital-sensitive elements (Al, K, Ti, Zr, Rb, Th, Si). 2) carbonate-sensitive elements (Ca, Mg, Mn, Sr), and 3) redox-sensitive elements (Mo, V, U, S).

5.1. Detrital-sensitive elements

Owing to the high chemical stability, Al is commonly associated with the detrital fraction of fine-grained sediments. Also, Al is the main proxy for clay minerals in hemipelagic rocks as it is quite stable during diagenesis (Calvert & Pedersen, 1993; Dean and Arthur, 1998; Sageman & Lyons, 2004; Tribovillard et al., 2006).

K occur associated with clay minerals of the illite group and/or related sub-products of K-feldespar (Weedon and Shackleton, 1997; Sageman and Lyons, 2004).

In marine shales, Ti and Zr generally occur at much lower concentrations than Al; however, due to their high stability under diagenetic conditions, these are very useful

proxies for continentally derived sediments (Bhatia and Crook, 1986; Sageman and Lyons, 2004).

Rb is one element that does not form any minerals of its own; instead it is present in minerals substituting for other elements of similar ionic radius such as K, which is commonly associated with illite and micas (Wedepohl, 1971).

In mudrocks Si can be found related to a variety of silicate minerals (e.g. quartz, feldspars) and phyllosilicates (e.g. clays, micas) (Pearce and Jarvis, 1992; Pearce et al., 1999, Brumsack, 2006). Its use is more meaningful in the form of a Si/Al ratio; this ratio basically diminishes the Si signal in clays while enhances the signal of quartz (Turner, 2016). Excesses in concentrations of Si/Al may indicate high biogenic or authigenic input within the system (Sageman and Lyons, 2004; Rowe et al, 2008; Ross and Bustin, 2009). Cross-plots of detrital sensitive elements with Al allow to infer whether an element is associated with detrital input or not, from which a positive correlation suggests detrital provenance whereas negative indicates either authigenic or biogenic origin (Tribovillard et al., 2006).

In this work, positive correlations were obtained from cross-plots of detrital-sensitive elements with Al (Figure 41), implying that the coexistence of higher concentrations of Ti, K, Rb, Zr, Th are of detrital affinity within the Woodford strata.

Remarkable observations from Figure 41 are the well-defined segregation between hard and soft beds. Hard beds are characterized by low concentrations of detrital-sensitive elements (Al, Ti, K, Rb, Zr, Th) along with an excess of Si over Al, which together suggest that hard beds within the Woodford Shale are more of biogenic/authigenic affinity. Soft beds on the other hand present higher concentrations

of Al, Ti, K, Rb, Zr, Th and moderate to low Si concentrations, which suggest that soft beds within the Woodford contain more detrital-derived sediments (without excluding the combination of authigenic plus detrital).

These previous observations fall in accordance with our petrographic results, where the higher contents of biogenic particles (radiolarian and spicules) are more evident within lithofacies of Cherts and Siliceous Mudstones (Figure 25 and Figure 24), whereas the higher contents of detritus (silt-sized quartz) occur within the lithofacies of Argillaceous and Siliceous Shales (Figure 21 and Figure 22).

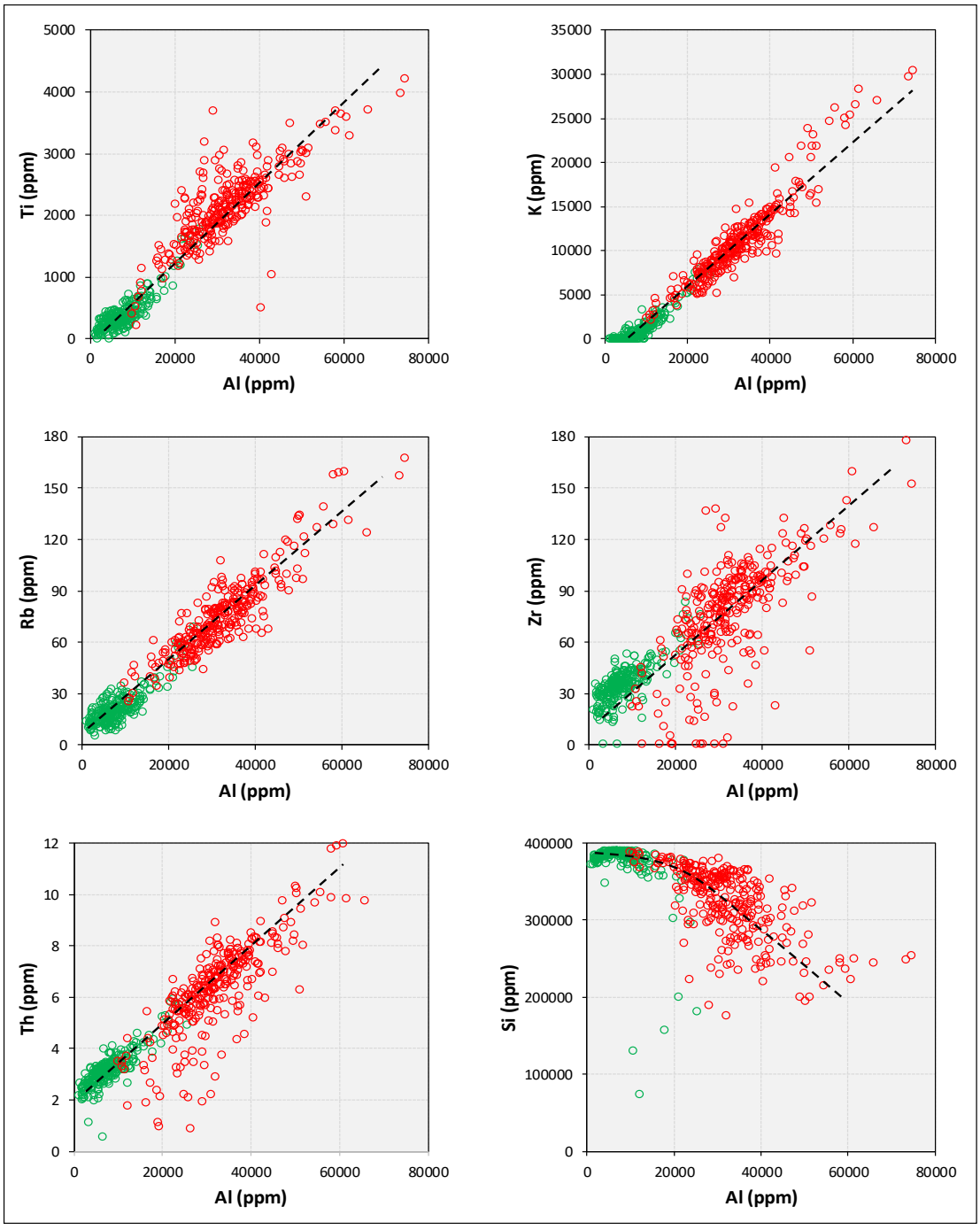

Figure 41. Cross plots of detrital-sensitive elements differentiated by hard (green dots) and soft (red dots) beds. Ti, Zr, K, Rb and Th all together show positive covariance with Al, and suggest a dominance of detrital input in soft beds over the hard ones. Hard beds, on the other hand, reveal an excess of Si over Al, along with minor concentrations of Ti, Zr, K, Rb and Th, thus suggesting a more authigenic or biogenic origin of hard beds. The segregation of data points into soft and hard samples confirms the importance of distinguishing these two rock types in the field, as they record much of the stratigraphic heterogeneities at the bed scale.

5.2. Carbonate-Sensitive Elements

Ca, Mg, Mn and Sr commonly coexist within carbonate minerals in the majority of black shale deposits (Vine and Tourtelot, 1970; Brumsack, 2006).

Ca is present in high concentrations in several minerals including calcite, dolomite, anhydrite and gypsum. But also, it can occur within in phosphates, feldspars, and clay minerals. Mg is a major constituent of silicates, carbonates, sulphates, phosphates and borates (Salminen et al., 2005). However, usually enrichments of Mg are strongly related to dolomite (Wedepohl, 1971). Despite its easy mobility, Mn is related with Ca and Sr, and usually occurs substituting Fe in dolomite to form ankerite (Brumsack, 1989; Calvert and Pedersen, 1993; Hild and Brumsack, 1998). Sr may be related to a variety of rock forming minerals including feldspars, gypsum, calcite and dolomite (Salminen et al., 2005). In ancient sedimentary environments, Sr is related to precipitates of aragonite and its transformation into primary calcite, which might imply the presence of skeletal particles or allochems (Katz, et al., 1972). Sr can occur within phosphatic deposits as is the case of phosphate nodules of the Woodford Shale, which are enriched in Sr (Siy, 1988).

From this work, it is worth mentioning that overall in the Woodford shale at the Speake Ranch section, the signals for Ca, Mg, Mn and Sr were extremely weak. Putting numbers into context for this study, truly carbonate-rich samples confirmed by XRD (carbonates >50%) typically contains: Ca>30000 ppm, Mg>15000 ppm, Mn>500 ppm and Sr>200 ppm. In about 98% of Woodford samples these signals plotted way below the threshold values (Figure 42), thus making only few samples useful for interpretations based on their carbonate proxies. This finding basically confirms that mudrock strata of

the Woodford Shale at Speake Ranch outcrop are not the case of calcareous-siliceous-argillaceous deposits. Instead they are predominantly siliceous-argillaceous, and mineralogically speaking should be considered a nearly carbonate clean formation, as well evidenced by the dolomitic beds that account for less than 7% of the total lithofacies across the section (Figure 9).

Cross-plots of carbonate-sensitive elements reveal a good inverse relationship between Ca, Mg, and Mn with Al (Figure 42). Assuming that in the Woodford Shale, aluminum-rich beds are regarded as being of detrital affinity (Figure 41), the negative correlation between Al with Ca, Mg, and Mn, might discard the detrital origin of carbonates within the Woodford Shale (Figure 42). Rather, petrographic observations suggest more of a diagenetic or authigenic origin for dolomites instead of detrital origin, as evidenced by the presence of euhedral dolomite rhombs forming micro-mosaics with some relicts of the precursor shale fabric (Figure 26 and Figure 27).

The clear positive correlations between Ca versus Mg and Ca versus Mn (Figure 42), suggest that within the Woodford Shale most of the carbonates are also enriched in Mg and Mn together, confirming the typical abundant occurrence of dolomite and ankerite within the calcareous beds, as evidenced by the bulk XRD mineralogy results, where calcite does not occur within the shale matrix, but instead dolomite/ankerite make up the majority of the carbonate minerals in the matrix. In the Woodford Shale of this study, the only cases of calcite alone without dolomite/ankerite (or Ca without Mg or Mn) is as fillings of veins and concretions.

In regard to Sr, as anticipated it positively correlates with other carbonate proxies such as Ca, Mg, and Mn (Figure 43), and corroborates its affinity with dolomitic beds

across the Woodford Shale. However, besides that, it was observed a second important population of elevated Sr concentrations (Sr>200ppm) plotted along with very low concentrations of Mg and Mn (Figure 43). The most likely scenario for explaining the non-dolomitic source of the elevated Sr concentrations is the contribution from phosphate accumulations, as evidenced by the positive correlation between Sr and P (Figure 43). The non-dolomitic source of some elevated Sr concentrations is particularly valid for the upper Woodford member, where the phosphatic accumulations are typical not only in the form of nodules/concretions but also disseminated within the matrix of some siliceous shales. Thus, Sr in the Woodford Shale of this study is inferred to be partially in dolomite beds as well as in phosphates (restricted to the upper Woodford member).

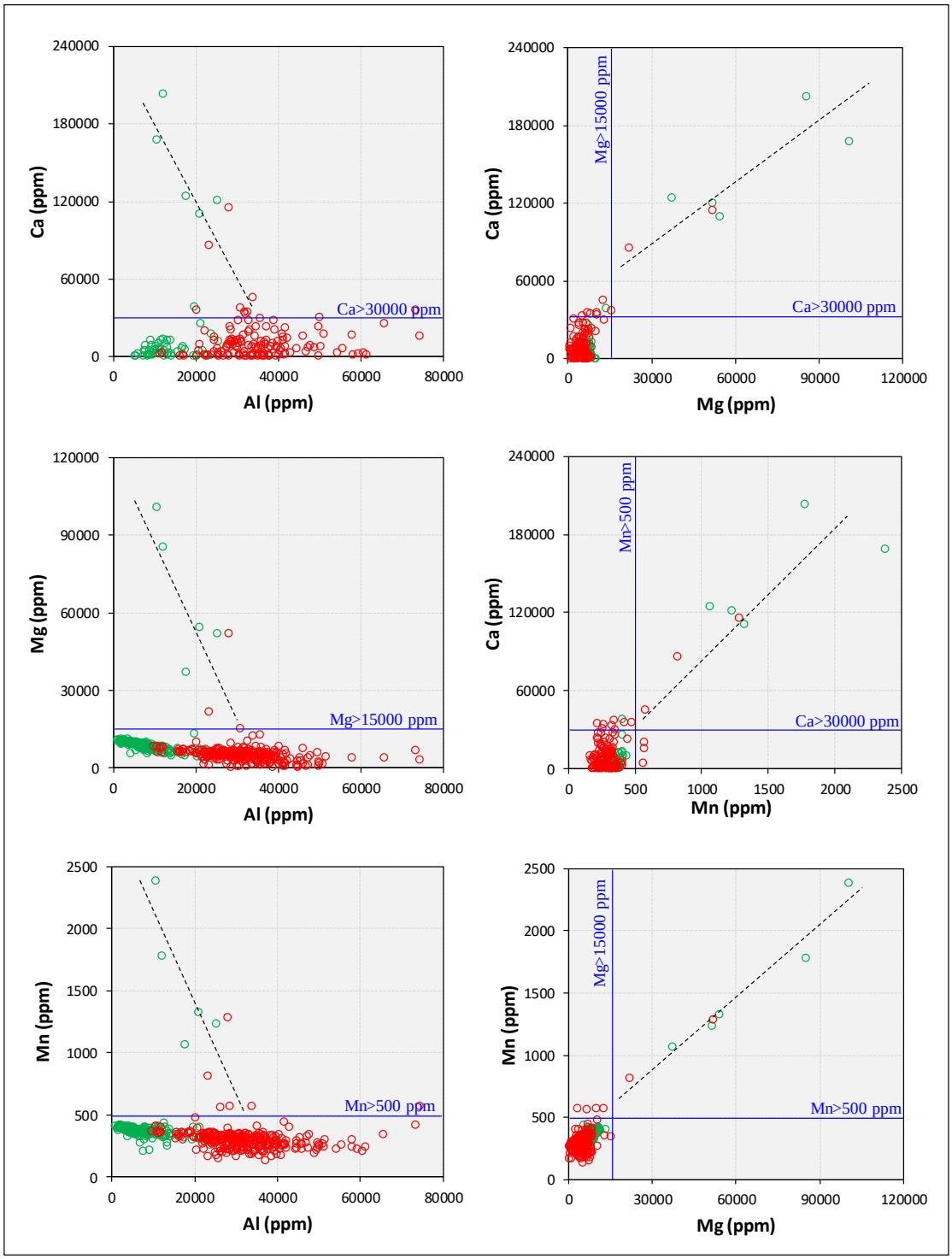

Figure 42. Cross plots of carbonate-sensitive elements differentiated by hard (green dots) and soft (red dots) beds. Carbonate proxies together Mg and Mn versus Ca confirms a dolomitic origin. Blue dashed lines correspond to our identified cutoff for carbonate-rich (dolomite>50%) samples, and below these values, signals of Ca, Mg, Mn, and Sr are considered background.

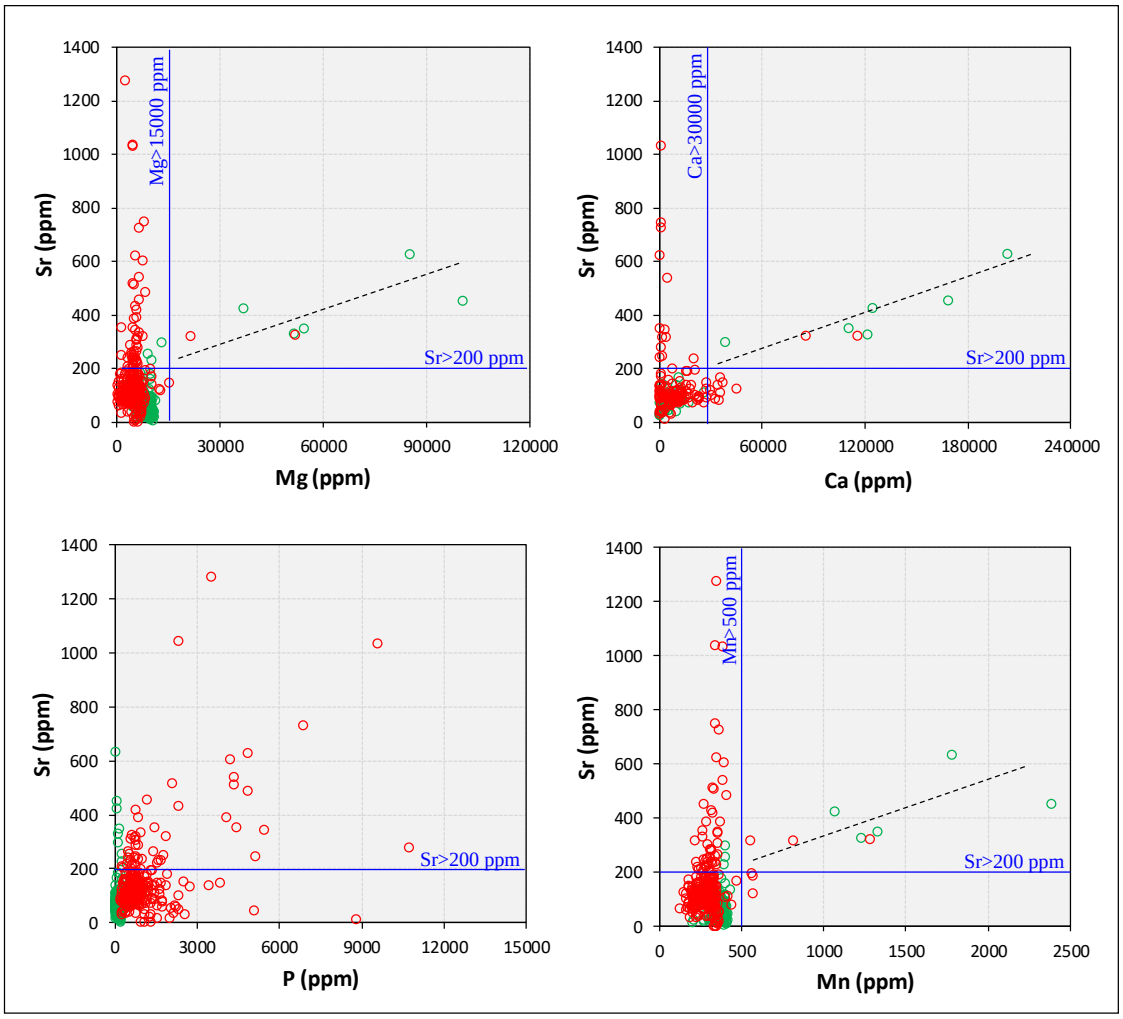

Figure 43. Cross plots of Sr versus carbonate-sensitive elements differentiated by hard (green dots) and soft (red dots) beds. The good positive correlation between Sr with Mg, Ca and Mn suggest in part the affiliation of elevated Sr with dolomite beds. Sr versus P partially support the association of high Sr concentrations with phosphates. Blue dashed lines correspond to our identified cutoff for carbonate-rich (dolomite>50%) samples, and below these values, signals of Ca, Mg, Mn, and Sr are considered background.

5.3. Redox-Sensitive Elements

Molybdenum (Mo), lacking of chemical reactivity under oxic conditions, is the most useful proxy for organic matter concentrations (Brumsack, 1989; Calvert and

Pedersen, 1993; Algeo and Maynard, 2004; Tribovillard et al., 2006). The fixation of Mo takes place in the sedimentary column close to the sediment-water interface. High Mo concentrations may indicate low sedimentation rates, and when Mo is accompanied with sulfide minerals, anoxic to euxinic conditions can be inferred (Brumsack, 1989).

In this work, positive covariance was obtained from cross plots of Mo versus TOC and Mo versus S (Figure 44), from which generalized anoxic-euxinic deposition accompanied by high levels of sulfur in the Woodford Shale is suggested. Also, generally soft beds (shales) are interpreted to be relatively more anoxic-euxinic than hard beds (cherts) based on the two well-defined populations in Figure 44.

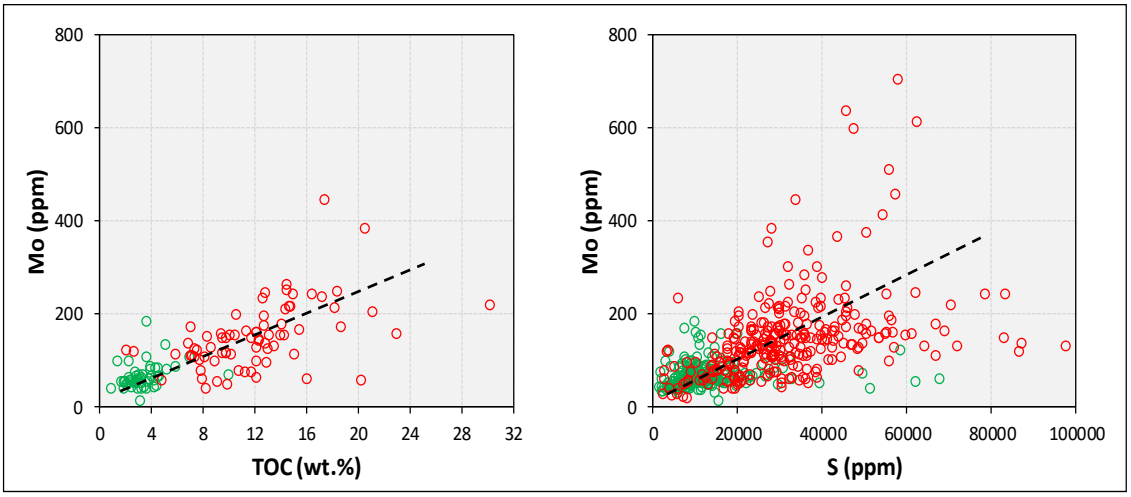

Figure 44. Cross plots of Molybdenum versus TOC and sulfur. Anoxic-euxinic with high levels of sulfur can be interpreted for the organic-rich strata of the Woodford Shale. Soft beds (red dots) tend to present higher Mo, S and TOC contents.

A widely-used approach to estimate paleo-hydrographic settings in anoxic environments is suggested by Algeo and Lyons (2006) and Algeo and Rowe (2012). Their study of four modern anoxic marine basins related Mo and TOC to the degree of basin restriction. From more to less restricted, the four modern analogs in their analysis were

the Black Sea (eastern Europe and western Asia), Framvaren Fjord (Norway), Cariaco Basin (Venezuela) and the Saanitch Inlet (British Columbia).

Based on Mo-TOC relationships from this study and adopting trends of modern analogs from Algeo and Rowe (2012), we infer that the entire Woodford Shale most likely experienced similar hydrographic restrictions fluctuating between Cariaco Basin (less restricted) to Framvaren Fjord (more restricted) (Figure 45). Similarly, Turner (2016) also interpreted degrees of basin restriction between high to moderate for both the lower and middle Woodford members.

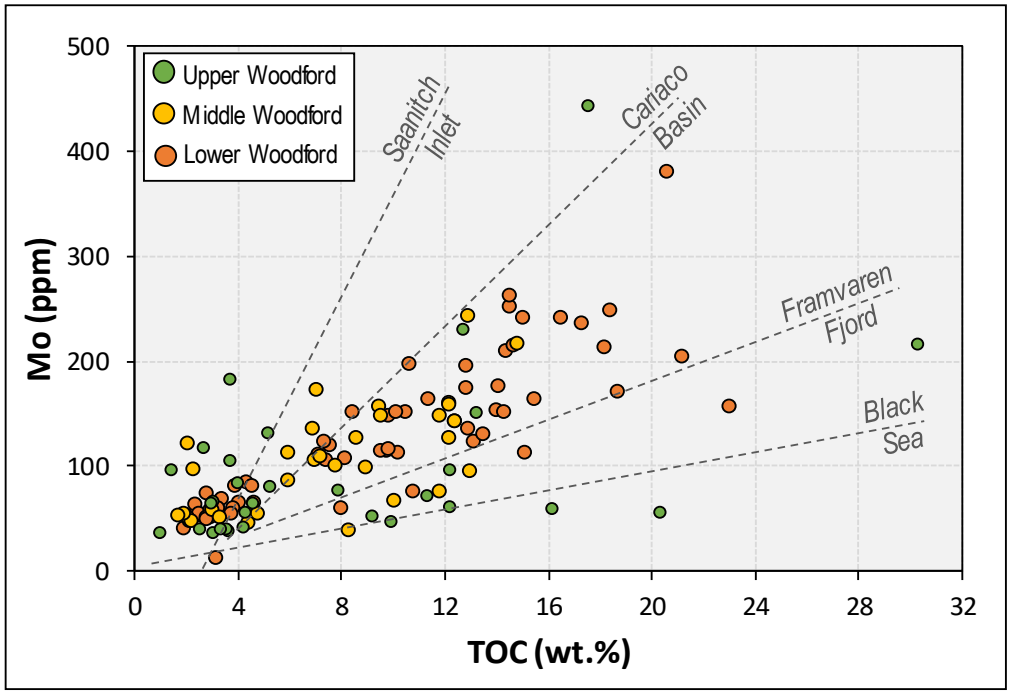

Figure 45. Cross plot of Mo versus TOC for interpreting degrees of basin restriction, adopting trends of modern analogs in Algeo and Rowe (2012).

Vanadium (V), though highly mobile under oxic conditions and burial diagenesis, is another redox-sensitive element chemically comparable to Mo (Calvert and Pedersen, 1993; Brumsack, 1989). However, since V is not trapped in solid solution by sulfide minerals, it cannot be a reliable indicator of sulphidic conditions or euxinia (Brumsack,

1989; Algeo and Maynard, 2004; Tribovillard et al., 2006). In the Woodford Shale of this study, cross plots of V versus TOC and Mo reveal weak but positive correlations mostly defined by the population of soft beds (Figure 46), implying a possible linkage of soft beds with more anoxic conditions compared with the conditions during deposition of hard beds (less V, Mo, and TOC).

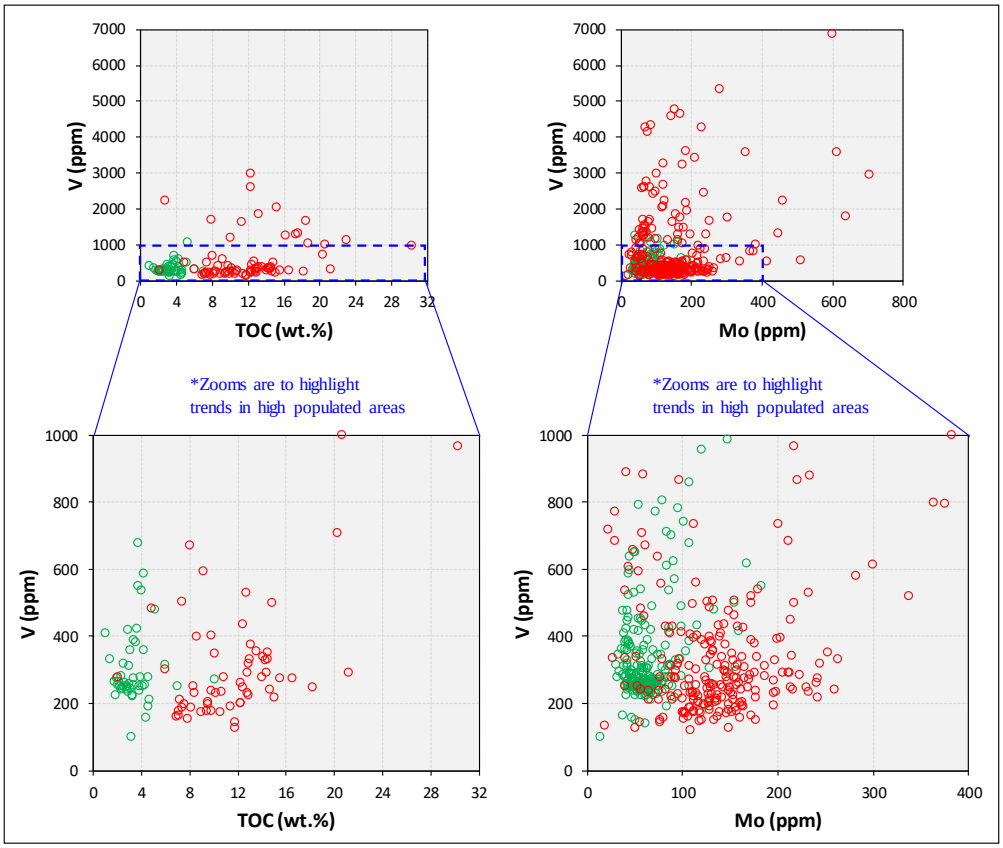

Figure 46. Cross plots of Vanadium versus TOC and Mo. Correlation between these variables is quite weak but positive, and it is particularly defined by data points of soft beds (red dots), confirming more anoxic conditions during the depositions of soft beds.

Uranium (U), commonly dissolved in sea waters, becomes absorbed and fixed within organic matter (Swanson, 1961; Calvert and Pedersen, 1993). It can also precipitate within sulfides and phosphates (Swanson, 1961). In anoxic basins, U enrichments are most likely to occur within sediments and not across the water column

(Algeo and Maynard, 2004; Tribovillard et al., 2006). Hence, a positive relationship can be obtained from U and organic matter, but not with bottom-water redox conditions. U can be easily remobilized or dissolved if oxygen reaches depths where U has accumulated (Tribovillard et al., 2006).

Anomalously to this study, cross plots of U versus TOC and Mo did not show clear positive correlations (Figure 47). Possibly, there is a stratigraphic control that conceals such expected direct relationships in cross-plots. For example, U signals from XRF are not only affected by organic matter (kerogen) but also by phosphates and bitumen, which are two extra components that also concentrate U particularly in the upper Woodford member. Whereas U enrichments of the middle and lower members are perhaps due to only organic matter. If correct, such an assumption would explain the outlier data points with elevated U and low TOC and Mo (Figure 47). To prove that, Figure 47 shows cross plots of U versus TOC and Mo but excluding the upper Woodford member which is the one that has the strongest affectation by phosphates and bitumen; as a result, plots show less dispersion and allows the definition of a positive trend between U-TOC and U-Mo. Thus, U might be a reliable proxy for redox conditions and organic richness in the lower and middle Woodford Shale, but not for the upper Woodford of this outcrop.

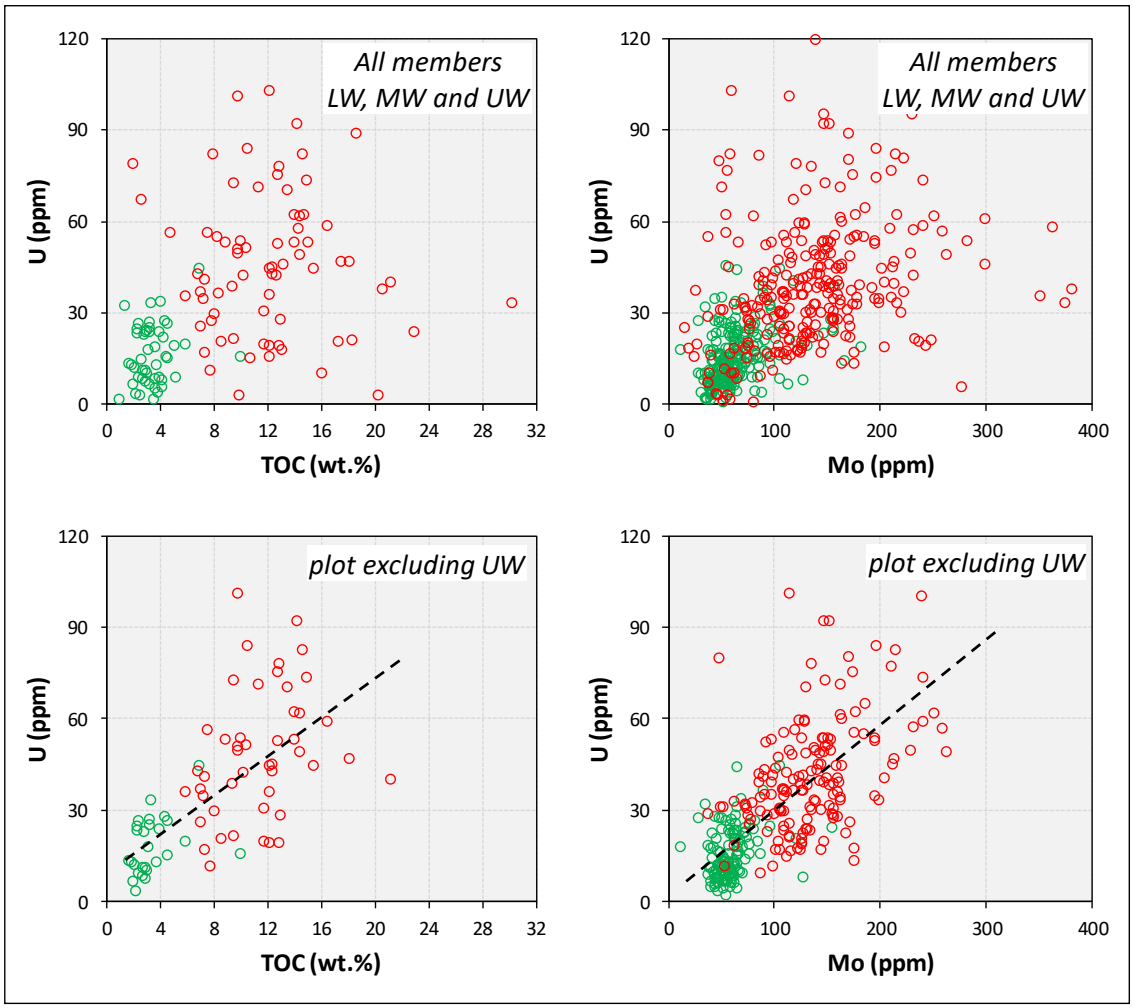

Figure 47. Cross plots of Uranium vs TOC and Mo. Correlations are very weak in the upper plots that corresponds with samples from all Woodford members. Lower plots on the other hand exclude samples from the upper Woodford (UW) and allow to highlight positive correlations between variables. Soft beds (red dots), hard beds (green dots).

5.4. Vertical Chemostratigraphic Zonation

Due to the large set of samples (n=560) and elemental proxies (n=12) distributed across the entire Woodford section, an approach based on hierarchical clustering analysis (HCA) was used to group elements based on their degree of similarity.

First, the input observations (samples) per each variable (elements) were standardized by subtracting the mean and dividing by the standard deviation. Then, inside the Minitab software, using the Euclidian distance and Ward's linkage method (Ward, 1963) seven clusters were identified based on the higher levels of similarity evidenced by a dendrogram, then for each sample (observation) an individual number of clusters from 1 to 6 was allocated to each sample. The output clusters have no geological meaning until an elemental enrichment and depletion ratio is computed per cluster. To do that in this work we used approaches in Phillips (1991) to calculate enrichment ratios (ER), which basically use the average concentration of each element in each cluster (1 to 6) divided by the average concentration of each element in the total number of samples (n=562); then, each cluster can be characterized by specific elemental enrichments (ER>1) or depletions (ER<1) as illustrated in a colored graded matrix in Table 3. The advantage of using this matrix of enrichment/depletion ratios is that it allowed us to compare and recognize almost unique combinations of enrichments or depletions per cluster, resulting in the identification of chemofacies (Table 3).

Cluster # Chemofacies	Elemental Characteristics	Interpretation	Si/Al	Al	K	Ti	Zr	Th	Ca	Mg	Mn	Sr	Mo	U	V	P	S
Cluster 1	Low Si/Al, V, P High Mo, S, U	High organics with detrital input and clays	0.234	1.512	1.642	1.534	1.426	1.355	1.612	1.320	1.025	1.142	1.689	1.771	0.460	0.751	2.070
Cluster 2	Low Si/Al High Ti, K, Al, S, Mo	Detrital input, clay-rich, with organics	0.335	1.254	1.271	1.335	1.229	1.173	0.622	0.654	0.868	1.231	1.240	1.198	0.605	0.695	1.319
Cluster 3	High Si/Al Low K, Al, Ti, Ca	Biogenic input, moderate organics	3.208	0.178	0.012	0.167	0.455	0.517	0.000	1.402	1.147	0.428	0.792	0.375	0.745	0.978	0.323
Cluster 4	Low Si/Al High Al, K, Ti, Zr, Th	Clay-rich, Detrital input, low organics	0.211	1.978	2.454	2.045	1.908	1.716	1.059	0.506	0.867	1.048	0.867	1.175	0.799	0.487	0.767
Cluster 5	Low Si/Al, Ca High V, Mo, Al, Ti, S	Detrital input, moderate clays, with organics	0.329	1.325	1.335	1.420	0.810	0.964	0.084	0.677	0.912	1.252	2.347	1.608	4.360	1.265	1.348
Cluster 6	Moderate Si/Al High P, Sr	Biogenic input with Phosphates	2.437	1.194	1.236	0.943	0.678	0.983	0.194	0.816	1.095	6.660	0.534	1.269	2.275	8.968	0.814

Table 3. Matrix of elemental enrichment ratios (ER) by cluster. The color gradient of this matrix ranges horizontally across each cluster based on variations of ER's among elements. The matrix became helpful by illustrating contrasts between elemental enrichments (ER>1) and depletions (ER<1) per each cluster; the darker the green color higher is the elemental ER>1, and conversely, the darker the red color the lower the elemental ER<1. Combinations of elemental enrichments and depletions per cluster were then translated into a particular chemofacies per cluster.

Once the chemofacies were identified per each sample, these were plotted vertically along with their individual elemental proxies (Figure 48), from which a vertical chemostratigraphic characterization could be made as follows:

Basal Woodford (0 to 35 ft), this zone comprises the lowermost Woodford strata, and is characterized by elevated concentrations of detrital and clay proxies such as Al, K, Ti, Zr, and Th that overall surpass their own concentrations throughout the rest of the section. This finding puts the lowermost Woodford as the most detrital-rich interval across the section (Figure 48). It can be noted that soft beds (shales) are the ones that fully contribute on the elevated responses of detrital proxies of this interval. There is little to no evidence of Ca, Mg and Sr within this basal Woodford (Figure 48). Few exceptions of moderate Ca are attributed to calcareous cements within sandstones and siltstones of this lowermost Woodford.

Lower Woodford (35 to 120 ft), this interval encompasses a general decreasing upward trend in Al, K, Ti, and Th reaching their minimum concentrations around 118 ft; motifs of Mo, U and S, depicts a complete cycle with an increasing trend overlaid by a decreasing one, and their highest and lowest concentrations sitting around feet 65 and 120 respectively (Figure 48). Very few and discrete peaks of Ca, Mg and Sr are evidenced in this lower Woodford. Chemofacies of this interval are dominated by low Si/Al ratios with the highest concentrations of Mo, S and U. At the top of the interval is a slight increase of interlayered chemofacies of more detrital affinity (Figure 48).

Middle Woodford (120 to 225 ft), compared with its underlying lower Woodford interval, ratios of Si/Al slightly increase within the middle interval, evidencing the subtle excess of Si within the hard beds (Figure 48). Within this middle interval, together Ti,

Zr, K, and Al depicts a general upward increase reaching their maximum concentrations around 185 ft (Figure 48). Mo and V remain fairly constant, while S shows a gradual increase up to 185 ft. From 185 ft and upward, concentrations of Ti, Zr, K, Al, and S decreases, while Mo and U increases (Figure 48). Chemofacies within this middle interval evidences intermittence in detrital input, intercalated with upward increments of biogenic pulses (Figure 48).

Upper Woodford (225 to 315 ft), in this interval concentrations of Si/Al abruptly increases upward, reaching maximum values around 270 ft, that then is capped by a decreasing trend of Si/Al (Figure 48). The high Si/Al ratios are merely due to the contribution of hard beds (cherts), soft beds do not show any excess of Si over Al (Figure 48). Concentrations of Ti, Zr, K and Al in the soft beds record their lowest values at about the same location where Si/Al reached its maximum, thus suggesting the zone between 260-275 ft as the most biogenic rich zone throughout the Woodford Shale (Figure 48). In this upper interval, as in no other portion within the lower and middle Woodford members, concentrations of Sr, V, and P all provide evidences of their highest values (Figure 48), which can be correlatable with the typical occurrence of phosphatic nodules/concretions of the upper Woodford. Both Mo and U, while high overall in the upper Woodford, a zone is highlighted between 260 to 275 ft where these two elements sharply decrease, pretty much aligned with the same zone of biogenic input and low radioactivity (Figure 48). Chemofacies of this upper Woodford interval evidences a high frequency interlayering between biogenic and detrital pulses, but with much lower clay and organic proxies within the soft beds (Figure 48).

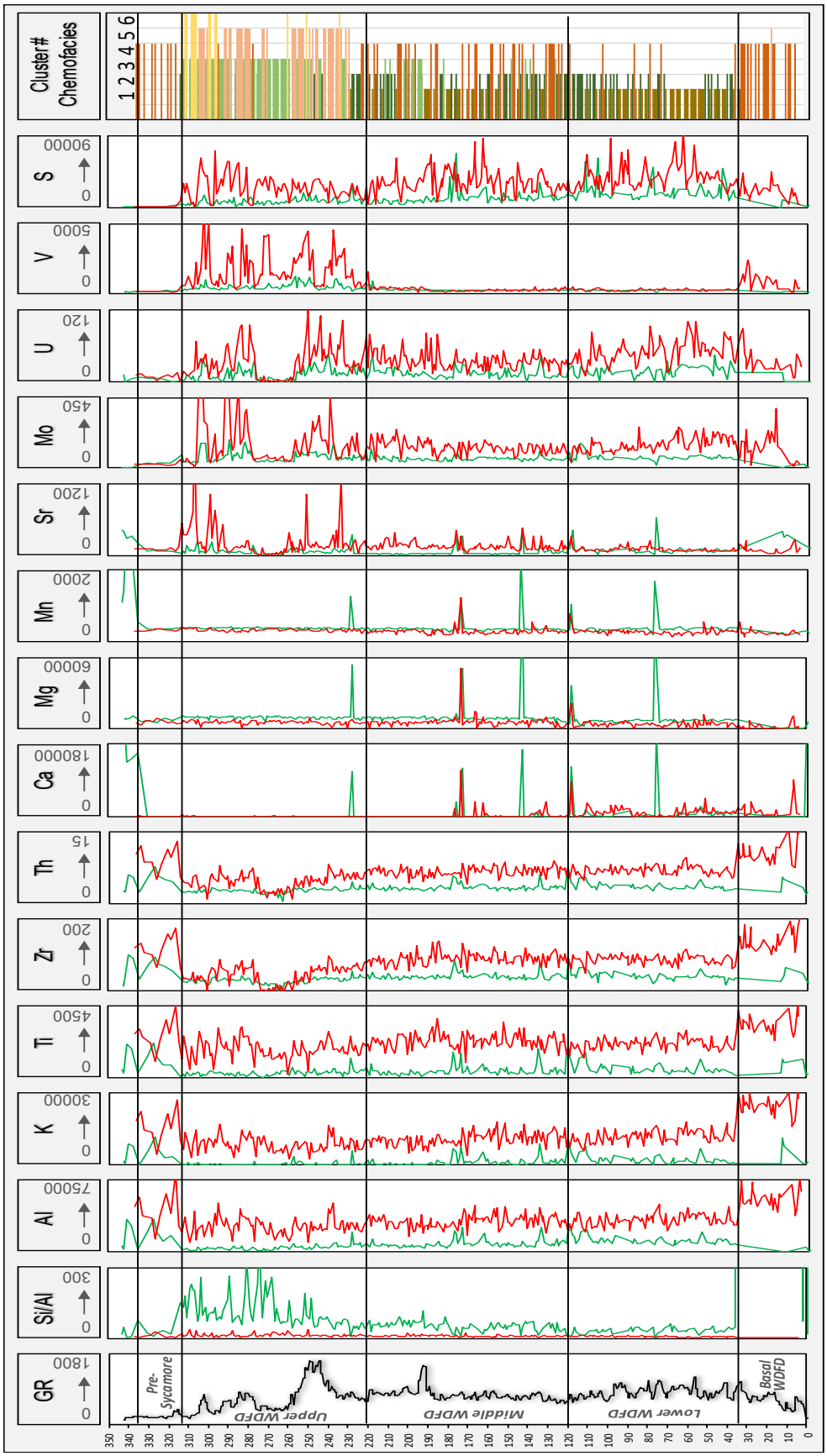

Figure 48. Vertical log of most common chemostratigraphic proxies across the entire Woodford section. Vertical resolution of data points is 0.5 ft and are differentiated by soft (red curves) or hard (green curves) beds. Right column corresponds with the chemofacies identified through the analysis of elemental enrichments ratios per cluster. For details on the significance of each cluster are Table 3

5.5. Elemental Proxies and Mineralogical Composition

In order to determine which are the main elemental signals that better represent the Woodford mineralogy in terms of quartz, clays and carbonates, elemental concentrations from XRF were compared with mineralogy from XRD.

Overall, quartz contents positively correlated with Si and Si/Al (Figure 49), and it is corroborated that hard beds are quartz-rich and tend to concentrate most of the excess of Si along with very minor amounts of Al; soft beds on the other hand, even with moderate to high excess of quartz content (20-75%), present very low Si/Al ratios, implying a great contribution of Si from quartz (Figure 49).

Elements presenting negative correlations with quartz contents are Ti and Zr (Figure 49), which suggests that quartz-rich beds within the Woodford do not host significant detrital fractions, so the high quartz contents within hard beds can be attributed to a non-detrital source, most likely occurring in the form of authigenic or biogenic silica.

For clay-rich samples (clays>15%) as expected, elements that show strong positive correlation with clay minerals are Al, K, and Th (Figure 50). Moreover, Ti and Zr also show positive correlation with clay minerals (Figure 50), meaning that within the Woodford Shale most of the detrital fraction is associated with clay-rich beds.

For the case of carbonate minerals, it was noted that elemental concentrations of Ca, Mg, and Mn positively correlate with carbonate contents and confirms the dominance of dolomite/ankerite in the Woodford carbonates, as evidenced by enrichments of Mg and Mn within carbonate beds (Figure 51).

At this point again, it is worth emphasizing the advantages of discriminating variables by the two most common rock types in the Woodford Shale, soft and hard beds

that appear as two very distinctive populations in cross plots and vertical profiles. In summary, soft beds are characterized by higher clay and TOC contents, low Si/Al ratios, and high Ti, Zr, K, Th and Al. Hard beds are very quartz-rich, with lower TOC contents, and low Ti, Zr, K, Th and Al concentrations. Statistically I found that almost regardless of their stratigraphic position, either a hard or soft bed found in the lower, middle or upper members will maintain such unique compositional properties.

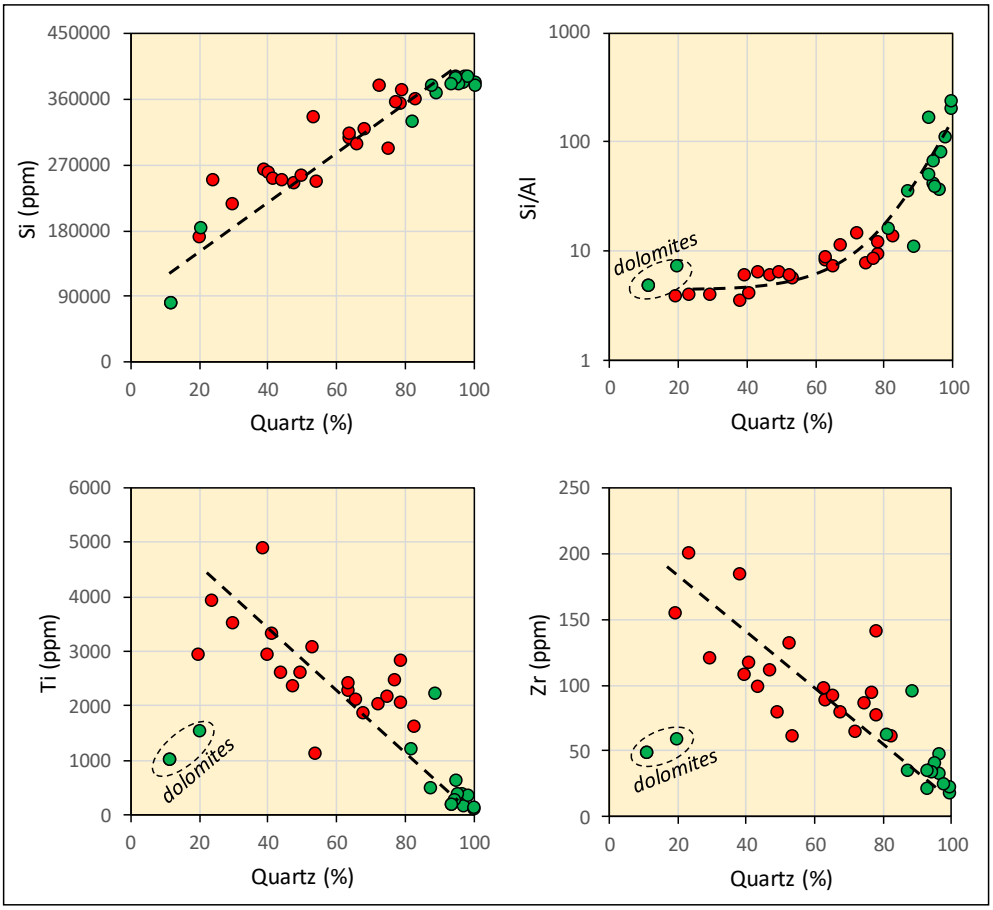

Figure 49. Cross plots of elemental proxies (XRF) versus quartz contents (XRD). Positive relationships are obtained from quartz with Si and Si/Al, whereas negative with Ti and Zr. Hard beds (green dots) are most likely enriched in biogenic or authigenic quartz, as evidenced by their very low Ti and Zr with very high quartz contents.

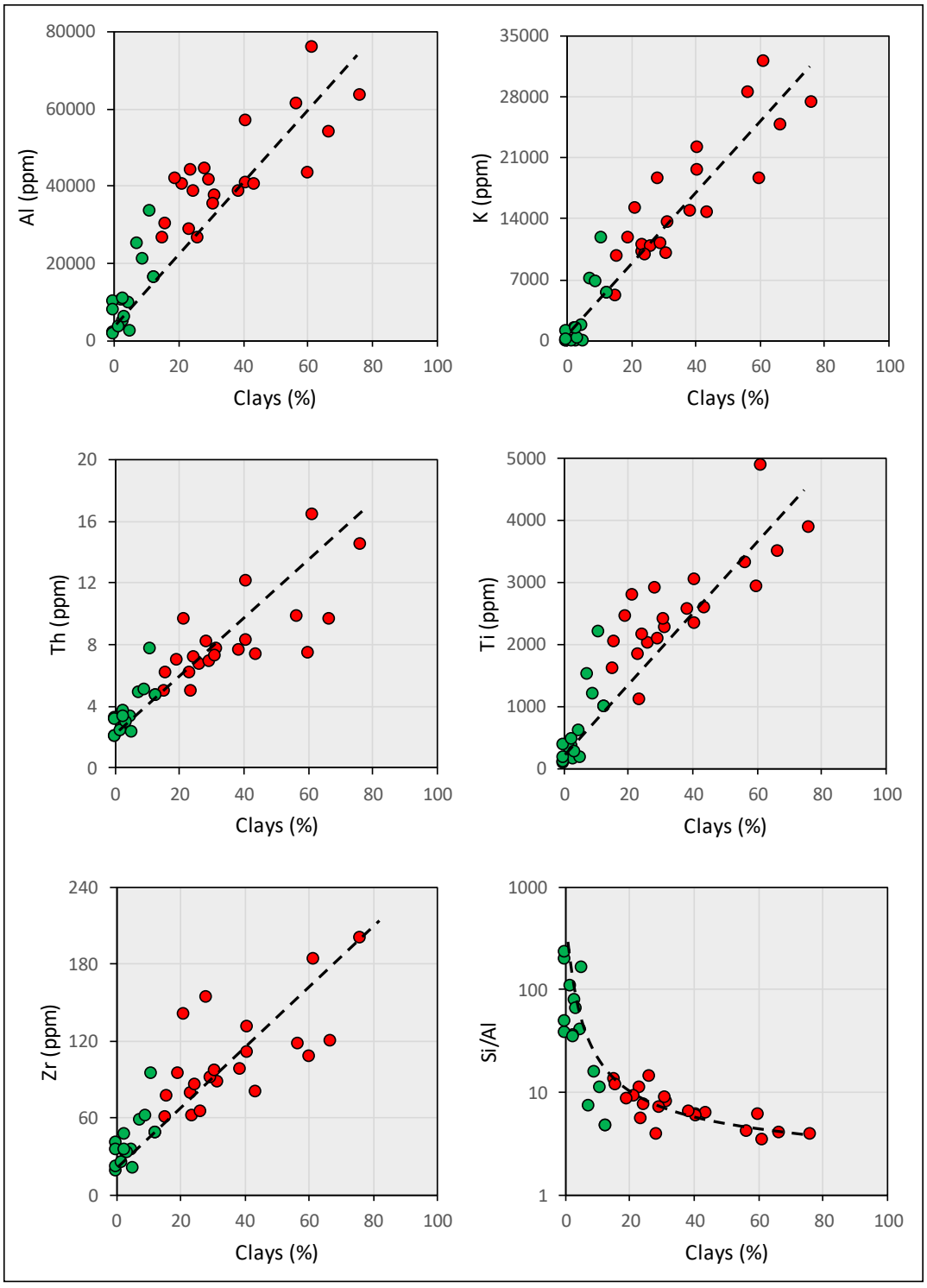

Figure 50. Cross plots of elemental proxies (XRF) versus clay contents (XRD). Clay-rich samples (clays >15%) are not only enriched in clay proxies such as Al, K and Th, but also in detrital proxies such as Ti and Zr, implying a higher detrital input associated with clays within soft beds (red dots).

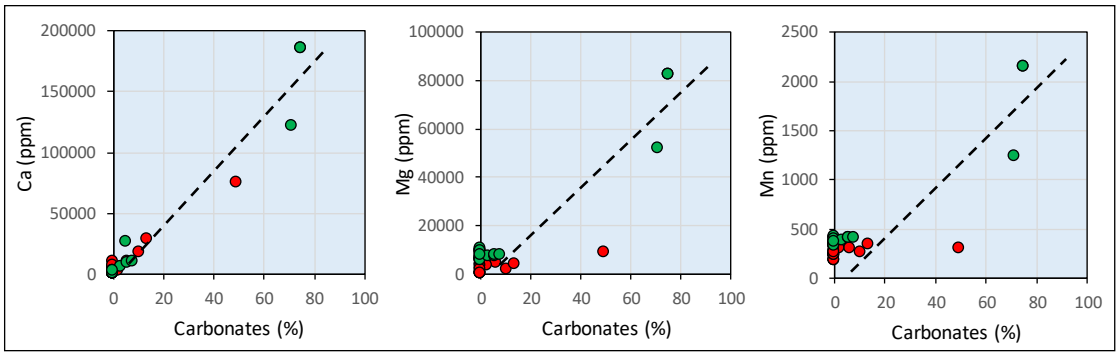

Figure 51. Cross plots of elemental proxies (XRF) versus carbonate contents (XRD). Together high Ca, Mg and Mn concentrations correlate positively with higher carbonate contents, and suppose dolomite/ankerite enrichments under higher Mg, Mn contents.

5.6. Elemental Proxies and Lithofacies

Several attempts were made using statistical analyses in order to quantitatively relate the elemental clusters (chemofacies) to unique groups of lithofacies. Multiple combinations of elements, under a different number of clusters, were tested versus the identified lithofacies. Results from this statistical correlation did not reveal meaningful outcomes, and resulted in most of the cases that chemofacies and lithofacies are not correlatable one-to-one.

Perhaps a reason for the lack of quantitative or one-to-one correlation between elemental proxies and lithofacies might be because lithofacies refer to material-based rock features (present-day fabric and composition), whereas elemental proxies from XRF usually combines signals from conditions at the time of deposition (i.e. water chemistry, particles source, redox conditions) plus post-depositional modifications (i.e. diagenesis, weathering). For example, taking the case of two different chemofacies, one rich in detrital quartz and the other rich in biogenic quartz, after correlation with lithofacies groups, both of them will fall within the range of the same quartz-rich lithofacies as they

share similar present-day composition no matter the origin of quartz; for that reason, it is suggested that chemofacies should not be treated as discrete numbers allocable to a single lithofacies. However, alternatively in this work, a qualitative integration of our lithofacies with elemental signals was achieved by plotting in box plots each elemental proxy per lithofacies, and visually using their relative proportions as if it were the case of predictive criteria, some groups of lithofacies can be easily identified by combinations of their elemental proxies (Figure 52).

Lithofacies of Argillaceous Shales present the highest values of Ti and Zr, accompanied by very low Si/Al ratios (Figure 52), suggesting these lithofacies as the most detrital in affinity. Conversely, in increasing order of Si/Al ratios, Siliceous Mudstones and Cherts appear as the most biogenic rich lithofacies, characterized by very high Si/Al ratios along with the lowest Ti and Zr signals (Figure 52). Corroborating this finding, petrographic observations revealed that particles of silt-sized detrital quartz are largely restricted to shale lithofacies. Indeed, none evidences of detritus (angular silt-quartz) appear within the radialrian-rich cherts, thus implying the non-coexistence of silt-size detrital quartz and silicified radiolarian within cherts.

Clay proxies (Al, K, and Th) all together confirm that Argillaceous Shales are the most clay-rich lithofacies within the Woodford Shale as identified by the highest concentrations of Al, K and Th (Figure 52). Following in decreasing order of clay signals, the lithofacies of Siliceous and Dolomitic shales appear with moderate contents of these elements (Figure 52), followed by the Siliceous Mudstones and Cherts as the least clay-rich lithofacies (Figure 52). Clay contents determined by bulk XRD also confirm that

argillaceous and siliceous shales are clay-rich (15-60%) while cherts and siliceous mudstones are clay-poor (clay<10%).

Elements sensitive to redox conditions and organic contents (Mo, U, and S) show that lithofacies of shales (Argillaceous, Siliceous and Dolomitic) together tend to concentrate most of the organic-sensitive elements among the Woodford strata (Figure 52). Only minor amounts of Mo, U and S appear within the lithofacies of Cherts, Siliceous and Dolomitic mudstones (Figure 52); this observation was previously confirmed by the distribution of TOC contents by lithofacies (Figure 37) in which soft beds (shales) are the ones that usually contain the highest TOC contents (>8wt.%), while hard beds (cherts) contain much lower TOC values (< 8wt.%).

In the case of phosphatic indicators, only the Brown Siliceous Shale lithofacies appears with marked enrichments of P, B and V (Figure 52); though difficult to identify a phosphatic-rich lithofacies by physical characteristics and/or petrographic observations, after going back and examining the stratigraphic occurrence of such anomalous P, Ba and V peaks it was noted that the Brown Siliceous Shale is restricted to the upper Woodford member, and correlate with numerous beds surrounding nodules and concretions. Thus, it is implied that the Brown Siliceous Shale lithofacies records the lithology of phosphatic influence and not necessarily corresponding to nodules or concretions, but rather to the matrix of shale beds as is the case of this Brown Siliceous Shale.

Carbonate elements, like Ca, Mg and Mn, are very restricted in abundance to the Dolomitic Mudstones and Siliceous-Dolomitic Shale lithofacies (Figure 52), with a pronounced enrichment within the Dolomitic Mudstone. Carbonate contents from XRD of this lithofacies surpasses 50% dolomite/ankerite, and their petrographic observations

reveal massive mosaics of crystalline dolomite (Figure 27). Dolomitic lithofacies within the Woodford Shale are interpreted to be the product of either early or late diagenetic modifications. Up to the most recrystallized beds of Dolomitic Mudstones, they preserve moderate amounts of Al, K, Th, Ti, Zr, U, and S that are markedly higher than in a typical Chert (Figure 52), thus implying elemental signals more affiliated with shale beds than cherts. Because of this we believe that the precursor for the majority of dolomitic lithofacies were the organic- and clay-rich shales, instead of cherts.

In summary, qualitative comparisons between elemental signals and lithofacies reveal the potential to roughly identify lithofacies based upon the combination of elemental signals obtained from XRF results. For example, within the Woodford Shale strata of this study, we recognized that Argillaceous and Siliceous Shales are identified by the highest concentrations of Al, K, Th, Ti, Zr, and Mo. Siliceous Mudstones and Cherts are identified by the highest Si/Al ratios and lowest Ti, Zr, Al, K, Th, Mo, U and S concentrations. Brown Siliceous Shales are identified by their highest concentrations of P, Ba, and V, and Dolomitic Mudstones are identified by the highest concentrations of Ca, Mg and Mn.

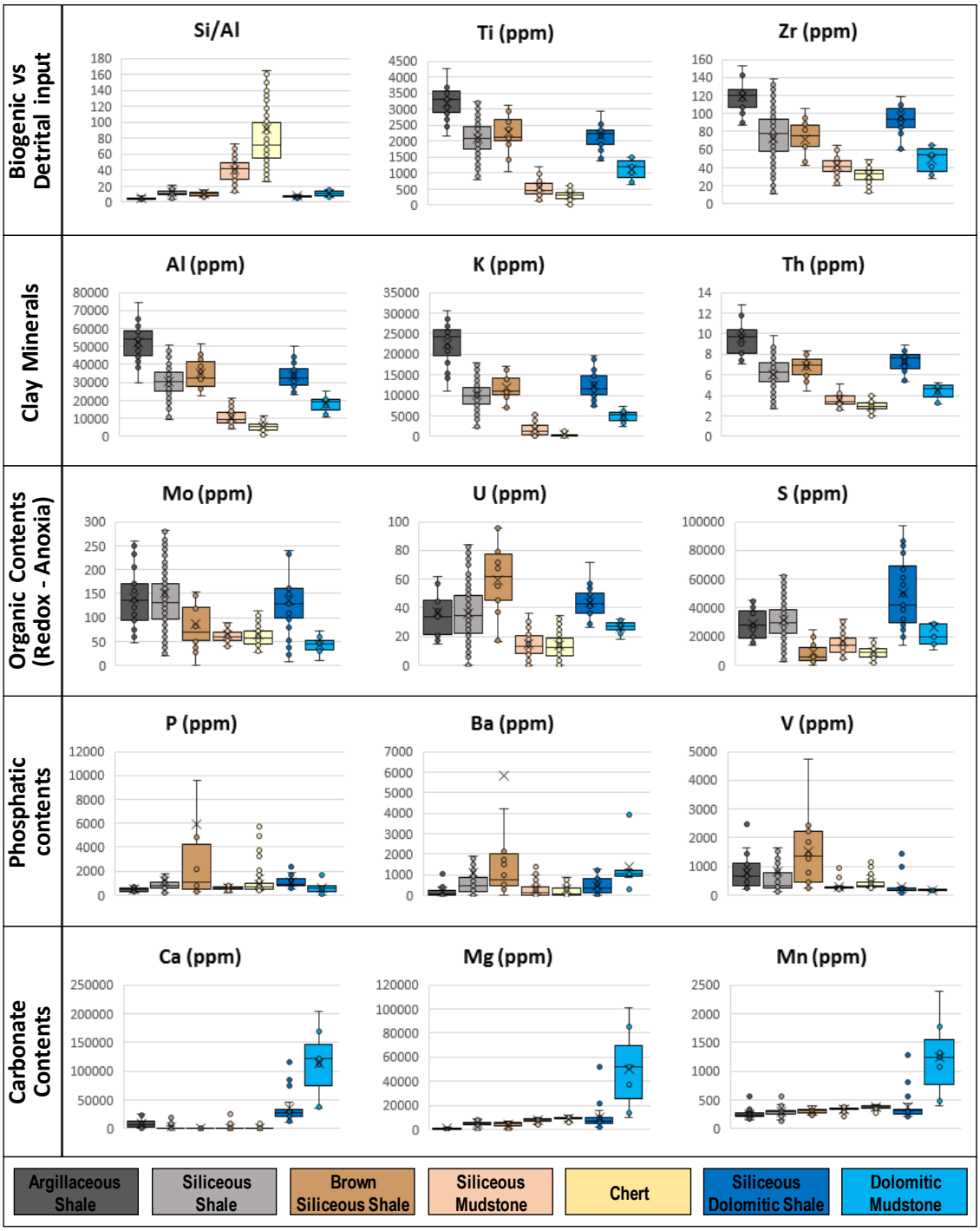

Figure 52. Box plots of elemental proxies plotted by lithofacies. Qualitative comparisons between elemental signals and lithofacies reveal the potential to roughly identify lithofacies based upon the combination of elements obtained from XRF results.

6. ROCK HARDNESS

Hardness results from the Speake Ranch outcrop revealed various aspects about the mechanical-stratigraphic heterogeneities of the Woodford Shale and were extensively covered in Becerra-Rondon (2017). She studied several controlling factors affecting this rock property, including rock fabric, mineralogy, organic richness and density, as well as making the calibration of hardness values with lab-measured UCS values. Accordingly, since much of the detail is given in her thesis, in this work rock hardness is only compared with lithofacies.

When grouped by lithofacies, rock hardness revealed very narrowed ranges per group (Figure 53), from high to low average hardness, Cherts are the hardest lithofacies (avg. 839 LH), followed by the Siliceous Mudstones (avg. 750 LH), Dolomitic Mudstones (avg. 684 LH), Siliceous-Dolomitic Shales (avg. 558 LH), Siliceous Shales (avg. 538 LH), and Brown Siliceous Shales (avg. 396). The Argillaceous Shales (avg. 309LH) are the least hard lithofacies among the Woodford strata. Another observable feature in Figure 53 is the narrow boundaries of the distribution of rock hardness values per lithofacies. In general, hard lithofacies such as chert and siliceous mudstones do not share any similar hardness value with soft lithofacies such as the argillaceous and siliceous shales, thus giving rise to a potential use of the micro-rebound hammer as a first screening technique for identifying lithofacies in well cores.

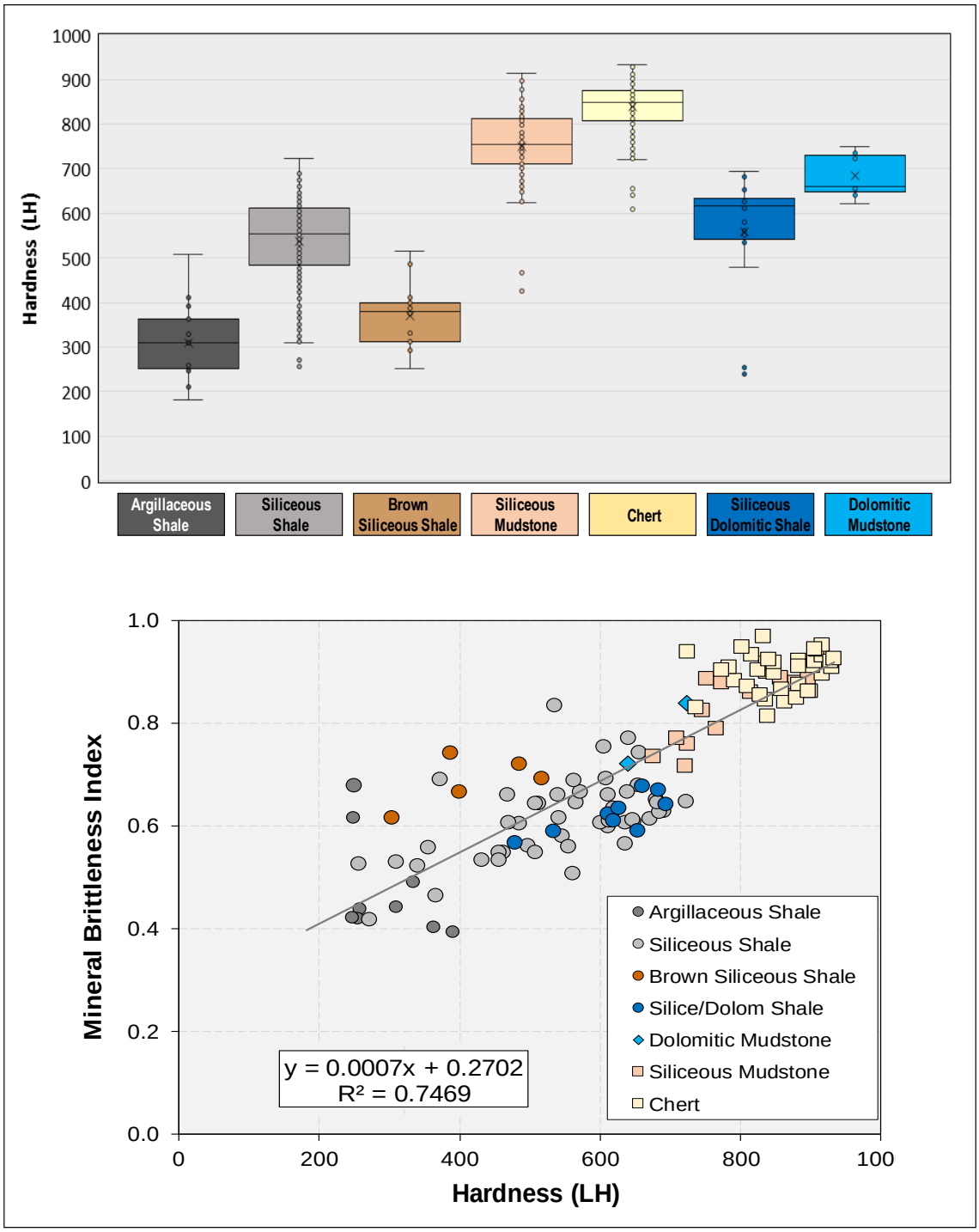

Figure 53. Distribution of rock hardness values by lithofacies. Mineral brittleness index versus hardness reveal a good positive correlation. Cherts and Siliceous mudstones appear as the most brittle lithofacies.

7. SUMMARY OF ROCK CHARACTERISTICS

In this work, rock characteristics constituted the backbone for further interpretations and correlation with more indirect data (well logs). Several analytical techniques were conducted under different scales of investigation and over a large set of samples, and many observations and findings have been documented. Thus, to synthesize, Table 4 and Table 5 compile rock characterization results distributed in respect to the informal Woodford subdivisions as well as by lithofacies recognized in this outcrop section.

Stratigraphic Subdivsion	Thickness (feet)	Weathering Response	Dominant Color	Radioactivity (cps)	Soft-to-Hard Ratio	Avg. Bed Thickness (cm)	Proportion of Lithofacies (%)	Mineralogy (Avg.%)	TOC (wt.%)
Sycamore Limestone	Section ends	Highly Resistant	Orange, grey	Min= 126 Avg= 173 Max= 187	Min= 0/100 Avg= 4/96 Max= 13/87	> 30	Crystall.Limestn= 80 Green Silic.Sh= 20	Quartz= 69.35 Clays= 5.15 Carbonts= 25.4	0
Pre-Sycamore Greenish	21	Soft Ponded lows	Pale Green	Min= 143 Avg= 217 Max= 397	Min= 0/100 Avg= 29/71 Max= 55/45	Soft= 5.97 Hard= 13.2	Impure Limestn= 4.8 Green Silty Sh= 61.9 Non-organic Chert= 33.3	Quartz= 71.4 Clays= 23.5 Carbonts= 3.2	<0.02
Upper Woodford	92	Resistant, develops ridges	Dark grey to Black	Min= 141 Avg= 652 Max= 1616	Min= 0/100 Avg= 38/62 Max= 100/0	Soft= 3.59 Hard= 6.52	Argill.Sh= 0 Silic.Sh= 41.0 Brw.Silic.Sh= 5.9 Silic.Mud= 2.4 Chert= 47.5 Cal/Dol.Sh= 1.1 Cal/Dol.Mud= 1.2	Quartz= 86.9 Clays= 9.7 Carbonts= 1	Min= 0.86 Avg= 7.71 Max= 30.2 SD ± 6.58
Middle Woodford	104	Medium resistant	Dark grey to Black	Min= 522 Avg= 754 Max= 1518	Min= 33/67 Avg= 74/26 Max= 100/0	Soft= 10.25 Hard= 2.62	Argill.Sh= 0.9 Silic.Sh= 48.4 Brw.Silic.Sh=1.9 Silic.Mud= 18.8 Chert= 25.8 Cal/Dol.Sh= 2.3 Cal/Dol.Mud= 1.9	Quartz= 71.2 Clays= 15 Carbonts= 11.3	Min= 1.62 Avg= 7.43 Max= 14.70 SD ± 3.99
Lower Woodford	105	Soft Ponded lows	Black	Min= 502 Avg= 810 Max= 1212	Min= 14/86 Avg= 87/13 Max= 100/0	Soft= 22.4 Hard= 3.3	Argill.Sh= 23 Silic.Sh= 36.6 Brw.Silic.Sh= 0 Silic.Mud= 19.3 Chert= 8.0 Cal/Dol.Sh= 11.2 Cal/Dol.Mud= 1.9	Quartz= 58.8 Clays= 28 Carbonts= 10.6	Min= 0.094 Avg= 9.39 Max= 22.9 SD ± 5.72
Basal Woodford	13	Soft Ponded lows	Mottled: olive green to brownish	Min= 318 Avg= 474 Max= 716	Min= 0/100 Avg= 73/27 Max= 100/0	Soft= >30 Hard= 26.4	Argill.Sh= 11.8 GreenArgill.Sh= 29.4 Brown.Arg.Sh= 23.5 Cal/Dol.Sh= 11.8 Sandstone= 23.5	Quartz= 38.9 Clays= 39 Carbonts= 17	< 2.9%
Hunton Limestone	section begins	Highly Resistant	Pale Yellowish	Min= 79 Avg= 109 Max= 178	Min= 0/100 Avg= 0/100 Max= 0/100	> 30	Crystall.Limestn= 100	Quartz= 2.4 Clays= 0 Carbonts= 97.6	0

Table 4. Summary of rock characteristics distributed by the informal Woodford subdivision at the Speake Ranch outcrop.

Lithofacies	Weathering Response	Microfabric	Quartz (%)	Clays (%)	Carbonates (%)	TOC (wt.%)	Si/Al	Ti, Zr, K, Al, Th	Ca, Mg, Mn	Mo, U, S	P, Ba, V	Hardness (LH)	Weight/Volume (g/cm3)
Argillaceous Shales	Soft, thinly fissile, papery-like	Well defined Preferred parallel orientation	Min= 29.6 Avg= 35.4 Max= 41.2	Min= 56.8 Avg= 61.84 Max= 66.89	Min= 0 Avg= 0 Max= 0	Min= 7.3 Avg= 15.07 Max= 22.9	Lowest	Highest	Low	High	Low	Min= 183 Avg= 309 Max= 410	Min= 1.81 Avg= 2.13 Max= 3.81
Siliceous Shales	Soft, fissile, slightly indurated	Subtle preferred parallel orientation	Min= 45.6 Avg= 67 Max= 85.7	Min= 12.4 Avg= 25.45 Max= 46.7	Min= 0 Avg= 0.75 Max= 6	Min= 5.8 Avg= 12.42 Max= 30.2	Low	High	Low	Highest	Low	Min= 309 Avg= 538 Max= 722	Min= 1.83 Avg= 2.27 Max= 3.33
Brown Siliceous Shales	Soft, Light weight	Subtle preferred parallel orientation	Min= 72.2 Avg= 73.55 Max= 74.9	Min= 24.8 Avg= 25.6 Max= 26.4	Min= 0 Avg= 0 Max= 0	Min= 1.9 Avg= 6.2 Max= 13.1	Low	High	Low	High	Highest	Min= 233 Avg= 396 Max= 516	Min= 1.98 Avg= 2.13 Max= 2.34
Siliceous Mudstones	Hard, massive	Random oriented microcrystalline aggregates	Min= 89.1 Avg= 92.6 Max= 96.1	Min= 3.9 Avg= 5.9 Max= 6.8	Min= 0 Avg= 0.4 Max= 0.8	Min= 1.8 Avg= 3.77 Max= 6.8	High	Low	Low	Low	Lowest	Min= 614 Avg= 750 Max= 913	Min= 2.24 Avg= 2.73 Max= 3.66
Chert	Hard, massive	Random oriented microcrystalline aggregates	Min= 87.4 Avg= 95.6 Max= 100	Min= 0 Avg= 2.0 Max= 5.4	Min= 0 Avg= 1.6 Max= 8.5	Min= 0.86 Avg= 3.1 Max= 9.8	Highest	Lowest	Lowest	Lowest	Low	Min= 721 Avg= 839 Max= 933	Min= 2.09 Avg= 2.81 Max= 3.15
Siliceous Dolomitic Shales	Soft, fissile, slightly indurated	Subtle preferred parallel orientation	Min= 19.6 Avg= 36.86 Max= 47.2	Min= 28.4 Avg= 36.01 Max= 40.95	Min= 10.5 Avg= 24.46 Max= 49.4	Min= 6.7 Avg= 10.6 Max= 20.5	Low	High	high	High	Low	Min= 482 Avg= 558 Max= 693	Min= 1.95 Avg= 2.30 Max= 3.14
Dolomitic Mudstone	Hard, Massive	Random oriented, crystalline mosaics	Min= 0 Avg= 10.6 Max= 20.2	Min= 0 Avg= 6.5 Max= 12.6	Min= 21 Avg= 48.76 Max= 71.2	Min= 0.09 Avg= 2.49 Max= 4.3	Low	Low	Highest	Low	Low	Min= 640 Avg= 684 Max= 750	Min= 2.36 Avg= 2.56 Max= 2.82

Table 5. Summary of rock characteristics distributed by lithofacies identified in the Woodford Shale at the Speake Ranch outcrop.

8. SEQUENCE STRATIGRAPHY

Accurate sequence stratigraphic interpretations usually combine knowledge of the depositional facies settings and how changes in those settings relate to variations in relative sea level (RSL). Slightly differing from classic models of sequence stratigraphy of clastic systems, in the Woodford Shale depositional model one must equally consider the interplay between extra-basinal (i.e. terrigenous) and intra-basinal (i.e. pelagic) sources/settings. For example, classic clastic models recognize the Transgressive System Tract (TST) as a decrease in continental input due to landward migration of the shoreline, and the Highstand System Tract (HST) as an increase in continental input due to basinward migration of the shoreline (Van Wagoner et al., 1990; Posamentier and Allen 1999). In the Woodford Shale case of distal portions of epicontinental shelves with important pelagic supply, an increase in detrital-derived input (clays) over biogenic pelagic silica might indicate a transgression. The most likely scenario for properly interpreting regression in distal regions is where terrigenous input increases at the expense of a significant decline in pelagic supply (biogenic silica and organics), as is the case of the uppermost portions of the Woodford strata.

The rock record of the Woodford depositional system of this study includes admixtures of abundant quartz (authigenic, biogenic and detrital), phyllosilicates (terrigenous and diagenetic), carbonates (diagenetic), and organic matter (pelagic and terrestrially-derived). Consequently, changes in climate, upwelling and basin circulation can be as equally important as water depth, as all of which appear to have influenced present-day lithofacies. The interpretation of upwelling and restricted bottom waters that contain high organic contents seldom coincide with increased clay contents, as is the case

of the HST in the upper Woodford. The clay- and organic-rich sediments, which are more common in lower and middle portions of the Woodford Shale, can record a reduction in upwelling and a probable more humid climate; in these intervals of increased clays (terrigenous) and organic contents sediments record transgression and not regression.

In analog examples from distal marine fine-grained settings, Bohacs (1993) and Bohacs et al., (2005) outlined multiple alternative interpretations beyond the classic sequence stratigraphy of shallow shelfal regions. He illustrates that accounting for variations in the type and rate of sediment delivery and deposition, as well as the type of sediment source (biogenic vs. terrigenous), the response in the record of depositional sequences vary from site to site. For example, in the Miocene Monterey Formation the major transgressive phase up to the maximum rate of flooding coincides with the largest TOC contents accompanied by high detritus supply and low to moderate biogenic silica. Thus, as opposed to the classic TST with declining continental input, the Monterey Formation and the Woodford Shale seem to share similarities of an increasing detrital input for the TST and increasing biogenic input for the HST.

Regarding hierarchy of the studied stratigraphic sequences, the Woodford Shale at Speake Ranch outcrop can be interpreted as recording a single large-scale depositional sequence, which is unconformably bounded at the base by the eroded Hunton Group and at its top by the pre-Sycamore deposits (Figure 54). Though lacking of absolute age dating based on biostratigraphy of conodonts from southern Oklahoma, the Woodford Shale deposition might cover a time span between 20 to 25 million years as suggested by Hass and Huddle (1965) and Amsden (1975), who reported conodont fauna in the Woodford strata from the early Late Devonian to earliest Mississippian (Kinderhookian).

Therefore, given a Woodford age range between 20 to 25 my, our interpreted large-scale sequence corresponds with a second-order depositional sequence according to hierarchical terminology in Vail et al. (1991) and Miall (1991). The second-order sequence in turn can be subdivided into a number of superimposed smaller third-order sequences and parasequence cycles bounded by regression surfaces (Figure 54), which all appear to occur in distal marine settings below the storm-wave base with no evidences of erosion or reworking. Other important regressive and flooding surfaces from smaller-scale sequences are present (Figure 54) and some of these are likely to be useful in regional correlations into the subsurface (Figure 56).

8.1. Description of Stratigraphic Sequences

Outcrop observations from the basal unconformity Sequence Boundary (SB) suggest subaerial exposure and erosion, as evidenced by the intense karstic and dissolution features over the top of the Hunton Group. In sharp contact above this basal SB, the succession shows an upward increasing GR parasequence (GRP1) (Figure 54), which is represented by abundant non-organic greenish claystones, siltstones and sandstones grading into the black shales of the lowermost Woodford Shale. Deposits comprised by the interval of GRP1 resulted from the earliest pulses of marine transgression, which led to the landward migration of the shoreline and creation of the transgressive surface of marine erosion (TSE). Rock attributes of the basal TSE at Speake Ranch outcrop suggest high-energy and oxygenated sedimentation related to the onset of marine incursion, it is evidenced by intercalations of bioturbated greenish and brownish claystones, and glauconitic sandstones with coarse reworked particles. Among the entire

Woodford succession, overlying the TSE, GRP1 corresponds with the most terrigenous strata (Figure 55), as evidenced by the largest detrital signals of Ti, Zr, K, Th and Al. The TSE at the base of the Woodford can be combined with the basal sequence boundary to form the SB/TSE. The presence of shallow marine deposits related to the TSE overlying the erosional SB at the top of the Hunton suggests that the second-order sequence begins with a TST, and Lowstand System Tract (LST) deposits were not preserved in the area of this study. It is known that before the deposition of the Woodford Shale a rapid sea-level drop related to a LST resulted in extensive subaerial exposure and fluvial incision of the Hunton carbonate ramp; however, since fluvial deposits were not observed at the base of incised valleys within the Hunton, a LST was not interpreted for this study.

Stratigraphically overlying the basal SB/TSE and GRP1, the third-order trend continues retrogradational (increasing GR upward) up to a flooding surface at the top of GRP3 (Figure 54). From GRP1 to GRP3 the interpreted transgression of the sea is represented by intercalations of organic-rich black argillaceous and siliceous shales that overall evidences a decrease in energy and accumulations rates, as well as very low bottom water oxygenation levels. Within the transgressive interval comprised by GRP1 to GRP3, bioturbation decreases and framboidal pyrite contents increase. Elevated redox proxies such as Mo, U and S all indicate an upward decline in water circulation (more restricted) that led to most stagnant and anoxic-euxinic conditions towards the top of GRP3. Average TOC and Hydrogen Index (HI) from this interval record their maximum values. In terms of basin sediment filling, the third-order transgressive deposits from GRP1 to GRP3 may correspond with the back-filling of the pre-Woodford topography. Stratigraphic correlations show thicknesses of the basal TST (GRP1 to GRP3) as highly

variable laterally (Figure 56). Differences are evident, as in some wells the Hunton/Woodford contact is thin and consists of a single GR spike, while in other wells the contact is thicker with GR responses gradually increasing upward (Figure 56).

Above the flooding surface capping GRP3, the stratigraphic succession shifts to a progradational trend represented by the decreasing upward GRP4 (Figure 54). Within this interval, frequency of organic-rich argillaceous shales beds decrease upward while siliceous mudstones and siliceous shales increase upward. The overall trend of GRP4 up to its third order regression surface suggest increased bottom oxygenation levels and presence of benthic fauna as evidenced by a decline in TOC contents, increase in bioturbation intensity and lighter rock colors. This interval also evidences a slight increase in detrital proxies (Ti and Zr) accompanied by declining of redox-sensitive elements (Mo, U, S).

At Speake Ranch outcrop the top of GRP4 marks an important turnaround point in the GR from a decreasing upward (GRP4) to an increasing upward trend (GRP5), the surface between these two GRP's is a third-order regressive surface (Figure 54) which coincides with the informal contact between the lower and middle Woodford members, and is likely one of the most traceable GR troughs across the Woodford strata (Figure 56). Rock characteristics of this regressive surface at the top of GRP4 include intense bioturbation, decrease in TOC contents and decrease in Hydrogen Index; elemental proxies include the lowering in Mo, U, and S concentrations.

Upwards, overlying the regressive surface at the top of GRP4, an overall trend of upward increasing GR forms another third-order transgressive trend that is capped by the maximum flooding surface (MFS) atop GRP7 (Figure 54). Within this third-order

transgressive cycle comprised by GRP5, GRP6 and GRP7, it is inferred that pelagic productivity in the form of biogenic silica increased from its underlying strata (GRP1 to GRP4). This can be evidenced by a general upward increasing in frequency of the radiolarian-bearing cherts and siliceous mudstones (Figure 55). GR responses and TOC contents are high within the transgression (GRP5 to GRP7) that led to the MFS. However, these are not as high compared to the more basal transgressive trend (GRP1 to GRP3). Organic matter accumulates most efficiently where circulation is reduced and considering that during the gradual reaching of maximum water depths also changes in water circulation occurred, this might give rise to a more circulated water system at the end of the MFS compared with the onset of transgression in the lower Woodford. Thus, maximum water depth (MFS) not necessarily must coincide with maximum water restriction, and perhaps in the Woodford Shale at Speake Ranch section, the maximum restriction was only reached around the earliest stages of marine transgression (GRP-1 to GRP3) making more efficient the preservation of higher organic contents. I interpret that at about the second-order MFS since there was more circulation of water masses (driven by upwelling), the high organic contents were not efficiently preserved either by dysoxia (oxidation) or auto-dilution from the abundant biogenic supply.

Once the second-order MFS was reached atop GRP7, the following upward trend is a large-scale HST with superimposed smaller scale parasequences (from GRP8 to GRP12) (Figure 54), which overall are characterized by decreasing-upward GR responses represented in greater proportions of cherty beds over shales. Capping the second-order HST a ‘hiatus’ type unconformity marks the upper sequence boundary (SB) of the entire Woodford Shale depositional system (Figure 54).

Internally, the HST of the Woodford Shale is interpreted to possess the strongest effects from upwelling and water circulation after the MFS. And yet, with low-energy deposition taking place under relatively elevated water depths (below the storm wave base), the general trend during the HST depicts regression of the sea level and shoreline progradation. However, diverging from the classic clastic model of shelfal regions, this type of regression in the Woodford Shale is not dominated by continentally-derived input from rivers, but instead is largely dominated by pelagic supply (biogenic silica) which in most of the GRP cycles the signal of biogenic/authigenic quartz overpasses the terrigenous signal (Figure 55). The biogenic silica blooms of the HST could be a response of the vigorous productivity influenced by upwelling as evidenced by the thick bedded radiolarian-rich cherts that dominates much of the upper Woodford member. Characteristics of the HST of the Woodford Shale at this location include high TOC contents (3-8 wt.%) not as high as in the TST (GRP1 to GRP7), chert frequency/thickness increases upward, detrital input decreases while biogenic supply increases, and phosphatic accumulations in matrix and concretions increases (Figure 55).

Near the top of the second-order HST, but a smaller scale in GRP11 one important peak of hyper productivity seems to be located across the Woodford. This interval contains abundant thick bedded radiolarite cherts, elevated Si/Al ratios and the lowest detrital input, additionally within the interval of GRP11, redox indicators (Mo and U) sharply decline to their minimum concentrations among the entire Woodford. GR responses also decrease and evidences no vertical change (blocky GRP) during the entire 20 ft of GRP11 (Figure 54). Besides that, in this interval of GRP11, phosphate concretions reached their maximum abundance (Figure 55), which in many cases are

draped by the under- and overlying bedding, suggesting they were formed before compaction and possibly under very low sedimentation rates.

Above the anomalous blocky GRP11 normal sedimentation settings are inferred to resume, as recorded by the decreasing upward GRP12. Still within the latest second-order HST, the type of sediment supply slightly shifts from being dominantly biogenic in GRP11 to mixed biogenic and detrital in GRP12. Concentrations of Al, K, Ti and Zr increases upward while Si/Al ratios decreases. Organic contents decrease and bioturbation increases upward, thus suggesting that once reached the maximum pelagic-biogenic supply in GRP11 the Woodford deposition slightly shifted to become less biogenic and more detrital in affinity. Sub-millimeter laminar concentrations of silt-sized detrital quartz as well as the increase in bioturbation, indicate that facies of the GRP12 were deposited near the storm wave base from where winnowing currents (with traction modes) and dysoxic-to-suboxic conditions become more common.

Finally, capping GRP12 at the very late stages of the second-order HST lies the upper boundary (SB) of the entire Woodford depositional sequence (Figure 54). This SB marks a sharp shift in sedimentary facies from the black, phosphatic and organic cherts of the Woodford Shale up to the grey-greenish non-organic mudstones of the pre-Sycamore deposits. Rather than appearing erosive as if it were the result of a rapid sea level drop, this SB actually appears more related to a 'hiatus' type unconformity, where declined sedimentation rates allowed the colonization of living benthic organisms. Characteristics of the upper SB include the intense bioturbation, bivalves, glauconite, and minimum-to-absent organic contents and redox indicators (U, Mo, V, S). Though not possible to demonstrate a hiatus (non-deposition) for the upper SB, lithological indicators

suggest low-energy, dysoxic/suboxic environments for the black Woodford cherts, which are directly overlaid by high energy and oxygenated bottoms of the greenish glauconitic and heavily bioturbated pre-Sycamore deposits. Based on conodonts biostratigraphy, Schwartzapfel (1990) and Noble (1995) interpreted a hiatus between the Woodford and Sycamore Formation in the Arbuckle area.

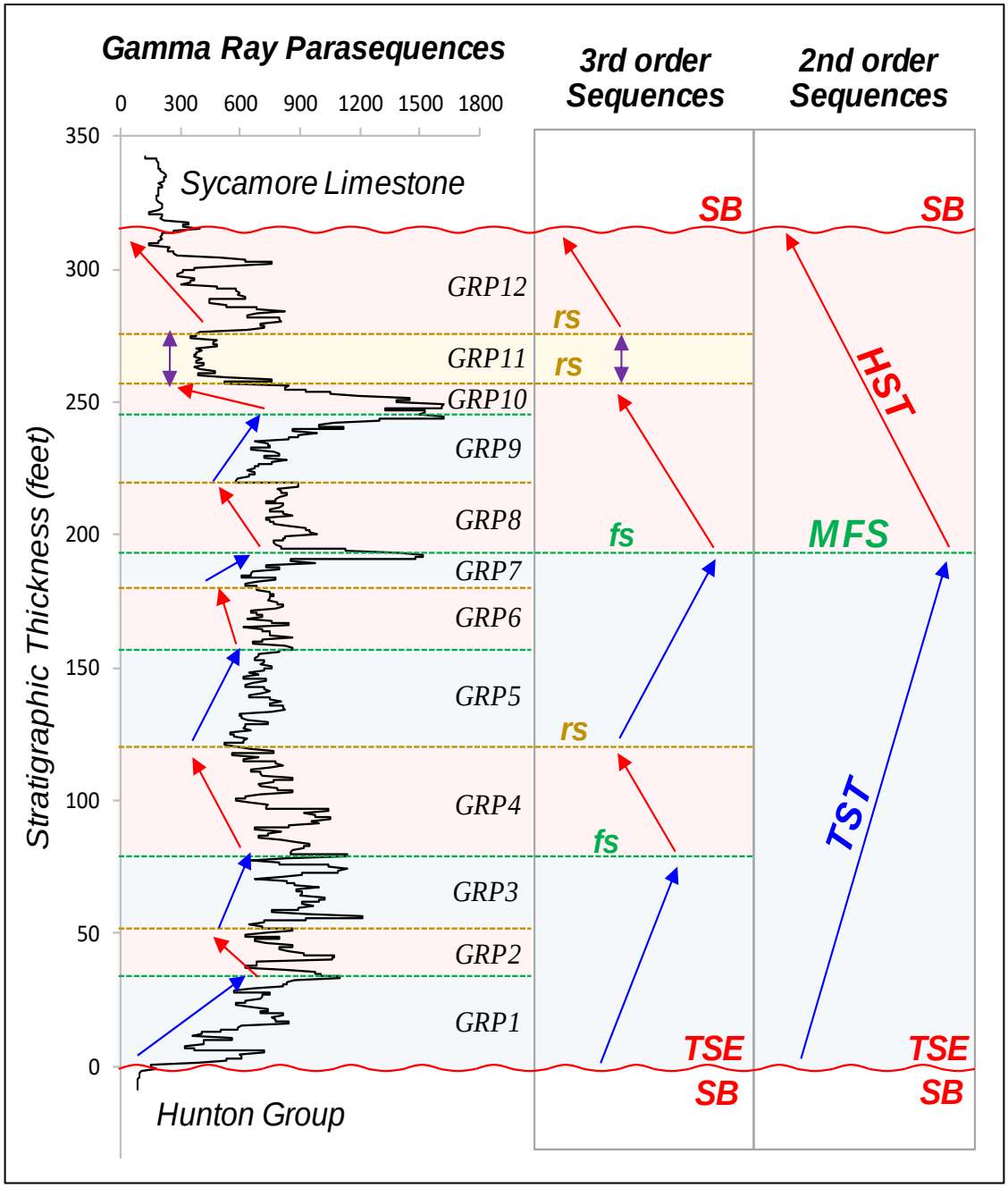

Figure 54. Outcrop-based sequence stratigraphic framework of the complete measured section at Speake Ranch. At the second-order scale, the Woodford Shale depicts a single sequence bounded by unconformities denoted as SB's. Superimposed upon the second-order sequence there are several higher order sequences and parasequences separated by flooding surfaces (fs) and regressive surfaces (rs). Blue arrows: increasing-upward GRP. Red arrows: decreasing-upward GRP. Purple arrow: blocky GRP. Sequence Boundary (SB). Maximum Flooding Surface (MFS). Transgressive Surface of Erosion (TSE). Transgressive System Tract (TST). Highstand System Tract (HST).

8.2. Synopsis of Sequence Stratigraphy Framework

– According to the integrated sequence stratigraphic framework interpreted at Speake Ranch outcrop, the Woodford Shale at this location overall records marine deposition of low energy under oxygen-deficient conditions possibly lying between middle to outer shelf regions.

– The generalized lack of evident traction-reworking structures, skeletal debris and scour surfaces, strongly suggest deposition mechanisms of pelagic and hemipelagic suspension settling below the storm-wave base.

– Main depositional controls on sediment type/supply and organic matter production/preservation were mostly driven by variations on water circulation which resulted from sea level fluctuations; coeval depositional conditions but of higher frequency were paleoproductivity as enhanced by upwelling and climate.

– The fact that 12 GRP's were identified across the complete Woodford measured section does not necessarily imply that sea level fluctuated that number of times during the ~20-to-25 my interval of the Woodford Shale; rather it might indicate cyclical changes that can be of a eustatic nature, a tectonic nature, autocyclic shifting of climate/water conditions, or a combination of these processes.

– From the most basal Woodford, the relative sea level rose up to a maximum flooding surface (MFS) to form the TST. During early transgression, given the mini-basins physiographic settings left by the underlying eroded Hunton maximum water restriction was achieved, which coupled with abundant clay input favored an efficient organic matter preservation as evidenced by the largest TOC contents hosted within the early TST (Figure 55).

– As transgression and rise in sea level continued, basin physiographic settings became less restricted and allowed water mixing via upwelling. At about middle stages of the TST sea level would have reached enough water depth over shelf regions to allow the mixing of nutrient- and oxygen-rich subsurface deep-water masses to ascend to surficial waters and promote the vigorous biota productivity and pelagic silica production. We hypothesized that from middle stages of the TST, upwelling pulses became more recurrent over shelf regions at variable durations and frequencies (most likely controlled by climatic forces within Milankovitch cycles).

– Relative sea level continued rising up to attain its MFS, but now since there is high pelagic siliceous input which largely overpasses the detrital input, the potential for auto-dilution from biogenic silica increased, and made conditions near the MFS little less efficient in preserving organic matter. As a result, our interpretation of the MFS within the Woodford Shale of this section do not coincide with the highest organic contents (Figure 55).

– After the MFS, a reduction in the rate of sea level rise forms the regressive phase or HST, which is dominated by pelagic supply that increases upward to its maximum near the top of the HST (Figure 55). It is just at the very late stages of the HST where terrigenous pulses become more intense and gradually outpace the biogenic supply that by then have decreased to its minimum as well as the organic contents.

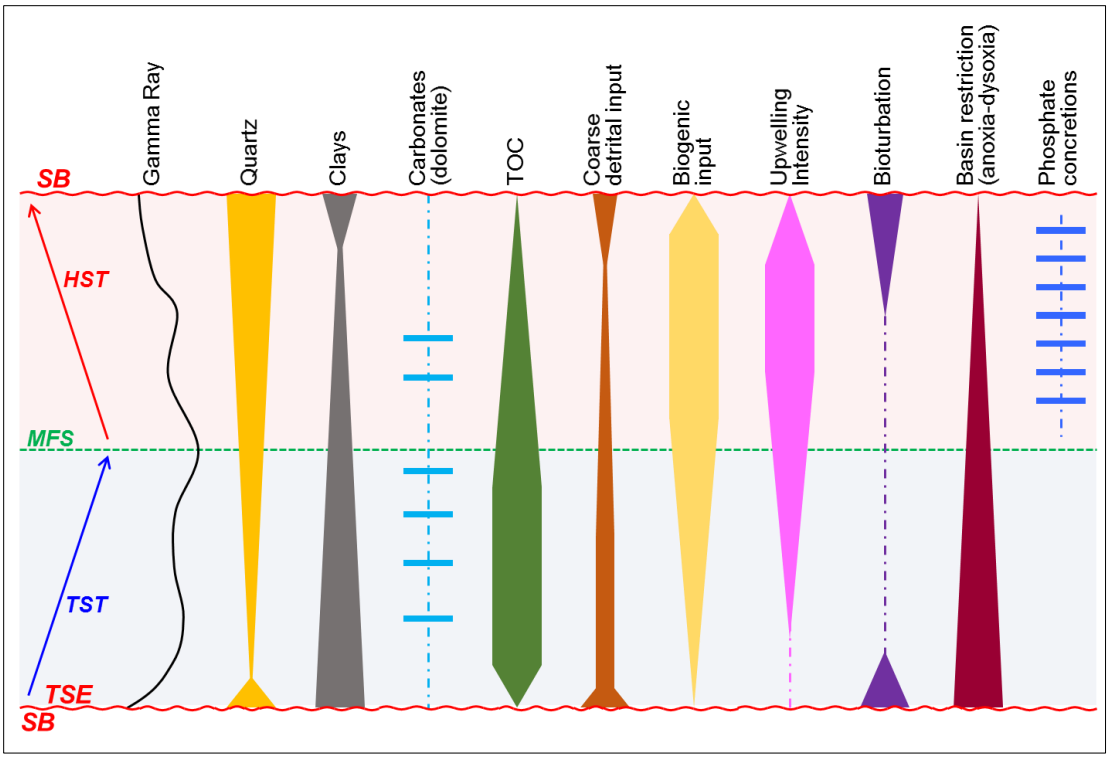

Figure 55. Idealized vertical variations of main features and controls across a second-order depositional sequence within the Woodford Shale of this study. Depending on the basin location, elements within a sequence of this type may be augmented or missing; for example, in proximal positions one would expect a HST more dominated by detrital input and less biogenic.

8.3. Outcrop-to-Subsurface Stratigraphic Correlation

In order to provide criteria of identifying and correlating packages in the subsurface, our outcrop-based stratigraphic interpretation was tied to subsurface well log responses. This is important as well-cores are not often readily available. Figure 56 shows a WNW-ESE panel of correlation which covers about 26 miles within the northern termination of the Ardmore Basin in Carter County.

Overall, gamma ray values are consistently high within the Woodford Shale across all wells. The Hunton/Woodford Shale contact corresponds with the basal SB of the second-order sequence, and is best picked by the abrupt GR change from a non-radioactive (clean GR) in the underlying Hunton to the highly radioactive overlying basal Woodford Shale (Figure 56). Atop the second-order sequence lies the upper SB which marks the contact between the Woodford Shale and Sycamore Formation. In all wells, the upper SB is best picked where the progradational trend (decreasing upward GRP) change to a blocky and slightly serrated GR pattern of the Sycamore Formation (Figure 56).

At about middle portions of the vertical section in all wells a MFS can be identified. This surface is picked at a major turnaround point where the underlying retrogradational trend (TST) changes to progradational (HST), and is represented by a change from upward-increasing to upward-decreasing GR (Figure 56). In some wells the MFS does not coincide with the largest GR peak, so it is better recognized by the large scale turnaround point previously described.

Superimposed upon the second-order sequence, there are several surfaces of third order that shows pretty consistent continuity across the majority of the study area (Figure

56), as is the case of the flooding surfaces (fs) and regression surfaces (rs). Lateral changes in thickness of the third-order packages varies from about 30 to 80 ft, which imply a reasonable vertical window for potential lateral well placement and horizontal drilling.

At higher stratigraphic frequencies occur twelve GRP's of possibly fourth-order, which over long distances present significant changes and for this study are considered not very reliable to correlate from well-to-well. Based on logs, smaller cycles of GRP's are in average thinner than 30 ft, and makes their correlation somehow ambiguous and quite risky if used for geosteering.

General observations from Figure 56 indicate an eastward thinning trend of the entire second-order sequence. Internally, the TST thickens northwestward of the outcrop location, whereas the HST thickens southeastward of the outcrop (Figure 56).

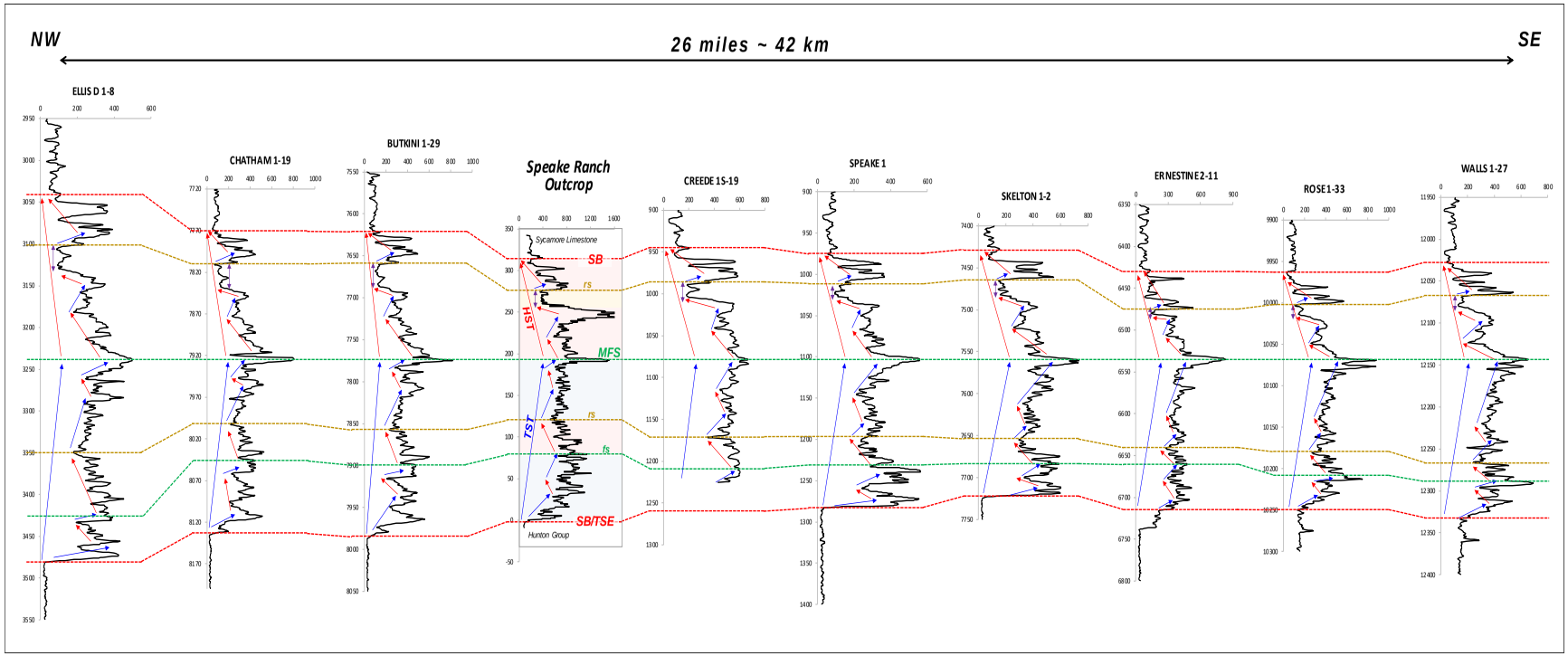

Figure 56. Outcrop-to-subsurface gamma ray correlation of sequence stratigraphic framework. Lateral variations in thicknesses show regional consistency and relatively symmetrical sequences. The basal interval is the least correlatable as it is related to the backfilling of pre-Woodford paleotopogaphy during the early stage of transgression. Red lines: second-order sequence boundaries (SB). Green lines: third-order flooding surfaces (fs). Yellow lines: third-order regressive surfaces (rs). Blue arrows: increasing-upward GRP. Red arrows: decreasing-upward GRP. Purple arrow: blocky GRP. Vertical scale of wells is in TVD (True Vertical Depth) with datum at the MFS. Cross section covers 26 miles oriented NW-SE. Refer to **Figure** 15 for exact location.

9. RESERVOIR IMPLICATIONS

Perhaps one of the most remarkable outcrop features of the Woodford Shale is its high frequency cyclical interbedding between soft and hard beds (Figure 57).

In prior studies of Slatt and Abousleiman (2011), Slatt (2013b), the Woodford Shale has been described at a variety of scales as consisting of brittle-ductile couplets, from which it was hypothesized that if subjected to artificial fracturing and proppant placement, the ductile layers after some time may deform and embed the proppant, resulting in fracture closing. Whereas brittle beds, as they have more rigid quartz-rich frameworks, they can better propagate the energy and develop more complex fracture networks, which when propped can hold clean conduits for the flow of hydrocarbons to the wellbore.

Thus, combining observations from the Woodford at the Speake Ranch outcrop and prior studies (Slatt and Abousleiman, 2011; Slatt, 2013b), we may speculate that the most favorable target intervals for horizontal drilling and completion corresponds to intervals of high-frequency interlayering of soft and hard beds. For this study, soft beds (fissile shales usually) are organic- and clay-rich layers which behave ductily and provide the organic material for generation and storage of hydrocarbons, thus as if they were depicting a 'hydrocarbon source rock' but at the centimeter scale. Hard beds (blocky cherts usually) are less organic-rich, but with quartz-rich layers which behave brittly, they constitute the fractured reservoir rock into which hydrocarbons can flow when the rock is hydraulically fractured.

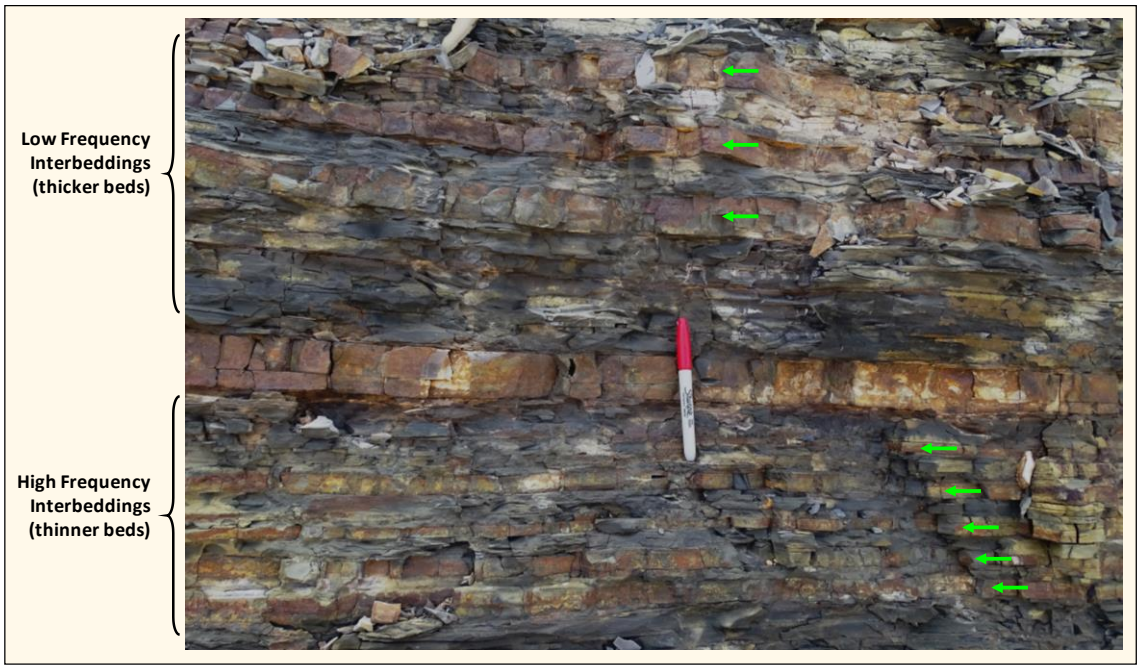

Figure 57. Typical interbedding observed in the Woodford Shale at Speake Ranch outcrop. Interbedding of low frequency accommodates fewer but thicker beds, whereas interbedding at high frequency accommodates a greater amount of thinner beds. Vertical fractures are more common within hard chert beds, but these fractures usually do not penetrate through the fissile shale beds. Green arrows indicate hard beds (cherty). Red marker for scale is 14 cm long.

First, simplifying the Woodford Shale lithology at the outcrop scale, soft and hard beds appear as the most dominant rock types (Figure 58, Figure 59), which their highly contrasting characteristics were corroborated from a variety of laboratory techniques. This allowed us to conclude that, almost regardless of their stratigraphic position, a soft or hard bed will maintain their unique characteristics.

Soft beds are fissile, laminated, contain more clay minerals and high TOC contents; hardness and brittleness values of soft beds are lower (Figure 59). Observations of the microfabric of soft beds shows a shale matrix consisting of parallel-like oriented clay minerals, with some embedded silt-sized quartz and organic matter (Figure 58). In

contrast, hard beds are blocky and massive in outcrops (Figure 58), quartz-rich, and present elevated Si/Al ratios that implies high biogenic/authigenic quartz. TOC contents and clay minerals are much lower in hard beds than in soft ones (Figure 59). The microfabric of hard beds (cherty) is largely made of microcrystalline quartz which forms massive aggregates (tightly interlocked) (Figure 58). Brittleness and hardness values of hard beds are higher (Figure 59). The presence of vertical fractures is more common through hard beds.

Thus, from a descriptive point of view, at the bed scale there clearly exists a sharp distinction between the two most dominant rock types, as evidenced by petrographic, geochemical, mineralogical and geomechanical properties.

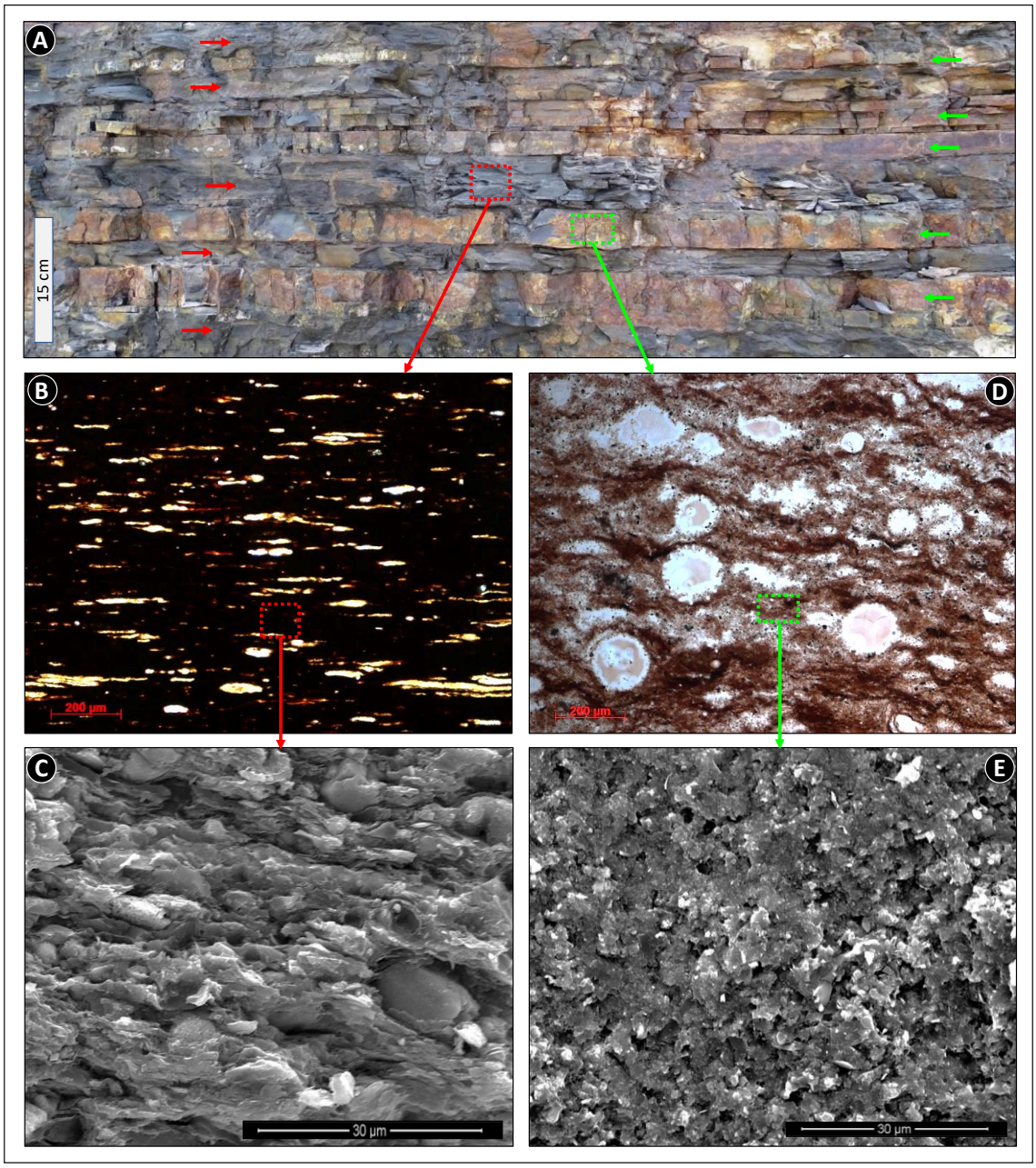

Figure 58. Differences between soft and hard beds. A) in outcrops, soft beds (red arrows) are fissile-laminated whereas hard beds (green arrows) are blocky and massive. B) thin section photomicrograph showing the dark organic-rich shale matrix and flattened *Tasmanites*. C) SEM photomicrograph showing the parallel-like preferred orientation of clay particles within a soft bed. D) thin section photomicrograph of a hard bed showing the patchy distribution of organic matter in the cherty matrix, with some embedded silicified radiolarian. E) SEM photomicrograph of the cherty matrix showing the tight interlocking of microcrystalline quartz aggregates.

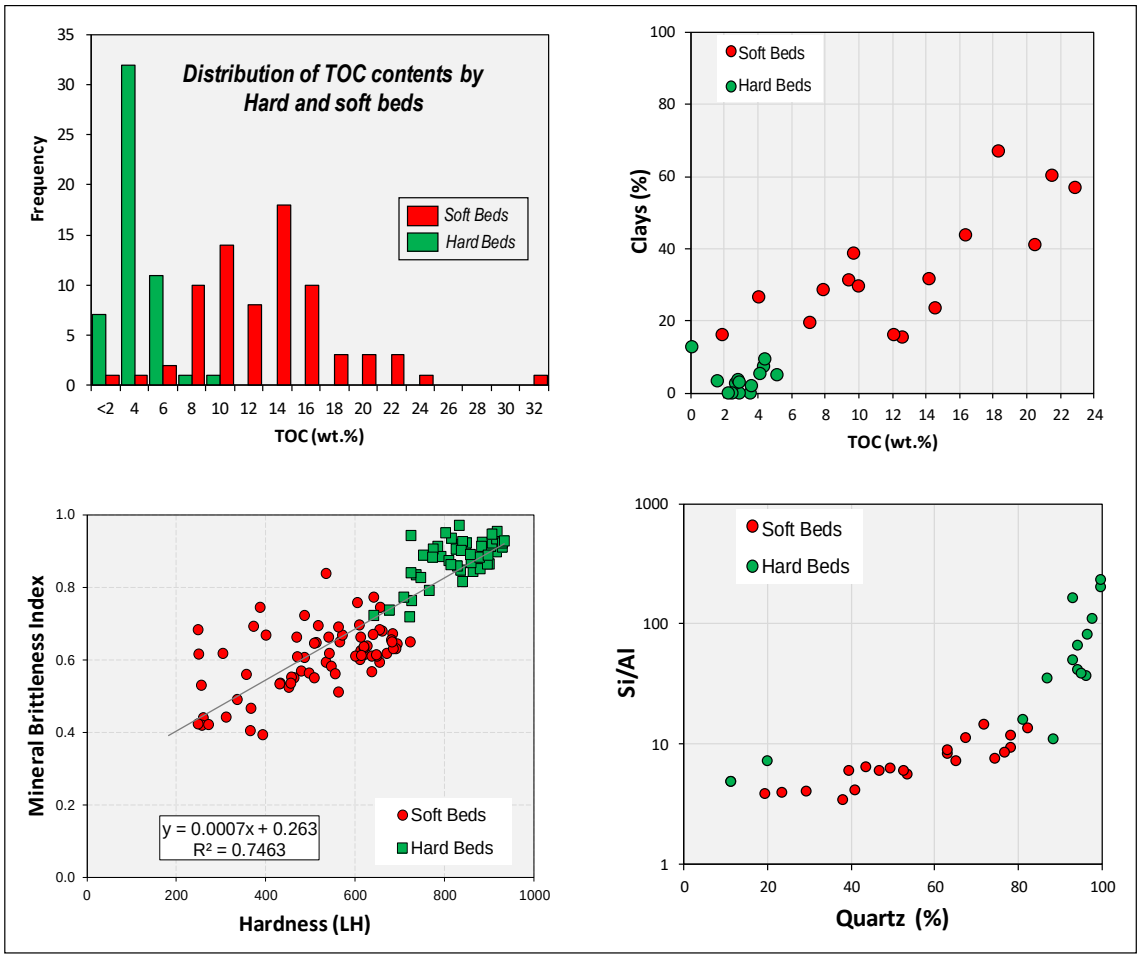

Figure 59. Differences between soft and hard beds as determined by TOC, clay and quartz contents, Si/Al ratios, brittleness index and hardness values. The two populations are well clustered and corroborates the highly contrasting nature between these two main rock types in the Woodford Shale. Hard beds (green dots) have low TOC and clay contents, but high quartz contents and high Brittleness index and hardness. Soft beds (red dots) are characterized by higher clays and TOC contents, and low hardness and brittleness index.

To identify target intervals in unconventional resources, the combination of reservoir quality (RQ) and completion quality (CQ) constitute the most commonly used parameters, which comparatively can be used in this work to interpret soft beds more related to affect RQ as they contribute with the source and storage of hydrocarbons, while hard beds affect CQ as they contribute with clean conduits (fractures) for fluid flow and

proppant placement. Additional geological understandings, perhaps more important than RQ and CQ itself, include the stratigraphic anisotropy or 'mechanical stratigraphy' as controls on well performance, from which has been suggested that the higher the bed frequency the greater will be the oil/gas production. The reasoning for that is because thinly interbedded intervals facilitate the creation of more complex fracture systems close to the wellbore and consequently more reservoir-fracture connectivity (Breyer et al., 2016).

Thus, to address the stratigraphic anisotropy with regards to the potential of RQ and CQ in the Speake Ranch outcrop, we then considered not only rock types (soft/hard), but also how beds are arranged vertically in terms of thickness and frequency. Several scenarios have been identified that relates differences in stratigraphic anisotropy at 1-foot intervals (Figure 60). To illustrate the different combinations, Figure 60 shows how intervals can be made of too much or too little numbers of beds. Depending on the bed thickness one could have a case of 50% soft and 50% hard, and if such interval is made of thinner beds the frequency of interbedding allows the stacking of more beds (Figure 60). Another case occurs when the same 50% soft and 50% hard is made of thicker beds, in this case only a few beds can be accommodated in one foot as they are too thick (Figure 60). Ideally, the scenario or stacking model that better favors both RQ and CQ is where soft-to-hard ratios are nearly 50/50 but made of thinner beds, in such a way more planes of weakness (bedding planes) become easier to be interconnected when artificially fractured.

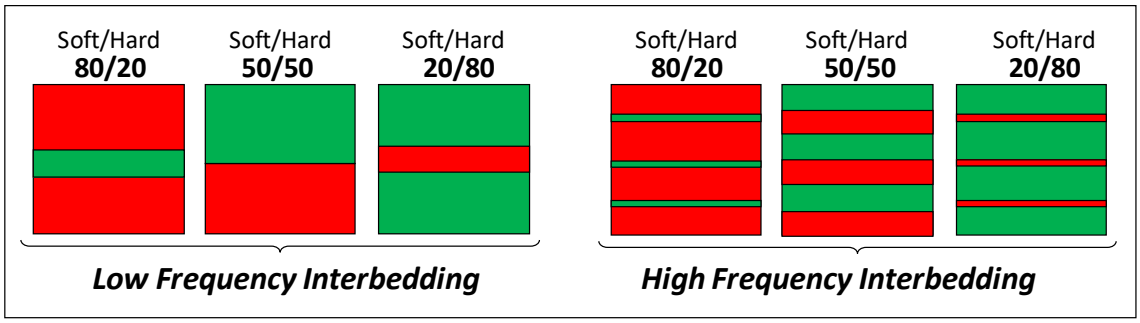

Figure 60. Idealized one-foot models to which Woodford Shale strata can be vertically stacked as a function of bed thickness and soft-to-hard ratios. Note that high frequency interbeddings consist of thinner beds while low frequency interbedding of thicker beds. Soft beds are in red and hard ones in green.

We then may assume that intervals with too many soft beds are excellent for RQ as they have good source and storage capacities for hydrocarbons provided by the shale matrix of soft beds (model 1 in Figure 61), but poor CQ. As they are relatively clay-rich and ductile they require higher pumping energies to break down, as well as artificial fractures might be potentially closed due to proppant embedment (model 1 in Figure 61). On the other hand, a scenario of too many hard beds is excellent for CQ as it is more brittle (frackable?) and able to hold propped fractures open for longer (Model 3 in Figure 61). Difficulties of too many hard beds are for RQ as the availability and deliverability of hydrocarbons is significantly reduced due to the lower TOC values and tightly interlocked quartz framework. According to my understanding, the best scenario might be existing a balance between RQ and CQ represented by a nearly 50/50 of soft and hard beds (Model 2 in Figure 61). This implies that the interval is not the most organic rich and porous, nor the most brittle, but after artificial fracturing will present better matrix-fracture connectivity for longer periods, which can be translated in better well performances.

Stacking Pattern	Characteristics	RQ and CQ	Woodford Examples
Model 3	**Hard >>> Soft** * Thick chert beds (8-12 cm) * Very thin shale beds (<3cm) * Moderate organic contents (<5%) * Very Hard (high UCS and Brittleness) * Moderate natural fracture intensity	**Better QC – Poor RQ** * Fracturability, high fracture conductivity * Efficient proppant placement * Low potential as a hydrocarbon source rock (Low expulsion efficiencies) * Poor matrix porosity	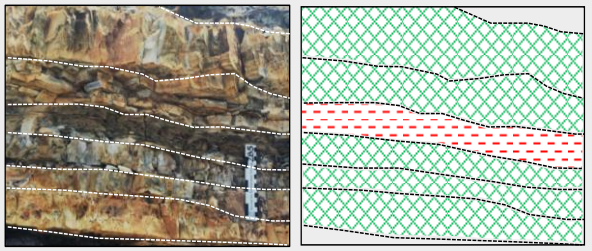
Model 2	**Soft ≈ Hard** * Homogeneous bed thickness (~4 cm) * High frequency interlayering (thinly) * Organic-rich shales and brittle cherts * Moderate Hardness * Very high natural fracture intensity	**Balance between RC and CQ** * Storage capacity in fractures of cherts as in the shale matrix primary porosity * Development of more complex hydraulic fractures * Excellent matrix-fracture connectivity * Efficient proppant placement	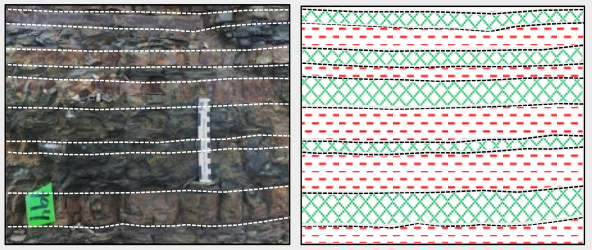
Model 1	**Soft >>> Hard** * Thick shale beds (>10cm) * Very thin scattered chert beds (<3cm) * Excellent organic contents (8-20%) * Low Hardness (high ductility) * Very low density of natural fractures	**Better RQ – Poor CQ** * Super high potential as a hydrocarbon source interval (with matrix storage) * High ductility, Low fracability * Poor reservoir connectivity * Proppant embedment	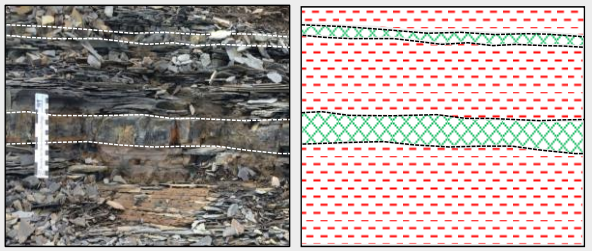

Figure 61. Idealized reservoir quality (RQ) and completion quality (CQ) as interpreted via stacking patterns between soft and hard beds. Actual examples of how the vertical arrangement differ depending on the soft-to-hard ratios and bed thickness. Example in model 1 is typical of the lower Woodford member in which soft beds dominate. Example of model 2 illustrates the typical 50/50 in which bed thicknesses of soft and hard beds are similar; this scenario of 50/50 dominates in the upper half of the middle Woodford as well as in the lower half of the upper Woodford member. Example in model 3 illustrates a dominance of thicker hard beds, which is very typical of the upper Woodford member.

Vertical variations of the soft-to-hard ratios and bed thicknesses of the Woodford Shale at Speake Ranch shows an overall upward thickening and increase in the amount of hard beds, accompanied by a thinning and upward decrease of soft beds (Figure 62). Specifically, thicker shale beds mostly predominate in the lower Woodford, while abundant and thicker cherty beds predominate in the upper Woodford (Figure 62). In between, from 190 to 250 ft, occur an interval where both soft and hard beds are similar in thickness (3-6 cm) but also their proportions soft-to-hard per foot are similar, indicating this interval is a good example of high frequency interbedding and 50/50 soft to hard ratios. Hardness values normalized per foot and plotted in the vertical also supports this observation as evidenced by the lowest values at the lower Woodford, highest values at the upper Woodford, and in between moderate values, which allow us to speculate that such an interval is not too soft to behave ductily, neither too hard to be drilled and fractured.

Recently, studies of the mechanical stratigraphy have become more common for unconventional resource shales as it seems to drive in great part the success of artificial fracturing and production. Caldwell (2013) compared productivity (EUR's) versus lateral well placement of many Woodford wells and revealed that intervals with too much clay required higher pumping pressures and presented inefficiencies in proppant placement. Using Eagle Ford wells, Breyer et al. (2016) found that oil production was significantly greater in zones where beds are thinner and the frequency of marls-to-limestones is higher. Thus, preliminary results from this thesis leave an open geological concept which deserves to be addressed with more detail and also to be validated using the intervals of lateral placement versus well productivity of Woodford wells.

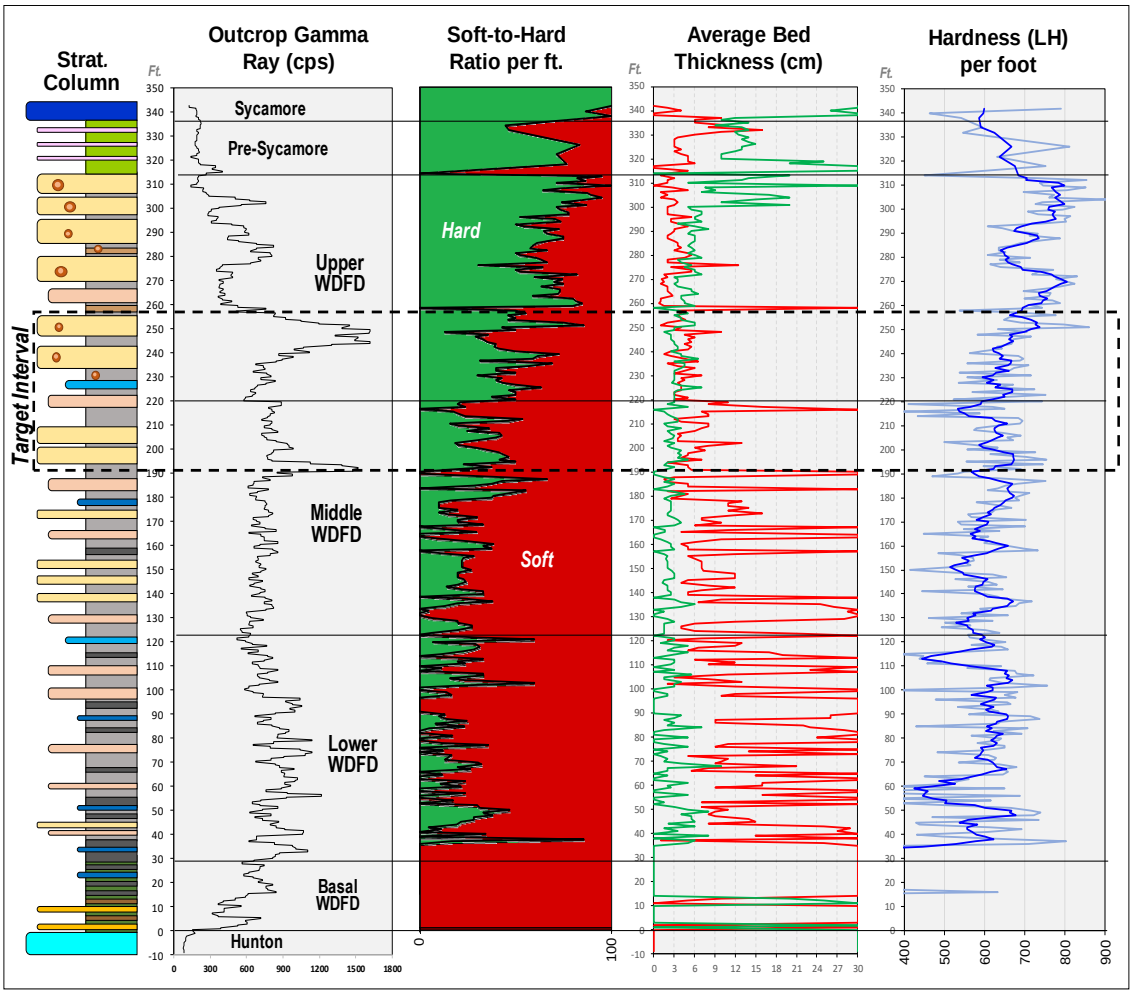

Figure 62. Vertical plot at one-foot resolution that shows the stratigraphic variability of soft-to-hard ratios, bed thickness and rock hardness. From bottom to top the amount of soft beds decreases while the hard ones increase. Bed thickness of soft beds decreases upward, while bed thickness of hard beds increases in the same direction. Hardness values evidence an upward increase very similar to the trend of increase observed for the proportion of hard beds. The potential target interval comprises the upper half of the middle Woodford and lower half of the upper member (190 to 250 ft). This interval presents a nearly 50/50 soft-to-hard ratio and bed thickness for both soft and hard beds is similar, implying a high frequency interbedding.

10. CONCLUSIONS

– The studied outcrop section at the Speake Ranch comprises the entire Woodford Shale (~320 ft thick), and partially its under- and overlying units, the Hunton Group and Sycamore Formation respectively.

– The outcrop exposure at the Speake Ranch locality allowed the documentation with direct rock indicators of the nature and relationship of the basal and upper Woodford formational contacts. The basal contact evidences the unconformable nature between the Hunton and lowermost Woodford; sedimentological indicators of the Hunton implies sub-areal exposure related to a drop in relative sea level. Overlying the Hunton limestones, glauconitic coarse sandstones and siltier-rich mudstones are evidence of shallower deposits that gradually shifts into organic-rich black shales, thus supporting the interpretation of rising sea level and the onset of marine transgression from the very base of the Woodford Shale.

– The upper Woodford contact occurs para-conformably with its overlying Pre-Sycamore deposits. A 20-ft transitional interval of silty claystones records the very late stages of HST deposits, where the biogenic input of the Woodford decreases, while the detrital and carbonate (with allochems and burrows) increases upward, thus suggesting more oxygenated bottom waters along with a reduction in the rate of sea level rise influenced by more continental-derived sedimentary input.

– Vertical stacking of lithofacies tied with outcrop gamma ray responses and chemostratigraphic proxies reveal a cyclical pattern interpreted as fourth-order or possibly fifth-order parasequence cycles superimposed onto a major second-order depositional sequence. The interpreted second-order depositional sequence begins with

the drop in seal level so that shelf regions became subaerially eroded to form the basal sequence boundary atop Hunton limestones. As sea level turned around and began rising, the shoreline moves landward and erodes to form the transgressive surface of marine erosion, which is combined with the basal sequence boundary to form the SB/TSE. With continued rise in sea level and deepening, more fine-grained detrital clay particles and organic material accumulate. Since the pre-Woodford paleotopography developed low relief, then water circulation was reduced in those lows during early stages of the TST and organic matter was more efficiently preserved. Sea level continued rising up to reach a maximum water depth, at which point any physiographic sill is outpaced giving rise to improved oceanic circulation, intense upwelling and more oxygenated waters, thus increasing organic productivity and giving rise to a more biogenic siliceous rich Highstand Systems Tract (HST).

– In outcrops, at the bed scale, the Woodford Shale lithology can be simplified as represented by two highly contrasting rock types (soft and hard) that were featured from a broader set of lab techniques (XRD, XRF, TOC, SEM, and Hardness). Soft beds are fissile, clay-rich, with high TOC, low Si/Al ratios, high Ti, Zr, K, Al and with low hardness and brittleness values. Hard beds are blocky and massive (usually), quartz-rich, with lower TOC, low Ti, Zr, K, Al and with much higher hardness and brittleness values. From the bed scale, statistically we found that almost regardless of their stratigraphic position, either a hard or soft bed will maintain their unique lithological properties throughout the section.

– Along the entire Woodford Shale there is a notorious upward enrichment in quartz-rich lithofacies, represented by an upward decrease in the soft-to-hard ratios.

Softer beds predominate in the lower Woodford, hard beds predominate in the upper Woodford, and there is a nearly 50/50 mix in the middle member. Beyond the proportion of soft over hard beds, the vertical distribution of bed thickness and frequency of interbedding better represents the degree of vertical heterogeneity between the two most contrasting rock types.

– Soft beds within the Woodford Shale present better properties as 'source for hydrocarbons' (higher in organics) coupled with relatively higher storage capacity in the form of matrix porosity. Hard beds, on the other hand, present better properties for completion quality as evidenced by its brittle behavior and abundance of natural fractures. The study of cyclical alternations of hard and soft beds within the Woodford allow to speculate that potential target zones for lateral placement correspond to a balance between reservoir quality provided by softer intervals and completion quality provided by harder intervals. If such assumption is correct the upper half of the middle Woodford and the lower half of the upper Woodford would be an optimum location for landing and completion for unconventional resources; this zone is made of high frequency interbeddings of soft and hard beds, thus the creation of connectivity (with hydro-fractures) from matrix to natural fractures would be more efficient, as well as proppant embedment will be diminished as shales are more siliceous and together with hard beds (cherty) can hold open conduits for hydrocarbons flow.

RECOMMENDATIONS AND FUTURE WORK

– There is an apparent anomaly with regards to the relationship between gamma ray response, TOC contents and Uranium (U). In Woodford hale outcrops, Krystyniak (2005) and Paxton et al. (2006) have shown that U is the major contributor to the total gamma ray response. In this study, the lower Woodford shows a good correlation of gamma ray with U and TOC. However, the upper member is not as highly correlated, but with the same trend of increasing U with increasing gamma ray. Interestingly, TOC is only correlated with U in the lower member, but not in the upper member, which is the interval with one of the highest gamma-ray responses. Phosphate nodules and concretions, which are present in abundance in the upper Woodford, can contain anomalously high U contents. Thus, caution is recommended while interpreting high gamma-ray responses in the upper Woodford as they may not provide a reliable indication of TOC.

– The origin of much of the micro-crystalline quartz in the Woodford Shale is still unclear. Although some appears to be biogenic, most of it in the mudstone matrix is too fine and shapes suggestive of radiolaria and/or spicules are not obvious. Although the interpretation of upwelling can favor biogenic silica early in its deposition, biogenic silica does undergo complex diagenesis, which involves several stages of recrystallization and re-distribution, which ends with authigenic quartz. It is possible that much of the original biogenic silica has recrystallized and today almost all quartz present in the Woodford may be diagenetic. SEM photomicrographs coupled with oxygen isotopes might provide information on the biogenic fingerprints of quartz that might allow clear differentiation between types of quartz.

– The Woodford Shale in some localities of southern Oklahoma contain carbonate minerals at variable proportions, although most samples analyzed in this study using XRD and XRF indicate that carbonates are irrelevant compared to silica contents. This minor carbonate occurs in a variety of forms, as in the matrix, as skeletal components, intraparticle-interparticle cements, veins and nodules. Its areal extent is unclear as is vertical distribution and how much carbonate has been remobilized and how much might have been lost during diagenesis, but investigation of the carbonate beds with SEM cathodoluminescence, geochemistry and wireline logs might provide useful information on the carbonate origin, diagenesis and identification. This understanding is important because carbonates might also improve or diminish petrophysical and geomechanical properties of the Woodford Shale.

– One important challenge in the characterization of the Woodford Shale are the small scale at which those soft-to-hard cycles occur. Usually conventional logs are delivered at 0.3 m (1-ft) vertical resolution, but the Woodford interbedding in most of the cases is couplets between 8 to 15 cm, and does not facilitate the detection of soft-to-hard ratios or bed thickness to study its mechanical stratigraphy. One alternative to validate our conclusions on the stratigraphic anisotropy of small resolution versus target zones might be the usage of borehole images or CT-core tomography, which easily allow the quantification and distinction between soft and hard beds.

– In northern Oklahoma, the Misener sandstone is an oil reservoir rock which is locally present in the base of, or below, the Woodford Shale according to some published information. In the study area at the Speake Ranch outcrop, possible Misener-like sandstones are present in the basal interval of the Woodford succession. Detailed facies

analysis and sediment provenance coupled with age dating of the Misener sandstones from outcrops or other wells should aid in constructing the facies model for the earliest stages of the Woodford deposition and aid in generating facies maps of this clastic unit in southern Oklahoma. To date very little geological information could be found on the Misener sandstone in southern Oklahoma. Implications with regards to the occurrence and distribution of pre-Woodford sandstone bodies in the subsurface of southern Oklahoma (with characteristics of a Misener sandstone), might be the presence of a permeable carrier bed and/or a potential conventional sandstone reservoir, as is the case of the Caddo and Aylesworth Fields where oil shows and production have been reported from a pre-Woodford clastic interval.

REFERENCES

Algeo, T.J. & Maynard, J., 2004, Trace-element behavior and redox facies in core shales of Upper Pennsylvanian Kansas-type cyclothems. Chemical Geology, v. 206, p. 289-318.

Algeo, T.J. & Lyons, T.W., 2006, Mo-total organic carbon covariation in modern anoxic marine environments: Implications for analysis of paleoredox and paleohydrographic conditions. Paleoceanography, v. 21, 23p.

Algeo, T.J., Lyons, T.W., Blakey, R.C., & Over, D.J., 2007, Hydrographic conditions of the Devono-Carboniferous North American Seaway inferred from sedimentary Mo-TOC relationships. Palaeogeography Palaeoclimatology Palaeoecology, v. 256, p. 204-230.

Algeo, T.J. & Rowe, H., 2012, Paleoceanographic applications of trace-metal concentration data. Chemical Geology, v. 324, p. 6-18.

Allen, R.W., 2000, Stratigraphy, mountain building and complex geological structures of the Ardmore Basin. Oklahoma Geological Society, Shale Shaker, v. 51, p. 10-21.

Amonette, J.E., 2002, Methods for determination of mineralogy and environmental availability. In: Dixon, J.B., Schulze, D.G. (Eds.), Soil Mineralogy with Environmental Applications, SSSA Book Series, v. 7. Soil Science Society of America, Madison, WI, p. 153-197.

Amsden, T.W. & Klapper, G., 1972, Misener Sandstone (Middle-Upper Devonian), north-central Oklahoma. AAPG Bulletin, v. 56, p. 2323-2334.

Amsden, T.W., 1975, Hunton Group (Late Ordovician, Silurian, and Early Devonian) in the Anadarko basin of Oklahoma. OGS Bulletin, v. 121, 214 p.

Andrews, R.D., 2011, Outcrop Characteristics for the Woodford Shale, Search and Discovery Article #80200. AAPG Mid-Continent Section meeting, Oklahoma City, OK-USA, October1-4.

Aoki, H., & Matsukura, Y., 2008, Estimating the unconfined compressive strength of intact rocks from Equotip hardness. Bulletin of Engineering Geology and the Environment, v. 67-1, p. 23-29.

Bhatia, M.R. & Crook, K.A.W., 1986, Trace element characteristics of graywackes and tectonic setting discrimination of sedimentary basins. Contributions to Mineralogy and Petrology, v. 92, p. 181-193.

Becerra-Rondon, D.M., 2017, Comprehensive characterization of the Woodford Shale at the I-35 outcrop, Arbuckles Mountains Area, Oklahoma. M.S. thesis, University of Oklahoma. In progress

Blackford, M.A., 2007, Electrostratigraphy, thickness, and petrophysical evaluation of the Woodford Shale, Arkoma Basin, Oklahoma. M.S. thesis, Oklahoma State University, 84 p.

Bohacs, K.M., 1993, Source quality variations tied to sequence development in the Monterey and associated formations, southwestern California in Katz, B.J., and Pratt, L.M., eds., Petroleum Source Rocks in a Sequence-Stratigraphic Framework: American Association of Petroleum Geologists, Studies in Geology, v. 7, p.177-204.

Bohacs, K.M., Grabowski, G.J., Carroll, A.R., Mankiewicz, P.J., Miskell-Gerhardt, K.J., Schwalbach, J.R., Wegner, M.B., Simo, J.A., 2005, Production, destruction, and dilution- the many paths to source-rock development. In: Harris, N.B., Eds., The Deposition of Organic-Carbon-Rich Sediments: Models, Mechanisms, and Consequences. SEPM (Society for Sedimentary Geology), Special Publication, p. 61-101

Bontempi, C.P., 2015, High resolution stratigraphy of thin bedded shales radiolarites, Woodford Shale, Arbuckle wilderness area, Oklahoma. MS thesis, University of Oklahoma, 81 p.

Breyer, J.A., Denne, R.A., Kosanke, T., Spaw, J.M., Funk, J., Christianson, P., Bush, D.A., & Nelson, R.A., 2016, Facies, fractures, pressure, and production in the Eagle Ford Shale (Cretaceous) between the San Marcos arch and the Maverick Basin, Texas, U.S.A., in J.A. Breyer, ed., The Eagle Ford Shale: A renaissance in U.S. oil production: AAPG Memoir 110, p. 363-384.

Brueseke, M.E., Hobbs, J.M., Bulen, C.L., Mertzman, S.A., Puckett, R.E., Walker, J.D., & Feldman, J., 2016, Cambrian intermediate-mafic magmatism along the Laurentian margin: Evidence for flood basalt volcanism from well cuttings in the Southern Oklahoma Aulacogen (USA). Lithos, v. 260, p. 164-177.

Brumsack, H.J., 1989, Geochemistry of recent TOC-rich sediments from the Gulf of California and the Black Sea. Geologische Rundschau, v. 78, p. 851-882.

Brumsack, H.J., 2006, The trace metal content of recent organic carbon-rich sediments: implications for Cretaceous black shale formation. Palaeogeography, Palaeoclimatology, Palaeoecology, v. 232-2, p. 344-361.

Caldwell, C.D., 2013, Cana Woodford Shale Play, Anadarko Basin: The Effects of Mudrock Lithologies and Mechanical Stratigraphy on Completion and Production. AAPG Search and Discovery Article, 43 p.

Calvert, S.E. & Pedersen, T.F., 1993, Geochemistry of recent oxic and anoxic marine sediments: implications for the geological record. Marine geology, v. 113, no. 1-2, p. 67-88.

Cardona-Valencia, L.F., 2014, Integrated characterization of the Woodford Shale in the southern Cherokee Platform, Oklahoma: Norman, Oklahoma, M.S. thesis, University of Oklahoma, 98 p.

Cardott, B.J., 2012, Thermal maturity of Woodford Shale gas and oil plays, Oklahoma, USA. Journal of Coal Geology, v. 103, p. 109-119.

Cardott, B.J., 2014, Woodford Shale play update: Expanded extent in the oil window. AAPG Search and Discovery Article #80409, 51 slides.

Carlucci, J.R., Westrop, S.R., Brett, C.E., & Burkhalter, R., 2014, Facies architecture and sequence stratigraphy of the Ordovician Bromide Formation (Oklahoma): a new perspective on a mixed carbonate-siliciclastic ramp. Facies, v. 60, p. 987-1012.

Champlin, S.C., 1958, The problem of the Welden, Sycamore and lower Caney in the eastern Arbuckle Mountains: Proceedings of the Oklahoma Academy of Science, p. 120-124.

Comer, J.B., & Hinch, H.H., 1987, Recognizing and quantifying expulsion of oil from the Woodford Formation and age-equivalent rocks in Oklahoma and Arkansas. AAPG Bulletin, v. 71, p. 844-858.

Comer, J.B., 2005, Facies distribution and hydrocarbon production potential of Woodford Shale in the southern Midcontinent, in: B.J. Cardott, ed., Unconventional energy resources in the southern Midcontinent, Oklahoma Geological Survey Circular 110, p. 51-62.

Comer, J.B., 2008, Woodford Shale in southern Midcontinent, USA-Transgressive system tract marine source rocks on an arid passive continental margin with persistent oceanic upwelling. AAPG Annual Convention, San Antonio, TX, poster, 3 panels.

Conant, L.C., & Swanson, V.E., 1961, Chattanooga Shale and related rocks of central Tennessee and nearby areas. U.S. Geological Survey Professional Paper 357, 91 p.

Connock, G.T., 2015, Paleoenvironmental interpretation of the Woodford Shale, Wyche Farm shale pit, Pontotoc County, Arkoma Basin, Oklahoma with primary focus on water column structure. M.S. thesis, University of Oklahoma, 253 p.

Cooper, C.L., 1932, A crustacean fauna from the Woodford Formation of Oklahoma. Journal of Paleontology, v. 6, p. 346-352.

Cornford, C., Gardner, P. & Burgess, C., 1998, Geochemical truths in large data sets. Part I: Geochemical screening data. Organic Geochemistry, v. 29, p. 519-530.

Curtis, C.D., Lipshie, S.R., Oertel, G., & Pearson, M.J., 1980, Clay orientation in some Upper Carboniferous mudrocks, its relationship to quartz content and some inferences about fissility, porosity and compactional history. Sedimentology, v. 27, p. 333-339.

Dean, W.E., & Arthur, M.A., 1998, Geochemical expressions of cyclicity in Cretaceous pelagic limestone sequences: Niobrara Formation, Western Interior Seaway. SEPM Concepts Sedimentol. Paleontol. v. 6, p. 227-255.

Donovan, R.N., 2001, Field study of the Sycamore Formation on Interstate Highway 35 in the Arbuckle Mountains, Oklahoma, in K.S. Johnson, ed., Silurian, Devonian, and Mississippian geology and petroleum in the southern Midcontinent, 1999 symposium, Oklahoma Geological Survey Circular 105, p. 139-149.

Ekwunife, I.C., 2017, High-Resolution Chemostratigraphy of The Woodford Shale in the McAlister Quarry, Ardmore Basin, Oklahoma. M.S. thesis, University of Oklahoma. In progress

Fay, R.O., 1989, Geology of the Arbuckle Mountains along Interstate 35, Carter and Murray Counties, Oklahoma. Oklahoma Geological Survey Guidebook 26, 50 p.

Ferrill, D.A., McGinnis, R.N., Morris, A.P., Smart, K.J., Sickmann, Z.T., Bentz, M., Lehrmann, D., & Evans, M.A., 2014, Control of mechanical stratigraphy on bed restricted jointing and normal faulting: eagle Ford Formation, south-central Texas, U.S.A., AAPG Bulletin v.98, p. 2477-2506.

Fishman, N.S., Ellis, G.S., Boehlke, A.R., Paxton, S.T., & Egenhoff, S.O., 2013, Gas storage in the Upper Devonian-Lower Mississippian Woodford Shale, Arbuckle Mountains, Oklahoma: How much of a role do chert beds play?, in J.Y. Chatellier and D.M. Jarvie, eds., Critical assessment of shale resource plays: AAPG Memoir 103, p. 81-107.

Gupta, N., Sarkar, S., & Marfurt, K.J., 2011, Seismic characterization of the Woodford Shale in the Anadarko Basin: SEG Annual Meeting, p. 1083-1087.

Ham, W.E., and others, 1973, Regional geology of the Arbuckle Mountains, Oklahoma: Oklahoma Geological Survey Special Publication 73-3, 61 p.

Hass, W.H., & Huddle, J.W., 1965, Late Devonian and Early Mississippian age of the Woodford Shale in Oklahoma as determined by conodonts, in Geological Survey research: U.S. Geological Survey Professional Paper 525-D, p. 125-132.

Hester, T.C., Schmoker, J.W., & Sahl, H.L., 1990, Log-derived regional source-rock characteristics of the Woodford Shale, Anadarko basin, Oklahoma: U.S. Geological Survey Bulletin 1866-D, 38 p.

Hild, E. & Brumsack, H.J., 1998, Major and minor element geochemistry of Lower Aptian sediments from the NW German Basin (core Hoheneggelsen KB 40). Cretaceous Research, v. 19, p. 615-633.

Hoffman, P., Dewey, J.F., & Burke, K., 1974, Aulacogens and their genetic relation to geosynclines, with a Proterozoic example from Great Slave Lake, Canada, in Modern and ancient geosynclinal sedimentation: SEPM Special Publication v. 19, p. 38-55.

Infante-Paez, L., Cardona, L. F., McCullough, B., & Slatt, R., 2016, Seismic analysis of paleotopography and stratigraphic controls on total organic carbon: Rich sweet spot distribution in the Woodford Shale, Oklahoma, USA. Interpretation, v.5-1, p. 33-47.

Ingram, R.L., 1953, Fissility of mudrocks: Geological Society of America, Bulletin, v. 64, p. 869-878.

Jarvie, D.M., Claxton, B.L. Henk, F., & Breyer, J.T., 2001, Oil and shale gas from the Barnett Shale, Fort Worth Basin, Texas. Proceedings of AAPG Annual Meeting, p. A100.

Jarvie, D.M., Hill, R.J., Ruble, T.E., & Pollastro, R.M., 2007, Unconventional shale-gas systems: The Mississippian Barnett Shale of north-central Texas as one model for thermogenic shale-gas assessment. AAPG Bulletin, v. 91, p. 475-499.

Johnson, K.S., & Cardott, B.J., 1992, Geologic framework and hydrocarbon source rocks of Oklahoma, in K.S. Johnson and B.J. Cardott, eds., Source rocks in the southern Midcontinent, 1990 symposium: OGS Circular 93, p. 21-37.

Katz, A., Sass, E., Holland, H.D., & Starinsky, A., 1972, Strontium behavior in the aragonite-calcite transformation: An experiment study at 40-98oC, Geochemica et Cosmochemica Acta, v. 36-4, p. 481-496.

Keller, G.R., & Stephenson, R.A., 2007, The southern Oklahoma and Dniepr-Donets aulacogens: A comparative analysis. Geological Society of America Memoirs, v. 200, p. 127-143.

Keller, G.R., 2012, A Regional Overview of Southern Oklahoma Structures, and some stuff about recent earthquakes. Oklahoma Geological Survey. Available at: http://www.ogs.ou.edu/MEETINGS/Presentations/OilGasMar2012/Keller_Southern_OK.pdf (Accessed: February 2017).

Kirkland, D.W., Denison, R.E., Summers, D.M., & Gormly, J.R., 1992, Geology and organic geochemistry of the Woodford Shale in the Criner Hills and western Arbuckle Mountains, Oklahoma. In: Johnson, K.S. & Cardott, B.J. (eds.) Source rocks in the southern mid-continent: 1990 Symposium: OGS Circular 93, p. 38-69.

Krystyniak, A.M., 2005, Outcrop-based gamma-ray characterization of the Woodford Shale of south-central Oklahoma. M.S. thesis, Oklahoma State University, 145 p.

Kuykendall, M.D., & Fritz R.D., 2001, Misener sandstone of Oklahoma: Oklahoma Geological Survey Circular 93-4, p. 117-134.

Lambert, M.W., 1993, Internal stratigraphy and organic facies of the Devonian-Mississippian Chattanooga (Woodford) Shale in Oklahoma and Kansas, in B.J. Katz and L.M. Pratt, eds., Source rocks in a sequence stratigraphic framework. AAPG Studies in Geology 37, p. 163-176.

Langford, F.F. & Blanc-Valleron, M.M., 1990, Interpreting Rock-Eval pyrolysis data using graphs of pyrolyzable hydrocarbons vs. total organic carbon. AAPG Bulletin, v. 74, p. 799-804.

Laubach, S.E., Olson, J.E., & Gross, M.R., 2009, Mechanical and fracture stratigraphy. AAPG Bulletin, v. 93-11, p. 1413-1426.

Lazar, O.R., Bohacs, K.M., Macquaker, J.H.S., Schieber, J., & Demko, T.M., 2015, Integrated approach for the nomenclature and description of the spectrum of fine-grained sedimentary rocks. Journal of Sedimentary Research, v. 85, p. 230-246.

Lee, J.S., 2015, Calibration of Rebound Hardness Numbers to Unconfined Compressive Strength in Shale Formations. Journal of Petroleum Technology, v. 67-1, p. 41-45.

Lewan, M., 1978, Laboratory Classification of Very Fine Grained Sedimentary Rocks. Geology, v. 6, p. 745-748.

Macquaker, J.H.S., & Adams, A.E., 2003, Maximizing information from fine-grained sedimentary rocks: an inclusive nomenclature for mudstones. Journal of Sedimentary Research, v. 73, p. 735-744.

Madden, M.E. Elwood, 2011, X-Ray Diffraction Laboratory Manual (unpublished report), The Devon Energy NanoLab, University of Oklahoma, Norman. 52 p.

McCullough, B.J., 2014, Sequence stratigraphic framework and characterization of the Woodford Shale on the southern Cherokee Platform of central Oklahoma. M.S. thesis, University of Oklahoma, 211 p.

Miall, A.D., 1991, Stratigraphic sequences and their chronostratigraphic correlation. Journal of Sedimentary Petrology, v. 61, p. 497-505.

Miceli-Romero, A., & Philp, R.P., 2012, Organic geochemistry of the Woodford Shale, southeastern Oklahoma: How variable can shales be?. AAPG Bulletin, v. 96, p. 493-517.

Milliken, K., 2014, A Compositional Classification for Grain Assemblages in Fine-Grained Sediments and Sedimentary Rocks. Journal of Sedimentary Research, v. 84-12, p. 1185-1199.

Molinares-Blanco, C.E., 2013, Stratigraphy and palynomorphs composition of the Woodford Shale in the Wyche Farm Shale Pit, Pontotoc County, Oklahoma. M.S. thesis, University of Oklahoma, 90 p.

Moore, D.M. & Reynolds, R.C., 1997, X-ray Diffraction and the Identification and Analysis of Clay Minerals. Oxford University Press, Oxford, New York, USA.

Noble, P.J., 1995, Regional sedimentation patterns associated with the passive- to active-margin transition, Ouachita Orogeny, southern Midcontinent, U.S.A., in K.S.

Johnson, ed., Structural styles in the southern Midcontinent, 1992 symposium, OGS Circular 97, p. 99-112.

Northcutt R.A. & Campbell J.A., 1995, Geologic Provinces of Oklahoma Map. Oklahoma Geological Survey. Available at: http://www.ogs.ou.edu/geolmapping/Geologic_Provinces_OF5-95.pdf (Accessed: February 2017).

Nowaczewski, V., 2011, Biomarker and paleontological investigations of the Late Devonian extinctions, Woodford Shale, southern Oklahoma. M.S. thesis, University of Kansas, 96 p.

O'Brien, N.R., & Slatt, R.M., 1990, Argillaceous Rock Atlas: New York, Springer-Verlag ed., 141 p.

Over, D.J., 1992, Conodonts and the Devonian-Carboniferous boundary in the Upper Woodford Shale, Arbuckle Mountains, south-central Oklahoma. Journal of Paleontology, v. 66, p. 293-311.

Over, D.J., 2002, The Frasnian/Famennian boundary in central and eastern United States. Palaeogeography, Palaeoclimatology, Palaeoecology, v. 181, p. 153-169.

Paxton, S.T., Cruse, A.M. & Krystyniak, A.M., 2006, Detailed fingerprints of global sea-level change revealed in Upper Devonian/Mississippian Woodford Shale of south-central Oklahoma, Proceedings of AAPG Annual Convention, p. 83.

Paxton, S.T., & Cardott, B.J., 2008, Oklahoma gas shales field trip, October 21 & 23, 2008: Oklahoma Geological Survey Open File Report 2, 110 p.

Pearce, T.J., & Jarvis, I., 1992, Applications of geochemical data to modelling sediment dispersal patterns in distal turbidites: Late Quaternary of the Madeira Abyssal Plain. Journal of Sedimentary Petrology, v. 62, p. 1112-1129.

Pearce, T.J., Besly, B.M., Wray, D.S., & Wright, D.K., 1999, Chemostratigraphy: a method to improve interwell correlation in barren sequences – a case study using onshore Duckmantian/Stephanian sequences (West Midlands, U.K.). Sedimentary Geology, v. 124, p. 197-220.

Pepper, A.S., & Corvi, P.J., 1995, Simple kinetic models of petroleum formation. Part I: oil and gas generation from kerogen: Marine and Petroleum Geology, v. 12, p. 291-319.

Peters, K.E., & Cassa, M.R., 1994, Applied source rock geochemistry, in Magoon, L.B., and Dow, W.G., eds., The petroleum system-From source to trap. AAPG Memoir 60, p. 93-117.

Phillips, N.D., 1991, Refined Subsidence Analyses as a Means to Constrain Late Cenozoic Fault Movement, Ventura Basin, California. MS Thesis, University of Texas at Austin, 545 p.

Posamentier, H.W., & Allen, G.P., 1999, Siliciclastic sequence stratigraphy: concepts and applications. Concepts in Sedimentology and Paleontology, v.7, 210 p.

Potter, P.E., Maynard, J.B., & Depetris, P.J., 2005, Mud and Mudstones: Introduction and Overview: Berlin, Springer ed., 297 p.

Puckette, J., Boardman, D.R. & Watney, W.L., 2013, Woodford Shale: Correlating rock properties in outcrop and core with wireline log characteristics: AAPG Search and Discovery Article #50885, 46 p.

Roberts, C.T., & Mitterer, R.M., 1992, Laminated black shale-bedded chert cyclicity in the Woodford Formation, southern Oklahoma, in K.S. Johnson and B.J. Cardott, eds., Source rocks in the southern Midcontinent, 1990 symposium: OGS Circular 93, p. 330-336.

Ross, D.J.K., & Bustin, R.M., 2009, Investigating the use of sedimentary geochemical proxies for paleoenvironment interpretation of thermally mature organic-rich strata: examples from the Devonian–Mississippian shales, Western Canadian Sedimentary Basin. Chemical Geology v. 260, p. 1-19.

Rowe, H.D., Loucks, R.G. Ruppel, S.C. & Rimmer, S.M., 2008, Mississippian Barnett formation, Fort Worth Basin, Texas: Bulk geochemical constraints on the severity of hydrographic restriction and the biogeochemical cycling and fate of iron. Chemical Geology, v. 257, p. 16-25.

Rowe, H.D., Ruppel, S.C., Rimmer, S.M., & Loucks, R.G., 2009, Core-based chemostratigraphy of the Barnett Shale, Permian Basin, Texas Gulf Coast Association of Geological Societies Transactions, v. 59, p. 675-686.

Rowe, H.D, Hughes, N., & Robinson, K., 2012, The quantification and application of handheld energy-dispersive x-ray fluorescence (ED-XRF) in mudrock chemostratigraphy and geochemistry. Chemical Geology, v.324-325, p.122-131.

Sageman, B.B. & Lyons, T.W., 2004, Geochemistry of fine-grained sediments and sedimentary rocks. In: Mackenzie, F. ed., Sediments, Diagenesis, and Sedimentary Rock. Treatise on Geochemistry, v. 7, p. 115-158.

Salminen R., Batista, M.J., Bidovec, M., Demetriades, A., DeVivo, B., DeVos, W., Duris, M., Gilucis, A., Gregorauskiene, V., Halamic, J., Heitzmann, P., Lima, A., Jordan, G., Klaver, G., Klein, P., Lis, J., Locutura, J., Marsina, K., Mazreku, A., O'Connor, P.J., Olsson, S.A., Ottesen, R.T., Petersell, V., Plant, J.A., & Reeder, S., 2005, Geochemical Atlas of Europe, Part 1: Background Information, Methodology and Maps. Geological Survey of Finland, 526 p. Available online at: http://www.gtk.fi/publ/foregsatlas/ (Accessed February 2017).

Schwartzapfel, J.A., 1990, Biostratigraphic investigations of late Paleozoic (Upper Devonian to Mississippian) Radiolaria within the Arbuckle Mountains and Ardmore basin of south-central Oklahoma, Ph.D. dissertation, University of Texas, 475 p.

Serna-Bernal, A., 2013, Geological Characterization of the Woodford Shale McAlister Cemetery Quarry, Criner Hills, Ardmore Basin, Oklahoma. M.S. thesis, University of Oklahoma, 141 p.

Siy, S.E., 1988, Geochemical and petrographic study of phosphate nodules of the Woodford Shale (Upper Devonian-Lower Mississippian) of southern Oklahoma. M.S. thesis, Texas Tech University, 172 p.

Slatt, R.M., & Abousleiman, Y., 2011, Merging sequence stratigraphy and geomechanics for unconventional gas shales. The Leading Edge, v. 30-3, p. 274-282.

Slatt, R.M., Buckner, N., Abousleiman, Y., Sierra, R., Philp, P., Micelli-Romero, A., Portas, R., O'Brien, N., Tran, M., Davis, R., & Wawrzyniec, T., 2012, Outcrop-behind outcrop (quarry): multiscale characterization of the Woodford gas shale, Oklahoma, in J. Breyer, ed., Shale reservoirs-Giant resources for the 21st century, AAPG Memoir 97, p. 382-402.

Slatt, R.M., & Rodriguez, N.D., 2012, Comparative sequence stratigraphy and organic geochemistry of gas shales: Commonality or coincidence?. Journal of Natural Gas Science and Engineering, v. 8, p. 68-84.

Slatt, R.M., 2013a, Stratigraphic reservoir characterization for petroleum geologists, geophysicists, and engineers, Elsevier ed. 2nd edition, 688p.

Slatt, R.M., 2013b, Sequence stratigraphy of the Woodford Shale and application to drilling and production: AAPG Search and Discovery Article #50792, Oral presentation AAPG Woodford Shale Forum, Oklahoma City, April 11, 2013.

Slatt, R.M., McCullough, B.J., Molinares-Blanco, C.E., & Baruch, E.T., 2016, Paleotopographic and Depositional Environmental Control on "Sweet Spot" locations in Some Unconventional Resource Shales. The Houston Geological Society Bulletin, v. 58-8, p. 37-39.

Spears, D.A., 1976, The fissility of some Carboniferous Shales: Sedimentology, v. 23, p. 721-725.

Sullivan, K.L., 1985, Organic facies variation of the Woodford Shale in western Oklahoma: Shale Shaker, v. 35, p. 76-89.

Suneson, N., 1996. The geology of the Ardmore Basin in the Lake Murray Stake Park Area, Oklahoma, prepared for the spring field meeting of the Oklahoma Academy of Science, 44 p.

Swanson, V.E., 1961, Geology and geochemistry of uranium in marine black shales, a review: U.S.G.S. Professional Paper 356-C, p. 67-112.

Taff, J.A., 1902, Description of the Atoka quadrangle: U.S. Geological Survey Geologic Atlas Folio 79, scale 1:125,000, 8 p.

Tissot, B.P., & Welte, D.H., 1984, Petroleum formation and occurrence. Springer-Verlag Berlin Heidelberg, Germany, 699 p.

Treanton, J.A., 2014, Outcrop-derived chemostratigraphy of the Woodford Shale, Murray County, Oklahoma. M.S. thesis, The University of Oklahoma, 83 p.

Tribovillard, N., Algeo, T.J., Lyons, T., & Riboulleau, A., 2006, Trace metals as paleoredox and paleoproductivity proxies: an update. Chemical Geology, v. 232, p. 12-32.

Turner, B.J., 2016, Utilization of Chemostratigraphic Proxies For Generating And Refining Sequence Stratigraphic Frameworks in Mudrocks and Shales, Ph.D dissertation, University of Oklahoma, 135 p.

Urban, J.B., 1960, Microfossils of the Woodford Shale (Devonian) of Oklahoma. M.S. thesis, University of Oklahoma, 77 p.

Vail, P.R., Audemard, F., Bowman, S.A., Eisner, P.N., & Perez-Cruz, C., 1991. The stratigraphic signatures of tectonics, eustasy and sedimentology - an overview. In: Einsele, G., Ricken, W., Seilacher, A., Eds., Cycles and Events in Stratigraphy. Springer-Verlag, Berlin, p. 617-659.

Van Wagoner, J.C., Mitchum, R.M., Campion, K.M., & Rahmanian, V.D., 1990, Siliciclastic sequence stratigraphy in well logs, cores, and outcrop. AAPG Methods in Exploration, v. 7, 55 p.

Villalba, D.M., 2016, Organic Geochemistry of The Woodford Shale, Cherokee Platform, OK and its Role in a Complex Petroleum System. M.S. Thesis, University of Oklahoma, 126 p.

Vine, J.D. & Tourtelot, E.B., 1970. Geochemistry of black shale deposits-A summary report. Economic Geology, v. 65, p. 253-272.

Von Almen, W.F., 1970, Palynomorphs of the Woodford Shale of south-central Oklahoma with observations on their significance in zonation and paleoecology. Ph.D. dissertation, Michigan State University, 179 p.

Wang, T., 2016, An Organic Geochemical Study of Woodford Shale and Woodford-Mississippian Tight Oil from Central Oklahoma. Ph.D. dissertation, University of Oklahoma, 299 p.

Ward, J.H., 1963, Hierarchical grouping to optimize an objective function. Journal of the American Statistical Association, v.69, p.236-244.

Wedepohl, K.H., 1971, Environmental influences on the chemical composition of shales and clays. In: Ahrens, L.H., Press, F., Runcorn, S.K., Urey, H.C., Eds., Physics and Chemistry of the Earth. Pergamon, Oxford, p. 305-333.

Weedon, G.P., & Shackleton, N.J., 1997. Inorganic geochemical composition of Oligocene to Miocene sediments and productivity variations in the Western

equatorial Atlantic: results from sites 926 and 929. Proceedings of the Ocean Drilling Program, Scientific Results, v. 154, p. 507-526.

Zahm CK, & Enderlin M., 2010, Characterization of rock strength in Cretaceous strata along the Stuart City Trend. Texas: Gulf Coast Association of Geological Societies Transactions, v. 60. p. 693-702.